Norges miljø- og biovitenskapelige universitet

Master's Thesis 2018 60 ECTS

Faculty of Environmental Sciences and Natural Resource Management

Acid Mine Drainage from Folldal Mine Tailings: Geochemical Characterization and Simulation

Samuel Kebede Gelena

Environment and Natural Resources - Specialization Sustainable Water and Sanitation, Health and Development

Abstract

The mining of certain minerals, such as copper and zinc is commonly connected with acid mine drainage (AMD) problems that can have serious impact on human health and cause ecological destruction. The Folldal mining area was intensively mined for copper, sulphur and zinc for about 200 years from 1747 to 1968. The main objectives of this research work were to predict the acid producing capacity of Folldal mine tailings by using static and kinetic tests and to develop geochemical models to quantify leachate composition. The static tests were carried out for 19 topsoil samples collected from different parts of the mining area. Humidity cell (small column) tests (kinetic tests) and large column test were performed to assess the sulphate and heavy metals leaching rates from the soil samples. Inverse geochemical modelling using PHREEQC codes was applied to explain possible mass transfer processes between column leachates of mine tailings and rainwater.

The net neutralization potential (NNP) and the neutralization potential ratio (NPR) calculated based on total concentration of sulphur and total inorganic carbon, TIC (static test), varied from -159 to 3.3 t $CaCO_3$ /1000 t and 0.01 to 11.5 respectively. The NNP in most samples were in an uncertainty zone (-20 to +20 t $CaCO_3$ /1000 t) and the NPR <1 which indicating that the Folldal mine tailings have a potential to produce acid.

The pH values in the leachate samples from humidity cell (small column) test varied from pH 3 to 8. The sulphate production rate in nearly all the leachate samples of the topsoil from the Folldal mining area was >10mg/kg/week, even after 20 weeks of rinsing/leaching, indicating that the tailing material on the surface will release acid over a long time.

Inverse geochemical modelling indicated that dissolution of pyrite, chalcopyrite, schwertmannite and sphalerite accounted for the high concentrations of sulphate, Cu and Zn observed in the study area. However the geochemical model for kinetic oxidation rate of pyrite, did not describe the observed large column test data sufficiently, probably because the PHREEQC model does not take dissolution of ultra-fine particles into account, as well as the impact of microbial activity.

Acknowledgements

I would like to thank my main supervisor Gudny Okkenhaug for giving me the chance to do my master thesis on such an interesting project and for her support and feedbacks during the whole time. I would like thank to my co-advisor Gijs Breedveld for helpful resources and comments. Special thanks should go to Åsgeir Almås for helping during field work and samples digestion. Furthermore I would like to thank you Irene, Valentina Zivanovic, Oddny Gimmingsrud for their help with analyzing the samples in the laboratory at the University of Norwegian Life Science (NMBU).

I would also like to thank Per Aagaard and Helge Hellevang for their comments and help on PHREEQC modelling. Last but not least, I would like to thank my wife Hamelmal Asfaw, my family and friends for understanding and encourage me.

Contents

1 Introduction

Investigation of the potentially acidic environment from leaching of sulphide ore mining and evaluation of various mitigation options are hot issues and quite challenging scientific problems. Tailings and waste rocks are the two most common mining wastes (Hudson-Edwards et al., 2011; Lindsay et al., 2015; Parbhakar-Fox and Lottermoser, 2015; Sutthirat, 2011). The tailings are mine dumps produced during mineral extraction and processing when the ores are crashed and milled. Whereas the waste rocks are generated during excavation and mining of the ores (Holmstrom, 2000). Frequently, huge amounts of sulphides minerals like pyrite, pyrrhotite and other ore minerals are present in these mine wastes (Hudson-Edwards et al., 2011). Usually waste rock piles and mill tailings from the mining, which contain sulphide minerals can be significant sources of acid mine drainage (AMD) (Molson et al., 2005, 2004). The mining of certain minerals, such as gold, copper, zinc and nickel, is commonly connected with AMD problems that can have serious human health and ecological destruction (Akcil and Koldas, 2006). AMD is formed when sulphide-bearing ores exposed to oxygen and water. For instance, oxidation of pyrite or pyrrhotite often produce AMD (Molson et al., 2004) which is characterized by a low-pH (< 4) in the drainage water, and high concentrations of sulphate (SO_4^{2-}), aluminium (Al), iron (Fe) and other toxic elements (Akcil and Koldas, 2006; Bussière, 2007; Dold, 2014; Molson et al., 2004; Sracek et al., 2004). The presence of high concentrations of trace element in the AMD affected areas (concentrations might be 1000 s of times higher compare to unaffected sites) and the corrosive nature of the acidic water unable to support many forms of aquatic life (Holmstrom, 2000; Kim and Chon, 2001).

This master thesis is focusing on acid generating tailings from the Folldal mining area. The study area was intensively mined for copper, sulphur and zinc for about 200 years from 1747 to 1968. Although the mining activity was responsible for growth of the economy of the area, the area has faced huge environmental problems due to the high copper concentrations in AMD. The Folldal mine tailings have been oxidized due to extended exposure to air and water. As a result local river and pore water are strongly contaminated by AMD. The consequence of the AMD generated from Folldal mine is clearly observable at the local river called Folla river. The numbers of fishes in the river, around the tailings (where the tributary run through the mine

tailing areas before joining the Folla river) are drastically decreased. In order to diminish the environmental problems on the area and to limit the generation of AMD, the Norwegian Environmental Agency has asked for reduction of copper discharge into water resources.

Several research works have been done in the Folldal mining area. For example, Norwegian Geotechnical Institute (NGI), has carried out various investigations in Folldal mining area and suggested several mediation techniques (NGI, 2014). These remediation methods recommended by NGI include dilution/neutralization of mine water with alkaline water from the nearby river (Klimpel, 2017) and cover the reactive mine and mining tailings areas (Tvedten, 2016). However, almost all the research activities carried out in this area was used static tests (based on total soil concentrations) only to evaluate/ quantify the acid mine drainage formation. There is an information gap on the kinetic tests to study the evolution of acid mine drainage (AMD) from reactive mine tailings. Therefore, this research work has compiled results from static tests, kinetic tests and geochemical simulations to evaluate acid generating potential of the Folldal mine tailings.

Static tests, which evaluate the balance between the acid-generating potential and acid-neutralizing potential for a given mine tailings are characterized by a wide uncertainty zone in which it is impossible to accurately predict the acid-producing potential (AP) (Bouzahzah et al., 2014; Cruz et al., 2001). Static tests are conducted at a given point in time, and do not account for the rate and evolution of the observed reactions rates (Adam et al., 1997). Subsequently, to better understand long-term AP, kinetic tests are commonly performed to provide more information about the reaction rates of the acid-generating and acid-neutralizing minerals.

The main aims of this research work are to predict acid producing capacity of Folldal mine tailings by using static and kinetic tests and to develop models to quantify leachates composition. Failure to accurately predict AMD leads to long-term impacts on ecosystems and human health, in addition to substantial financial consequences and reputational damage to operators (Parbhakar-Fox and Lottermoser, 2015). To achieve these objectives soil samples and leachate samples from humidity cell (small column tests) and large column test were analysed. Geochemical simulation model (PHREEQC code) was used to better understand of the complex reactions taking place within the Folldal mining activities and to predict future leaching.

Using geochemical modelling to investigate the acid mine drainage is quite common in the last decades. For instance, in the Adak mine tailings deposit in Sweden, an exhaustive environmental evaluation of the trace elements distribution in soil, sediments, plants and water was performed based on field data analysis and geochemical modelling with PHREEQC (Bhattacharya et al., 2006).

The specific objectives of this thesis work can be summarized as:

1) To examine the geochemical characteristics of Folldal topsoil influenced by mine tailings
2) To investigate how well the static test can predict the acid producing capacity of the tailings compared to the kinetic tests.
3) To develop a model for quantifying leachate composition in the study area, including inverse models and kinetic model by using the analyses results from large column test and soil geochemistry.

2 Folldal mining area

2.1 Overview

Folldal is located along the north western border of Hedmark county, in central Norway, 410 km North of Oslo, the capital city of Norway (Fig 2.1). The Folldal village settled at the foot of Rondeslottet and Snøhetta mountains. The study area is located at altitude of roughly 700 meters above sea level. Copper and sulphur mining was the main activity in Folldal area from 1748 to 1968.

Currently Folldal Mines, mining area and facilities (buildings, machinery and equipment), is a national technical-industrial cultural monument site and is protected by the Cultural Heritage Law, which does not allow alteration of the historical materials, structures and landscape. The area is one of the tourist attraction areas in Norway. The main attractions at Folldal Mines are old building from mining community, museum/ exhibition, Stoll 1, a mine dating back to the 1700s, and 600 metres train trip inside the mountain to Worms Hall (Folldal Gruver, 2018).

The climate of the area is distinguished by long and cold winters and short and relatively hot summers. This region is one of the most arid and temperate parts of Norway (Aanes, 1980) with average annual precipitation of 360 mm and annual mean temperature of 0.4 ^{o}C. The area receives the heaviest rainfall during the summer season (Fig 2.2).

Folla river is the largest river in the study area and the 3rd largest tributary of Glomma river which is the largest river in Norway (Aanes, 1980). The composition of the river has changed considerable by discharge of high concentration of sulphate, copper and trace elements from the mine tailings (Fig 2.3).

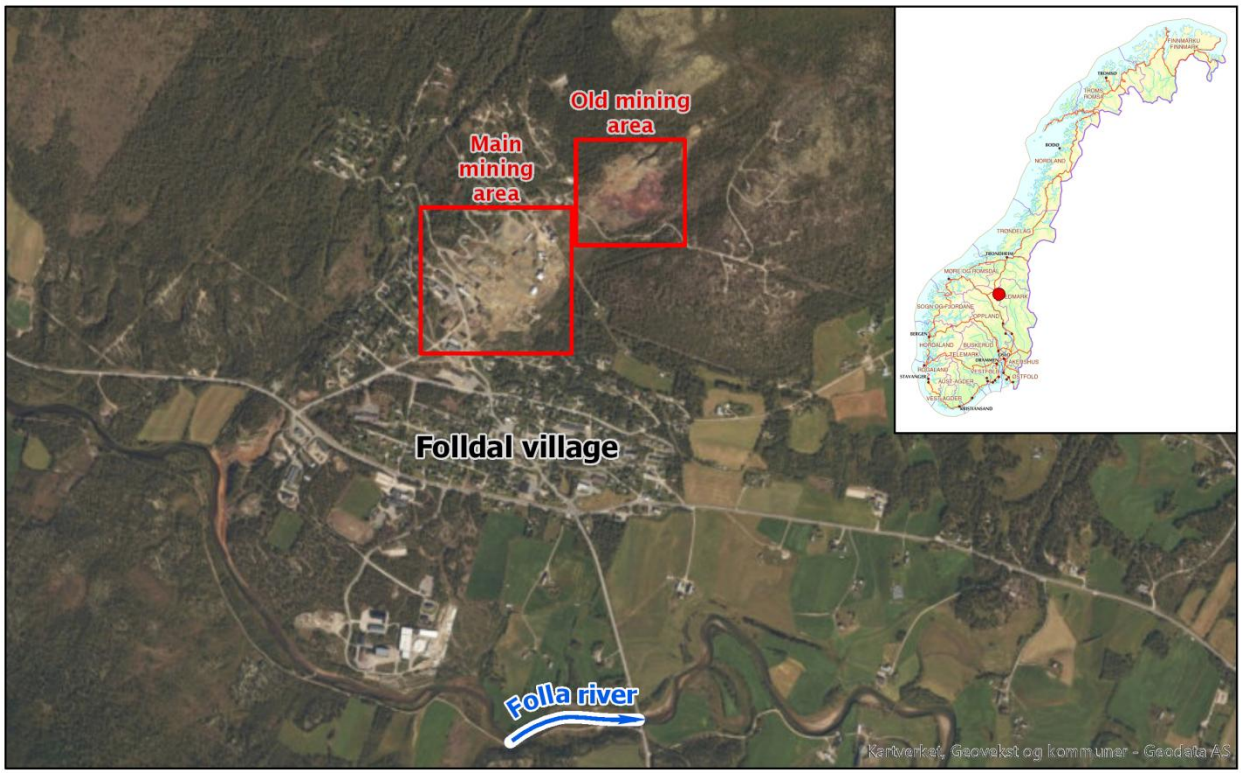

Fig 2.1 Location map of the study area, the blue arrow indicate direction of flow of Folla river (Modified from Kartverket, 2005).

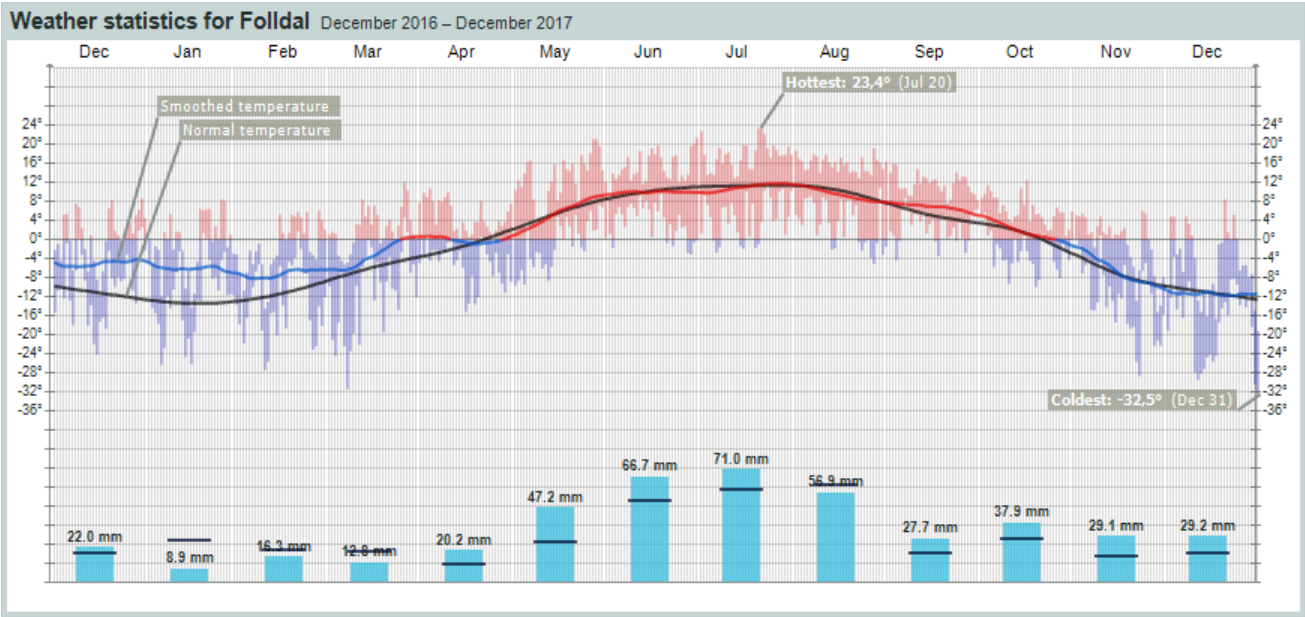

Fig 2.2 Annual weather statistics of Folldal area, the black lines show mean values, the red/blue line shows average temperature during the day (24 hr) (equalized for 30 days). The red/blue

areas show the temperature variations throughout the day (24 hr) with max- and min. The light blues bars show total precipitation this month, the black lines crossing are the normal (mean) value for precipitation.

Fig 2.3 The discharge of Acid mine drainage from Folldal mining tailings to Folla river

2.2 Geological setting

In Folldal area there are very large deposits of fluvio-glacial materials left from the last glacial period (Aanes, 1980). According to Bjerkgard and Bjorlykke (1994) there are five stratabound massive sulphide deposits of the volcanogenic massive type (VMS) situated at three different stratigraphic levels within the Fundsjø Group. The material transported and deposited by glaciers is poorly sorted, hard packed and varies in grain size from clay and fine sand to blocks. The fluvial material is sorted and rounded, composed of sand and gravel and some layers of organic material. The Fundsjø Group, a lithology belonging to the Upper Allochton of the Trondheim

region, consists in its lower part of metabasalts and gabbros while the upper part consists of tuffic rocks with intercalations of metasediment. A large subvolcanic trondhjemitic (tonalite) intrusion is present and the geochemistries of the volcanic rocks indicate an island arc setting (Bjerkgård and Bjørlykke, 1994b).

Lithologically, this region consist of Trondheim Nappe Complex (see Fig 2.4), the volcanogenic Fundsjø group, which consists of cambro-silurian sediment minerals of clay origin is overlaying the sedimentary Gula group (Aanes, 1980; Bjerkgård and Bjørlykke, 1996, 1994a, 1994b). The Gula group consists of psammitic-chlorite-mica schist, semipelites and quartzites that have intercalations of conglomerates and marbles. Thin layer of limestone sediment also occurs in this area (Aanes, 1980).

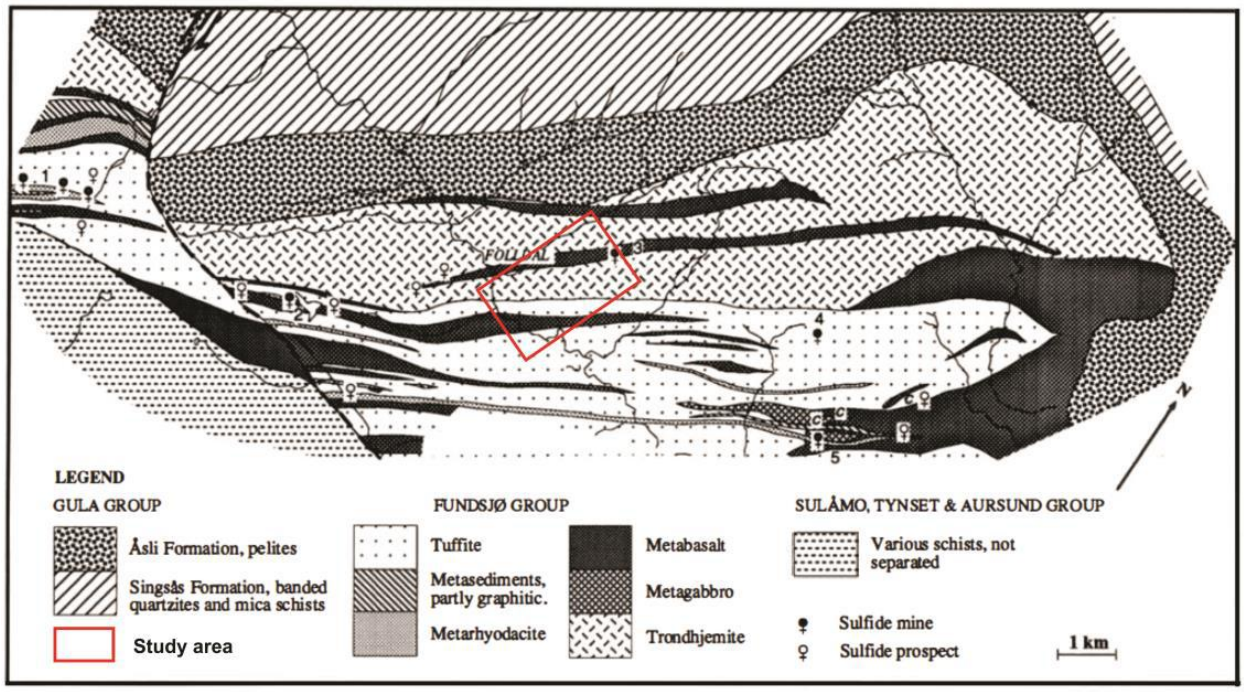

Fig 2.4 Geological map of Folldal area ((Modified from Bjerkgård and Bjørlykke, 1994a).

2.3 Mining history

In 1745 Ole Husum discovered ore in Folldal and three years later (1748) the mining was started. The first company started mining was called Fredrik Gaves Verk and mined copper, zinc and sulphur from 1748 to 1878 (Folldal Gruver, 2018). And then the mining activity was ceased until

Folldal Copper and Sulpher Co. Ltd mining company established in 1906. This mining company was active before it was closed down by 1941. However, small mining in and around Folldal was continued until 1968. From 1748 to 1968 a total of 4.45 million tons ore were extracted from Folldal mining area (Bjerkgård and Bjørlykke, 1996, 1994b, 1994a).

2.4 Mine tailings

Tailings are mixtures of crushed rock and processing fluids from mills, washeries, which are produced during mineral extraction and processing (Hudson-Edwards et al., 2001; Kossoff et al., 2014). Waste rock is produced during excavation and mining of the ore. These kinds of wastes often contain large amounts of different sulphides, such as pyrite (FeS_2), pyrrhotite ($Fe_{1-x}S$ where x can be a value between 0 and 0.2) and other ore minerals. Such waste, exposed to weathering, is a source of acid mine drainage.

The ratio of tailings to ore (concentrate) is commonly very high, generally around 200:1 (Kossoff et al., 2014). The main mine located in central Folldal consisted of 14 different levels, where the deepest level reached down to a total depth of 700 meters. From the opening in 1748 until it was close down in 1941, 1.5 billion tons of ore with 1.9% Cu and 1.1% Zn were extracted by underground mining (Geological Survey of Norway, 2014).

Waste materials (tailings and waste rocks) from Folldal were disposed of in different areas from north of the old mine and towards the river Folla (Fig 2.1). Previous investigations and measurements by (NGI, 2014) have shown that there are four main sources of pollution of Folla river, that is drainage from the mine and four landfills: sludge pool area (A), industrial area (C), main depot (S) and old mine/tailings (N) (Fig 2.5). NGI (2014) also mapped the thickness of the tailing impoundments (Fig 2.6).

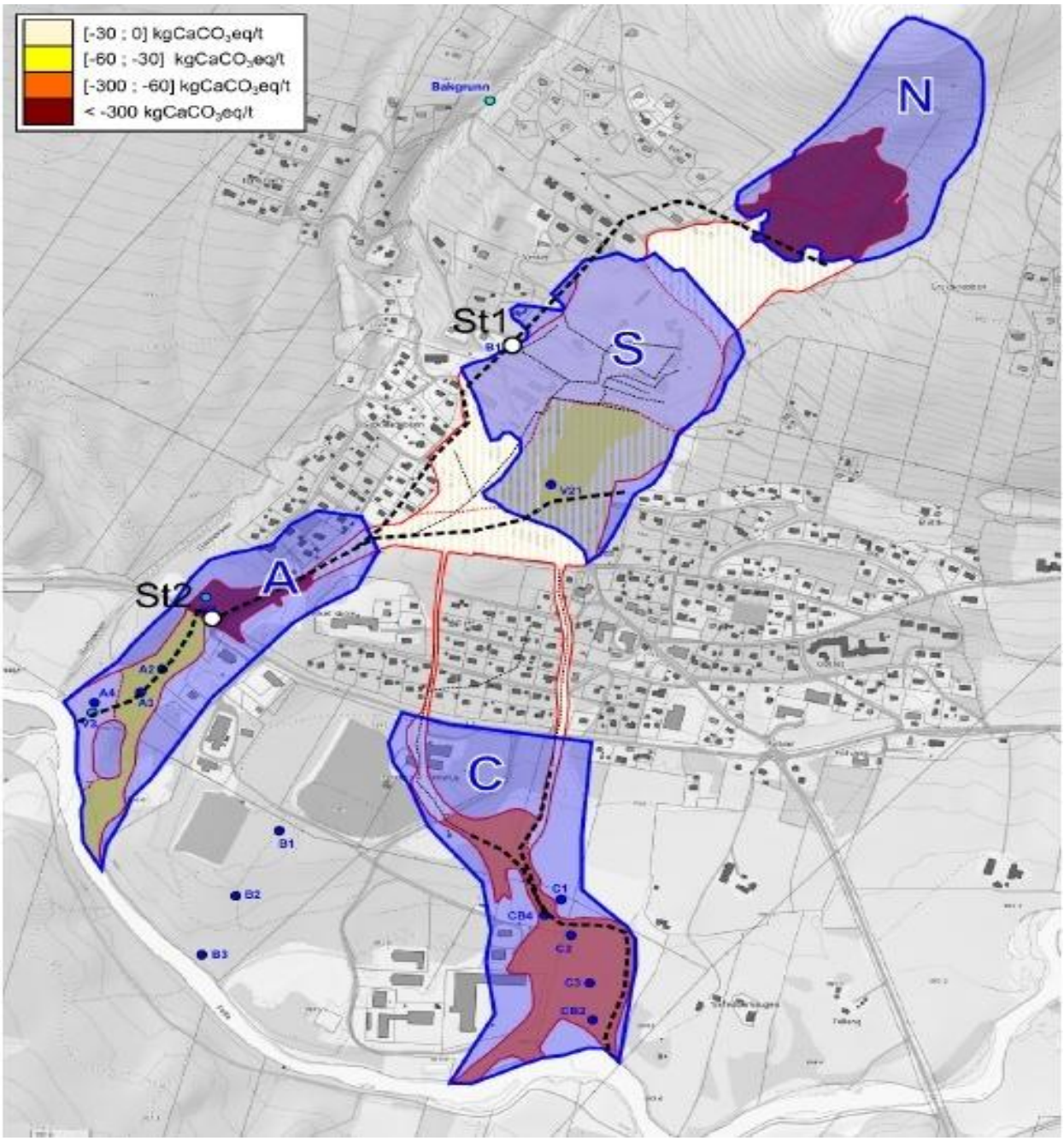

Fig 2.5 The tailings area and sources of Cu contamination in Folldal mining. The shaded and labelled polygon representing: sludge pool area (A), industrial area (C), main depot (S) and old tailings (N) (from NGI, 2014).

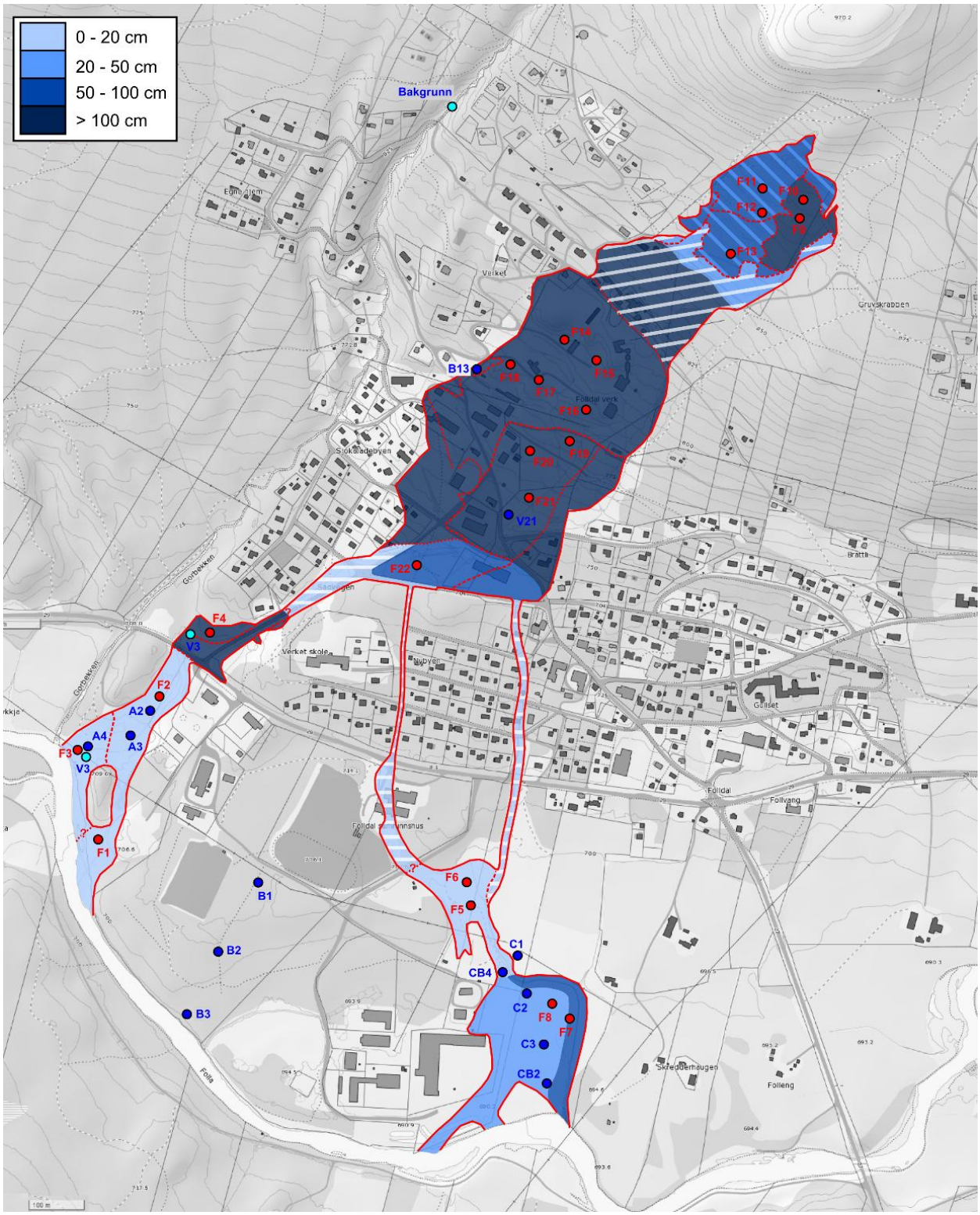

Fig 2.6 The thickness of mine tailings in Folldal. The lightest blue areas represents 0-20 cm, and the darkest blue represents a thickness >100 cm. Map from (NGI, 2014).

Fig 2.7 indicated that the area is severely affected by the acid generating from the mine tailings. Since the pH of the soil of reactive tailings is quite low the plants cannot tolerate in this area.

Fig 2.7 The acid mine drainage discharging to Folla river (A) and bird eye view of Folldal Main mine area: production buildings and workers cottages (B) (Folldal Gruver, 2015).

3 Acid Mine Drainage (AMD)

Acid mine drainage (AMD) is strongly acidic water, generally containing high concentrations of metals, sulphides, and salts and if it is left untreated, it can contaminate ground and surface water, damaging the health of plants, humans, wildlife, and aquatic species (Georgopoulou et al., 1996; MacIngova and Luptakova, 2012). Even though the chemistry of AMD generation is straightforward, the final product is a function of the geology of the mining site, the availability of water and oxygen, the presence of microorganisms and temperature of the area (CSIR, 2009). Because of these factors are extremely variable from place to place, the prediction, prevention and treatment of AMD need carefully and site specific investigation. AMD is produced when sulphide-bearing material is exposed to oxygen and water (Akcil and Koldas, 2006). Even though the process occurs naturally, mining activity promote AMD formation by increasing the quantity of sulphides exposed. Oxidation of sulphide mineral ores is identified as the main source of AMD (Kefeni et al., 2017).

Among the metal sulphides ores, pyrite ore (FeS_2) is one of the key mineral responsible for generation of AMD due to its ease of oxidation when exposed to oxygen and water (Blodau, 2006; Chen et al., 2014; Hansen, 2015; Plante et al., 2012). Therefore the process of AMD production is well exemplified by considering the reactions during the oxidation of pyrite (FeS_2) and the equations of the chemical reactions can be found in various papers (Akcil and Koldas, 2006; Banks et al., 1997; Blodau, 2006; Chen et al., 2014; Kefeni et al., 2017; Ruihua et al., 2011; Simate and Ndlovu, 2014).

The first important reaction is the oxidation of pyrite by oxygen and water, which releases ferrous iron (dissolved iron), sulphate and protons into solution.

$$FeS_2 + 7/2\ O_2(g) + H_2O \rightarrow Fe^{2+} + 2SO_4^{2-} + 2H^+ \qquad (3.1)$$

The formation of the dissolved Fe^{2+}, SO_4^{2-} and H^+ in Equation 3.1 shows an increase in the total dissolved solids and acidity of the water.

If there is sufficient oxidizing agent available in the surrounding environment, much of the ferrous iron will oxidize to ferric iron, according to the following reaction (Akcil and Koldas, 2006):

$$Fe^{2+} + 1/4O_2 + H^+ \rightarrow Fe^{3+} + 1/2H_2O \quad (3.2)$$

At the pH range between 2.3 and 3.5, ferric iron precipitates as $Fe(OH)_3$ and to a lesser degree as jarosite ($KFe_3^{3+}(OH)_6(SO_4)_2$), leaving little Fe^{3+} in solution and also decreasing pH:

$$Fe^{3+} + 3H_2O \rightarrow Fe(OH)_{3\ solid} + 3H^+ \quad (3.3)$$

Some Fe^{3+} formed from Equation (3.2) and that does not precipitate from Equation (3.3) may be used to oxidize the pyrite additionally (indirect oxidation) and form new Fe^{2+}, SO_4^{2-} and H^+, according to the following:

$$FeS_2 + 14Fe^{3+} + 8H_2O \rightarrow 15Fe^{2+} + 2SO_4^{2-} + 16\ H^+ \quad (3.4)$$

The equations 3.1 to 3.3 can be combined and simplified as:

$$FeS_2 + 15/4O_2 + 7/2H_2O \rightarrow Fe(OH)_3 + 2\ SO_4^{2-} + 4H^+ \quad (3.5)$$

Equation 3.5 indicates the overall reaction of pyrite oxidation with oxygen as major oxidant. The 1 mole of pyrite oxidation will release of 4 moles of protons, consequently decrease the pH and increase acidity into the environment.

The oxidation of other metal-sulphide minerals may be described by similar overall reactions. It should be noted that not all of the sulphides will generate acidity under natural conditions (e.g. galena (PbS), sphalerite (ZnS)).

Fig 3.1 shows summary of various the reactions take place during pyrite oxidation. Firstly, FeS_2 reacts with O_2 following Equation (3.1), either through a direct reaction ((a) in or through dissolution followed by oxidation (a'), but in both cases the rates remain low. Secondly, FeS_2 react with Fe^{3+} (Equation 3.4) and it is fast and yields a low pH (Fig 3.1(c)). The produced Fe^{2+}

by reaction 3.1 and/or 3.4 might be oxidized by O_2 to Fe^{3+} (Equation 3.2, Fig 3.1(b)). However, only at low pH Fe^{3+} remain in solution since it otherwise precipitates as $Fe(OH)_3$ (Equation 3.3, Fig 3.1(d)).

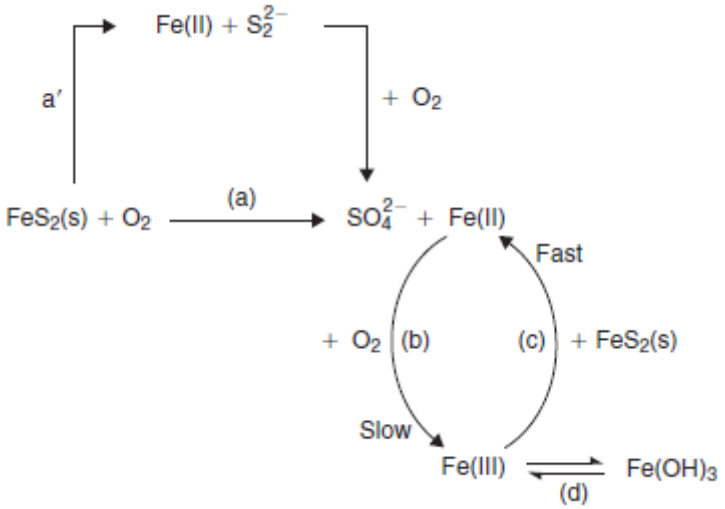

Fig 3.1 Reaction pathways in the pyrite oxidation (Stumm and Morgan, 1996).

Not only chemical, but also biological and physical factors are important for determining the rate of acid generation (Akcil and Koldas, 2006). For example physical factors like waste rock and/or tailings permeability, are particularly important. The tailings with high permeability have a higher diffusion rate of oxygen, which contributes to higher chemical reaction rates. This leads to increase temperatures and consequently increased oxygen entrance through convection. On the other hand bacteria have a major role in the oxidation process of sulphide minerals by accelerate the reaction rates (Skousen et al., 1998). Acidithiobacillus ferroxidans bacteria, anaerobic autotroph bacterium is one of the most common bacteria that has a capability to oxidize pyrite and uses the reactions as an energy supply (Akcil and Koldas, 2006). The environmental conditions must be favourable for ferroxidans bacteria and it is most active in water with a pH of less than 3.2.

Due to low pH, high concentrations of potentially toxic dissolved metals, metalloids and sulphate, AMD causes a severe pollution problem to current and future generations (Akcil and Koldas, 2006; Chen et al., 2014; Hansen, 2015; Kefeni et al., 2017; Morin and Hutt, 2001;

Simate and Ndlovu, 2014; Sracek et al., 2004). Dissolved iron (Fe^{2+}) is one the most abundant and common in majority AMD. It reacts with dissolved oxygen to produce iron oxide precipitates Equation (3.2), which is commonly called "yellow boy," and can stifle life all along the way by embedding on stream or ocean beds. Thus, small aquatic life that feeds from the bottom of the ocean or streams can be severely affected and may finally die out (Hansen, 2015). The impact does not end with only small aquatic life; it has also a negative impact on the food chain.

Moreover, formation of $Fe(OH)_3$ precipitate, intensifies the condition by lowering the pH and damage most of the microorganism existing in the water (Agrawal and Sahu, 2009). Because of the corrosive nature, AMD interacts with rocks and soils that containing different types of mineral ore and easily aggravating the solubility of toxic metals. Therefore, the formed AMD water elevates the level of dissolved metals in the receiving water resources and strongly influences the aquatic organisms.

4 Methodologies and Procedures

In order to investigate the formation of acid mining drainage and build models to simulate the kinetic reactions and leachate composition of Folldal mine tailings, detail hydrogeochemical analysis were required. As a results samples were collected from the study area (Fig 2.1) and prepared in a very carefully manners.

4.1 Field work

A total of 19 top layer (<15 cm depth) soil samples were collected from the Folldal mining area in June 2017 (Table 4.1). The samples were collected from the four sub-areas (See section 2.4 and Fig 2.5). Soil sample F1 - F3 were collected from the old mine area (N); soil samples F4- F9 from main depot area (S); sample F10- 14 from sludge pool area (A) and F15- F17 from industrial area (C) (Figs 2.5 and 4.1). In addition two soil samples (F18 and F19) were collected from the other side (south) of the Folla river (Fig 4.1), by assuming the impact of mining is less at these sites and to use as background. The samples were collected in small plastic bags (polyethylene) and transported to Soil Science Laboratory of Norwegian University of Life Science (NMBU). The soil samples were stored in the cold room (4 ^{o}C) until further analyses were carried out.

Table 4.1: Summary of field work

Samp-le	Depth (cm)*	Vegetation covers	Remarks
F1	3-5	Short brush trees, some of dwarf bottlebrush plants	
F2	5-7	Dense vegetation of dwarf bottlebrush	
F3	7-10	Scarcely vegetation cover	
F4	4-6	5-7 m long trees	
F5	7- 10	No vegetation, but there are some roots in the soil	
F6	6- 10	Very few vegetation cover	
F7	4-8	Dense vegetation cover, up to 8 m tall	
F8	10-15	Scarcely vegetated	
F9	10-15	Grass and short plants	
F10	5-10	Young short trees	Near to stream discharging to Folla river
F11	5- 10	Dead plants	Reddish soil
F12	10-15	Dense forest	
F13	5- 10	Bare land	
F14	10- 15	Short trees(1-3 m)	Thick A-horizon
F15	6-8	Large trees (up to 15 m)	On the creek
F16	10-15	Bare land	
F17	8- 10	Short trees(3 -7 m)	Just above Folla river
F18	8-10	Relatively dense forests, up to 20-30 m tall	Background soil on the south east of Folla river
F19	10-15	Big trees, up to 20-40 m tall	Background soil on the south east of Folla river (Fig 4.1)

*Depth from where the samples collected

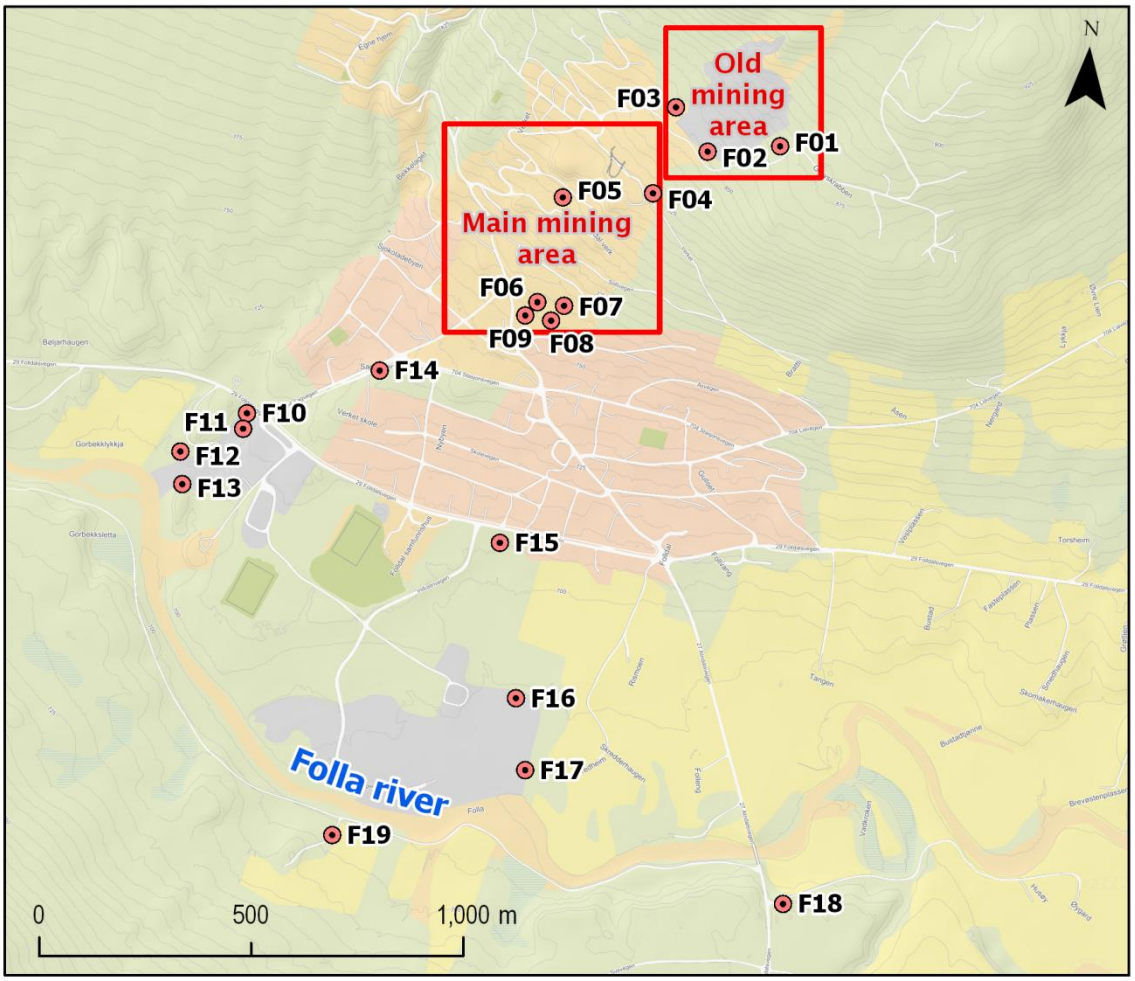

Fig 4.1 Soil samples location in Folldal mining, samples F18, F19 were collected south of Folla river. The circle and the rectangle mapped with red color were locations, where the reactive tailings and pre-oxidizing tailings were collected respectively.

4.2 Sample preparations and chemical analysis

4.2.1 Soil sample preparations and digestion

To prepare for further analyses the samples were dried at 40 ^{0}C for three days and then sieved on the 2 mm sieve size. The materials above 2 mm sieve (gravel, pebble, and plants root) were excluded.

Each sample was homogenised gently and then few grams of the samples were sampled for analysing total concentrations. The samples were grinded by Mortar Grinder, RM 200. About

0.2 g of the grinded samples were measured and transferred to beakers to digest with ultra pure nitric acid (UP-HNO_3). By digestion processes, the solid matrixes of the samples are completely decomposed and form solution, so that they introduced into determination step (Inductively Coupled Plasma Optical Emission Spectroscopy (ICP-OES)). Five millilitres (5 mL) of UP-HNO_3 were added on each sample and the samples were put in ultraclave. The ultraclave raises the pressure and temperature through microwave irradiation and increase the speed of thermal decomposition of the samples and solubility of elements in solution. ICP-OES analytical technique, an elemental analysis method that uses the emission spectra of a sample to identify and quantify the elements present was used for the detection of chemical elements including iron (Fe), sulphur (S), copper (Cu), aluminium (Al), zinc (Zn), calcium (Ca), magnesium (Mg), and sodium (Na).

4.2.2 Quality assessments of soil sample analysis

Limit of Detection (LOD), and Limit of Quantification (LOQ) of ICP-OES to analysis total soil concentration were given for each element (Table 4.2). The LOD and LOQ are terms used to describe the smallest concentration of a measurement that can be reliably measured by an analytical procedure. Three replicates of blanks were used to control the quality of measurements and concentrations of most of the element in the blanks were less than LOD (Table 4.2).

Three replicates of Standard Reference Material® 2709a (SRM 2709a), San Joaquin soil and certified/ reference values were used to check the accuracy of analytical method. The green shaded values of SRM 2709a indicated accurate methods of analysis with a stated 95% confidence level. The green shaded values showed that the measured values of SRM 2709a were within 95% confidence interval of reference/certified values. The yellow shaded values of SRM 2709a were indicate moderately accurate procedure of analysis (Table 4.2).

4.2.3 Total organic carbon (TOC) and total inorganic carbon (TIC)

Total organic carbon (TOC) and total carbon (TC) of the soil samples were anlysed at ALS Laboratory Group. Total carbon content was determined in dried sediments and total organic carbon was analysed in the dried and acidified samples using a LECO CR-412 Carbon Analyzer. The soil samples were combusted at 1.350 °C by using the LECO CR-412 and any carbon present converted to CO_2. The sample gas flows into a non-dispersive infrared (NDIR) detection

cell. A non-dispersive infrared (NDIR) detection cell measured the mass of CO_2 present in the sample. The mass of CO_2 was converted to percent carbon (%C) based on the dry sample weight. The total inorganic carbon (TIC) of the given sample was determined by subtracting the TOC from the TC.

Table 4.2: Standard reference materials and their certified values used to assess the quality of total soil concentration analyses

Quality assessment	Al (%)	Ca (%)	Cu (mg/kg)	Fe (%)	Mg (%)	S (mg/kg)	Zn (mg/kg)
LOD in (w/w)x1000	0.95	2.16	0.13	2.70	0.76	3.45	0.04
LOQ in (w/w)x1000	3.16	7.20	0.45	9.00	2.52	11.49	0.12
Blank	<LOD	<LOD	<LOD	<LOD	<LOD	<LOD	<0. 12
Blank	<LOD	<0,007	<LOD	<LOD	<LOD	<LOD	<0.12
Blank	<LOD	<LOD	<LOD	<LOD	<0,003	<LOD	<0.12
SRM 2709a	4.2	1.6	32	3.3	1.4	630	110
SRM 2709a	4.1	1.5	31	3.2	1.4	620	100
SRM 2709a	4.0	1.5	31	3.1	1.3	630	100
Reference Values *	7.37±16	1.91±0.09	33.9 ± 0.5	3.36±0.07	1.46±0.02		103 ± 4

* Reference Values (Dry-Mass Basis) for selected elements in SRM 2709a (See Table_A 2 andTable_A 3 in Appendix A).

4.3 Humidity cell test/ small column tests

For the environmental impact assessment various types of kinetic tests are often used to predict the longer-term weathering characteristics of a mine tailings (Holmstrom, 2000). Column test and humidity cell test are the two most common kinetic tests types (Bouzahzah et al., 2012; Frostad et al., 2002; Lapakko and White III, 2000; Sapsford et al., 2009).

Humidity cells testing is involving repetitive oxidation and leaching cycles on a sample (Holmstrom, 2000). From the 19 collected soil samples, 16 samples were selected and used to fill in the humidity cell tests. A total of 16 humidity cells/small column tests (30 cm in height, 1.8

cm internal diameter) were built at the NMBU laboratory (Fig 4.2). The small columns were filled with 25 g of tailings, and to avoid erosion about 5 g of plastic bubbles and 10 g of pure coarse quartz sand were used and filled above the soil samples (Fig 4.2). Milli-q water (50 ml) was added from top on each column once per week. The experiments were carried out for consecutive 20 weeks.

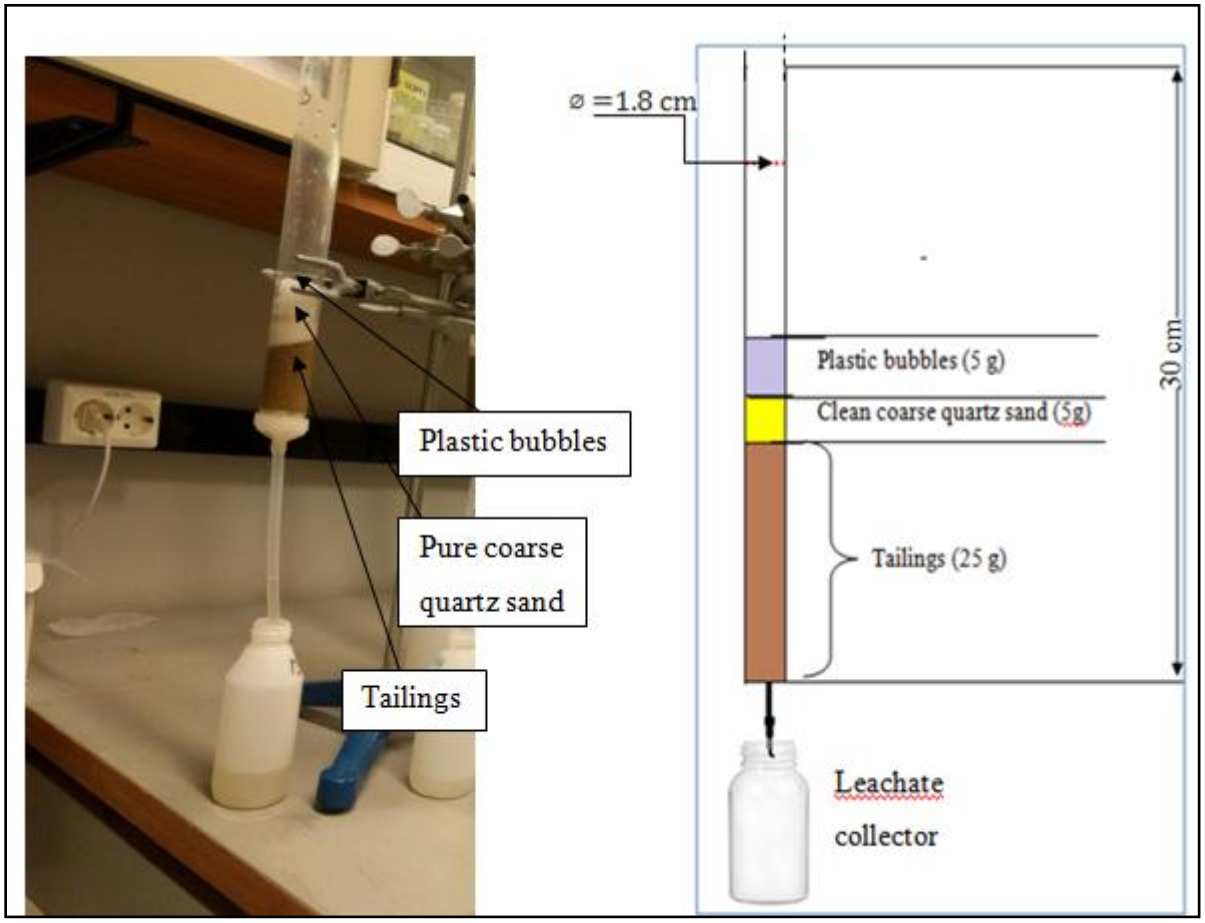

Fig 4.2 Setup of humidity cells (small column tests) at NMBU. The location and amount of filled materials is written on the left figure.

4.3.1 Leachate samples analysis

The leachates samples from the columns were collected in three different plastic tubes: (a) 10 ml for SO_4^{2-}, (b) 10 ml and for other elements (Al, Cu, Fe, Zn, and S) for inductive coupled plasma mass spectrometry (ICP-MS) analysis, and (c) about 10 ml for pH and electrical conductivity (EC) measurements. The ICP-MS combines a high temperature ICP (Inductive Coupled Plasma)

sources with a mass spectrometer (MS). The ICP source converts the atoms of the elements into ions and then the ions are separated and detected by the MS.

The pH values of the samples were measured shortly after sampling every week by PHM210 Standard pH meter. pH values 4 and 7 were used to calibrate the pH meter. Similarly, electrical conductivity (EC) of the leachate samples was measured by Metrohm-712 Conductometer every week, shortly after the leachate water comes out of the column tests.

The leachate samples for other elements analyses were filtered at 0.45 μm (Santorius Stedim millipore filters) and acidified to pH <2 with 10% of ultra pure nitric acid (UP-HNO_3). The acidified leachate samples were stored in refrigerator (a 4 ^oC) until the further geochemical analyses were carried out.

The collected water samples for sulphate analysis were neither filtered nor acidified. Ion chromatography (IC) was used to determine the sulphate concentrations in the leachates. From the measured sulphate concentrations, total sulphur concentrations in the soil samples were calculated by using 1/3 conversion factor (that is total sulphur ≈ measured sulphate concentration x 1/3). The conversion factor (1/3) is quotient of molecular weight of sulphur (32 kg/mol) to molecular weight of sulphate (96 kg/mol). The results of measured sulphur and the calculated sulphur were quite similar (Fig 5.1 and Table 5.3) for all samples in the first 4 weeks. Therefore, sulphate concentrations were not analyzed after the 4^{th} week.

4.3.2 Quality assessment for leachate samples analyses

The LOD and LOQ values measured by ICP-MS for the elements in leachate samples from both humidity cell/small column tests and large scale column tests are presented in Table 4.3. Similar to soil samples analyses, three blanks were used to calibrate the instrument used to analyses leachate samples. The concentration in the blank samples was less than LOD for most of the elements (Table 4.3).

1643H and ION-96.4 reference materials (the materials collected from mouth of Grand River in Southern Ontario during 2009) were used to determine the quality of analytical procedures (See Table_A 1 and Table_A 4 in Appendix A). The concentrations of all elements measured by ICP-MS/ ICP-OES from 1643H reference materials were within 95% confidence interval with the

references values of 1643H. That is why the value of the element in 1643H samples was shaded with green colour (Table 4.3).

Table 4.3: Standard reference materials and their certified values used to assess the quality of leachate samples analysis

Quality assessment	Al (µg/L	Ca (µg/L)	Cu (µg/L)	Fe µg/L)	Mg (µg/L)	S (µg/L)	Zn (µg/L)	SO_4^{2-} (µg/L)
LOD (w/w)	7.4	657.4	5.3	116.7	8.0	50.4	3.5	<LD
LOQ (w/w)	24.6	2191.3	17.7	389.0	26.8	167.9	11.7	<LD
Blank	<25	<LD	<LD	<LD	<LD	<LD	<LD	<LD
Blank	<25	<LD	<LD	0.07	<LD	<LD	<LD	<LD
Blank	<25	<LD	<LD	<LD	<LD	<LD	<LD	<LD
1643H	130	33000	22	99	8200	2600	82	
Certified values	141.8 ± 8.6	32300 ± 1100	22.76 ± 0.31	98.1 ± 1.4	8037 ± 98	2500	78.5 ± 2.2	
ION-96.4	<25	99000	<LD	19	26000	27000	<LD	81800
Certified values		95500 ± 7500			25500 ± 2100			76300 ± 4200

4.4 Large scale column test

In addition to humidity cell tests, the leachate samples collected from large column test (from June 2016 to October 2017) were analysed. Tvedten (2016) built four column tests in NGI to access the impact of cover material on AMD and to recommend better mitigation materials. The focus of Tvedten study was evaluating the performance of multilayered covers for limiting acid mine drainage from the Folldal mining area. In this thesis the leachates from one column filled with reactive tailings column (K3 in Tvedten thesis) were analysed and used in geochemical modelling and in predicting acid producing capacity of the tailings. The description the column used in this thesis is summarized in Table 4.4.

The column has 50 cm length and 15 cm internal diameter. The column test was carried out at NGI lab since May 2016 to assess the hydro-geochemical behaviour of tailings (Fig 4.3). The column was filled with 30 cm reactive tailings, from the Folldal mining area and contain 1.3-12.5% of sulphur concentration and coded as K3 (Tvedten, 2016). At the beginning of each wetting cycle, every month 1.5 L of distilled water was added at the top of the column (Tvedten, 2016). The amount of the water added to the column in every 30 days (1.5 L) corresponded to a mean of three months value of precipitation (85 mm) in Folldal area.

Fig 4.3 Picture of large columns: the left column is filled with reactive tailings (Source Tvedten, 2016)

The Leachate samples from the column were collected once a week and stored in cold room (4 ^{o}C) for further analysis. EC and pH were measured shortly after the samples were collected. For this thesis nine samples were selected and analysed from the collected leachate samples. Geochemical analyses were conducted for: S, Fe, Al, Ca, Mg, Na, Cu and Zn concentrations) (see Table 4.4 and Table _A 6 in Appendix D).

Table 4.4: Description and geochemical analysis of the soil sample that filled in the large column test (modified from Tvedten, 2016).

Length (cm)	Filled with	Reactive tailings chemistry							
50	30 cm of reactive tailings	Fe (mg/kg)	Al (mg/kg)	Ca (mg/kg)	Cu (mg/kg)	Zn (mg/kg)	S (mg/kg)	SO_4^{2-} (mg/kg)	TIC (%)
		147000	2070	401	3340	49	51400	42400	0.023

4.5 Acid Mine Drainage (AMD) Prediction Methods

The main purpose of mine tailing characterization is to determine the AMD potential for a site. Prediction of the AMD potential is an iterative process that is investigated during exploration, development, operation and closure of a mine site with prediction methods including the following assessments (CEN/TR, 2012a; Robertson and Kirsten, 1989):

• Previous work/mining in area

• Environmental and geological models

• Tests that determine metal leaching

• Static tests

• Kinetic tests in the laboratory or field

• Mathematical models

Of these methods, the static, kinetic predictive tests and geochemical models were used in this thesis. These methods are outlined below.

4.5.1 Static Methods

A static test is comparatively fast to perform and inexpensive, but gives only indicative information based on total composition of the mine tailing material. Static prediction methods measure the theoretical balance between acid potential (AP) and neutralizing potential (NP) components of the mine tailings. The first test to be widely employed was the acid base accounting (ABA) method by (Norsk Standard, 2011; Sobek et al., 1978).

The acid potential (AP) is calculated based on the sulphur content (either total or sulphide sulphur) (Morin and Hutt, 2001; Norsk Standard, 2011) as follows:

1) Expressed as H^+ content in mol/Kg (Equation 4.1).

$$AP = 0.625 * ws \quad (4.1)$$

where,

0.625 is the conversion factor (that is by taking into consideration of units and that 1 mol of sulphur in pyrite creates 2 moles of H^+)

ws is the sulphur (either total or sulphide sulphur) content as mass fraction in percent.

2) Expressed as carbonate equivalents ($CaCO_3$) in Kg/t (Equation 4.2)

$$AP = 31.25 * ws \quad (4.2)$$

where,

31.25 is the conversion factor (ratio of molecular masses of calcium carbonate (100 g/mol) and sulphur (32 g/mol)) and then multiplied by 10 to convert percent (parts per hundred) to parts per thousand.

In order to be able to calculate the final ABA, the neutralization potential (NP) of the waste material have to be determined. According to Dold (2017) only the carbonate neutralization potential (CNP) is considered for standard ABA calculation. Therefore quantification of carbonate concentration in the samples is recommended.

The total inorganic carbon (TIC) concentrations were assumed to be associated to the carbonate minerals like calcite or dolomite and are expressed as $CaCO_3$ (Dold, 2017). The carbonate quantification was expressed in t $CaCO_3$/1000 t (Equations 4.3 and 4.4) , in order to be able to calculate the final ABA with the AP Equation 4.5 (Sherlock, 1995).

$$NP \approx CNP = (\%CO_2 \text{ - inorganic}) \times 22.73 \text{ (t } CaCO_3/1000 \text{ t)} \quad (4.3)$$

where, 22.73 is the conversion factor (ratio of molecular mass of calcium carbonate (100 kg/mol) and carbon dioxide (44 kg/mol)) and then multiplied by 10 to convert percent to parts per thousand (t/ 1000 t).

or

$$NP \approx CNP = (\%C \text{ - inorganic}) \times 83.33 \text{ (t } CaCO_3/1000 \text{ t)} \quad (4.4)$$

where,

83.33 is the conversion factor (ratio of molecular masses of calcium carbonate (100 kg/mol) and carbon (12 kg/mol)) and then multiplied by 10 to convert percent to parts per thousand (t/ 1000 t).

Since TIC in the soil samples from Folldal mining area was given by % C, in this thesis Equation (4.4) was used to determine NP.

Although there are many different ways to present the ABA results, the most common are the net neutralization potential (NNP) and Neutralization Potential Ratio (NPR)

$$NNP = NP - AP \quad (4.5)$$

$$NPR = \frac{NP}{AP} \quad (4.6)$$

If the result of Equation (4.5) is negative, this means that the material will form AMD, as there is an excess of AP (sulphides= pyrite) in relation to the carbonate content. If the result is positive, there is enough NP (carbonates = calcite) to maintain the material neutral (Dold, 2017). If the result of Equation (4.6) is < 1, the mine tailings have a potential to produce AMD.

The standard ABA test assumes that:

• All the sulphur is in sulphate (SO_4^{2-})

• Pyrite (ferrous iron sulphide) completely oxidizes to sulphate and ferric iron

• Ferric iron precipitates as $Fe(OH)_3$

The static test in this thesis was calculated by using Equations 4.5 and 4.6.

However, the application of static tests alone may not be sufficient to determine the actual potential of the tailings to generate AMD. To better evaluating the AMD of the mine tailings, assembling static and kinetic tests are strongly recommended (Benzaazoua et al., 2001; Morin and Hutt, 2001).

4.5.2 Kinetic Methods

The static tests (Section 4.5.1) were discussed in order to predict if a sample has the potential to acidify the geochemical system or if it will maintain neutral or even go alkaline. On the other hand kinetic test is used to investigate in which time frame the acidity or neutrality of geochemical system will occur (Dold, 2017).

The kinetic test gives more detailed information on behaviour based on reaction rates under specified conditions. It is used to analyse the interpretation of the static test data; determine the long term rate of acid production and metal leaching (CEN/TR, 2012a).

The various laboratory and field techniques have been proposed to carry out kinetic methods (Coastech Research Inc., 1989) and include:

• Humidity Cells test

• Column test

• Lysimeter test

• Field test pad

The differences between these tests are based on the scale, duration, complexity, cost and data requirements. Humidity cell and column tests are the most commonly used methods to determine the rate of AMD formation and are used in this thesis. In these methods it is possible to measure metals and sulphate concentration, and pH of the leachates over time.

4.5.2.1 Sulphide oxidation rate - sulphate production rate

The mineral reaction rates are commonly given as the amount of mineral (moles) reacted per time unit and surface area (Nicholson and Scharer, 1994; Williamson and Rimstidt, 1994). The overall oxidation process of iron sulphides, represented by the most common sulphide mineral, pyrite is described by Equation 3.5 (see chapter 3).

The reaction rate might be affected by the secondary minerals formed and whether or not these secondary minerals are effectively washed out during the rinse cycles. If the effects of secondary minerals are ignored, the reacting minerals may become sum up which would lead to a reduction of the oxidation rate of sulphides and availability of the neutralising minerals (CEN/TR, 2012a).

The leachate collected represents the result of the reactions taking place within the material being tested: I.e. sulphide oxidation; mineral dissolution; silicate mineral weathering; and mineral precipitation (CEN/TR, 2012a, 2012b; Morin and Hutt, 2001; Nicholson and Scharer, 1994). The reaction rate of sulphide oxidation within the mixed mine tailings material in the columns can be calculated by assessing sulphate release rate (sulphate production rate, SPR). Morin and Hutt (2001) described rate of sulphide oxidation by sulphate production rate (Equation 4.7).

$$\text{SPR (mg. Kg}^{-1}\text{.wk}^{-1}\text{)} = \frac{Sulphate\ \ (mg/L) * Volume\ \ Leachate\ \ Collected\ \ (L)}{Sample\ \ weight\ (kg) * rinsing\ \ interval\ \ (week)} \qquad (4.7)$$

where

SPR is sulphate production rate in mg/kg per week (wk^{-1})

4.5.2.2 Leaching rates

The leaching rate (L_R) refers to the amount of element leached per mass and time unit. Morin and Hutt (2001) estimated the leaching rate by applying Equation 4.8.

$$L_R = \frac{C\ x\ V_r}{M_s\ x\ t_r} \qquad (4.8)$$

where, L_R is the leaching rate (mg/kg/wk), C is concentration (mg/L), V_r is rinse volume (L), M_s is sample weight (kg) and t_r is rinsing interval (week)

4.6 Geochemical simulations

The data obtained from the large column test were used to simulate the ongoing conditions of acid mine drainage in the study area. Hydrogeochemical and mass transport models were developed by PHREEQC code (Parkhurst and Appelo, 1999, 2013) with the standard set of thermodynamic data in the default phreeqc.dat database file.

PHREEQC is a computer program for simulating one-dimensional calculations of different chemical reactions and processes in water (Parkhurst and Appelo, 2013). The program has a capacity to model kinetic reactions and numerous authors used PHREEQC in geochemical transport modelling of AMD (Eary and Williamson, 2006; Holmstrom, 2000; Papassiopi et al., 2014; Salmon, 2003). The database contains the chemical definitions and constants needed to perform the kinetic calculations (Parkhurst and Appelo, 2013).

Two hydrogeochemical models were developed in this thesis to simulate (1) presence of reactant minerals and, (2) kinetic rate of pyrite oxidation. The analytical results obtained from the large column test were used in the models.

4.6.1 Inverse modelling code

The inverse modelling has mostly been used in investigating geochemical properties and mass transfer in water resources (Armienta et al., 2001; Belkhiri et al., 2012; Dai et al., 2006; Sharif et al., 2008) and evaluation of water quality changes in connection with mining activities (Desbarats et al., 2011; Namaghi and Li, 2016; Seal et al., 2008). It is programmed to determine the geochemical reactions going on from the compositional differences between two aqueous solutions (in initial and final solution). The inverse modelling was simulated to calculate the changes in the mineral phases when the infiltrating rainwater (initial solution) to change to the observed leachate water composition (final solution) (Parkhurst and Appelo, 2013). The program balances the concentration of the aqueous species from an initial solution and quantifies the mole transfers of the minerals and gases that yield to the composition of the second aqueous solution. The input data used in the inverse model in this thesis is given in Appendix E1.

4.6.1.1 Model setup

In the inverse modelling the two solutions and phases required were defined based on rainwater data from Appelo and Postma (2005) and leachate collected from the large column test (Table 4.5). The reacting phases involved in the formation of AMD in the mine tailings (Table 4.6),

were based on the pyrite oxidation reactions (see chapter 3) and the geological study of Folldal area (refer section 2.2). Mineral pyrite, O_2(g), pyrrhotite, K-mica, chlorite and halite phases were specified as dissolving species, while amorphous $Fe(OH)_3$ defined as precipitating phases. Gypsum, K-feldspar, schwertmannite, chalcopyrite, sphalerite, jarosite, and albite mineral phases were not assigned either dissolving or precipitation. Because these minerals can be present in the soil and may precipitate as secondary minerals. Presence of halite was assumed as possible fossil seawater in the glacial sediments (Bjerkgård and Bjørlykke, 1996, 1994a, 1994b). CO_2 and alkalinity were not considered in the model, no carbon or carbonates were detected in the soil sample used in large column test. The TIC content in soil sample from Folldal area that filled in large column was quite low (TIC 0.023%) (see Table 4.4).

Table 4.5: Compositions of the two solutions: initial (rainwater) and final (leachate composition from the large column) solutions used in the inverse model.

Parameters	Rainwater* (µmol/L)	Leachate composition (mg/L)
pH	5.6	1.9
T (^{0}C)	2.2	1
Na^+	10	9.7
Mg^{2+}	5	110
Al^{3+}		130
SO_4^{2-}	31.1	4200
K^+	5	1.7
Ca^{2+}	16	120
Mn^{2+}		2.9
Fe^{2+}		4100
Cu^{2+}		160
Zn^{2+}		3.9
Cl^-	11 charge**	5.2 ***
O_2 (g)	865	SI= -0.69****

Modified from Appelo and Postma (2005), ** a charge-balance equation is used the solution to adjust the activity of Cl to produce electroneutrality in the solution; * the result was taken from NGI (2014); ****SI= saturation index*

Table 4.6 Phases used in the inverse model

Dissolution	No restriction	Precipitation
O_2 (g) Pyrite [FeS_2] Pyrrhotite [FeS] K-mica [$KAl_3Si_3O_{10}(OH)_2$] Chlorite [$Mg_5Al_2Si_3O_{10}(OH)_8$] Halite [NaCl]	Gypsum [$CaSO_4 \cdot 2H_2O$] K-feldspar [$KAlSi_3O_8$] Schwertmannite [$Fe_8O_8(OH)_6SO_4$] Chalcopyrite [$FeCuS_2$] Sphalerite [ZnS] Jarosite [$KFe_3(SO_4)_2(OH_6$] Albite [$NaAlSi_3O_8$] Gibbsite [Al(OH)3]	Amorphous Ferric hydroxide [$Fe(OH)_3$]

4.6.2 Kinetic of pyrite oxidation

The kinetic model is used to simulate chemical reactions that do not attain equilibrium within the experimental or model time frames (Parkhurst and Appelo, 1999, 2013). A kinetic geochemical model was established to estimate the rate of iron released from the tailings and formation of AMD from pyrite oxidation. The kinetics PHREEQC code was used to simulate the kinetically controlled pyrite oxidation (formation of AMD). The input file in this thesis is given in Appendix E2.

4.6.2.1 Kinetics code

The kinetics keyword permits the user to specify rate expressions for modelling a kinetically controlled reaction of a solid or solute, such as pyrite. The aqueous oxidation of pyrite (FeS_2) involves different kinetic reactions and can be driven by molecular oxygen (O_2) or ferric iron (Fe^{3+}), depending on the pH and bacteria presence. The two pathways were described by Equations 3.4 and 3.5 in chapter 3.

The rate expressions of pyrite oxidation were defined according to following equations:

$$r = 10^{-8.19}\ m_{O_2}^{0.5}{}_{O2}\ m_{H^+}^{-0.11} \tag{4.9}$$

$$r = 6.3x10^{-4}\ m_{Fe^{3+}}^{0.92} \left(1 + {m_{Fe^{2+}}}/{10^{-6}}\right)^{-0.43} \tag{4.10}$$

$$r=1.9x10^{-6}\, m_{Fe^{3+}}^{0.28}\ \left(1+{}^{m_{Fe^{2+}}}/_{10^{-6}}\right)^{-0.52}\ m_{H^+}^{-0.3} \qquad (4.11)$$

where, r is rate of pyrite oxidation in (mol/m^2/s) and m is the concentration (molality). Equation (4.9) is oxidation by O_2 based on Williamson and Rimstidt (1994); Equations (4.10 and 4.11) is oxidation by Fe^{3+} when oxygen is present (4.10) and when oxygen is absent (4.11) (Appelo and Postma, 2005). All the rates given by Equations (4.9 - 4.11) must be multiplied with initial surface area (m^2) and concentration (g/L) of pyrite to obtain the reaction in mol/L/s.

The initial surface area of pyrite, A_0, was estimated from the following equation (Equation 4.11) for geometric surface area, assuming that the pyrite grains are cubic shape (Eary and Williamson, 2006).

$$A_0=\frac{2[(ab)+(bc)+(ac)]}{(\mathrm{abc})*\rho} \qquad (4.11)$$

where a, b and c are the dimensions of the particle and ρ is the density of pyrite. It was assumed a grain size of 0.01 μm, for aquifer sediment containing pyrite, and 5.01 g/cm^3 pyrite density (Appelo and Postma, 2005).

5 Results

5.1 Total soil concentration

The analytical results of total soil concentration show considerable variations between the samples location in the Folldal mining area (Table 5.1 and Table_A 5 in Appendix C). Aluminium (Al) concentration in the soil samples varied from 10 g/kg (F11) to 36 g/kg (F4). The minimum and maximum iron (Fe) concentration in the soil samples were 18 g/kg (F18) and 56 g/kg (F17) respectively. Total sulphur (S) concentration in the soil samples varied between 0.04 g/kg (F18) and 20 g/kg (F11). The lowest copper (Cu) and zinc (Zn) concentration were found in the background soil samples (F18 and F19), while the maximum concentrations were observed in F11 soil sample.

Although the minimum concentrations were measured in background soil samples, there were some indications which supported that the background soils were also affected by mining activities. Particularly, F19 were more influenced, mainly because it is closest to where a stream from the mine tailings joins the Folla river (Table 5.1 and Fig 4.1).

5.2 EC and pH of soil samples

The electrical conductivity (EC) and pH results of the soil samples showed substantial variations. The EC values varied approximately from 29 µs/cm to 2109 µs/cm (Table 5.1). The lowest and highest EC values were measured in sample F18 and F11 respectively. In comparison with the previous study from Folldal area (Klimpel, 2017; Rodés, 2014; Tvedten, 2016), EC values of the topsoil samples were significantly lower. This might be because these soil samples were collected from the top soil and probably the mobile/dissolved ions have partly been leached out to a lower horizon.

Table 5.1: Total element concentration, pH, EC and total organic and inorganic carbon concentration in the tailings samples from Folldal mining area.

Sample name	EC (µs/cm)	pH	Al (g/kg)	Cu (g/kg)	Fe (g/kg)	S (g/kg)	Zn (g/kg)	TOC (%TS)	TIC (%TS)
F1	181	3.8	28	0.10	53	0.93	0.07	0.83	0.01
F2	183	7.5	26	0.18	40	1.4	0.12	0.40	0.04
F3	236	3.8	19	0.09	43	2.3	0.04	0.63	<0.01
F4	89	7.2	36	0.12	46	0.52	0.15	0.34	<0.01
F5	154	3.8	28	0.12	52	0.83	0.08	0.34	<0.01
F6	318	5.9	17	0.28	27	1.3	0.11	0.83	0.04
F7	224	7.2	19	0.08	19	0.66	0.22	6.92	0.32
F8	128	7.2	20	0.10	23	0.48	0.32	3.73	0.04
F9	100	6.4	24	0.03	21	0.81	0.07	3.82	0.02
F10	196	7.6	19	0.08	27	0.68	0.12	0.81	0.15
F11	2109	7.6	10	1.10	55	20	2	0.17	1.48
F12	56	5.1	23	0.20	26	0.14	0.1	1.05	0.01
F13	179	4.3	22	0.12	41	1.20	0.09	0.17	<0.01
F14	32	4.9	24	0.04	24	0.05	0.06	0.17	0.11
F15	50	4.8	20	0.02	21	0.11	0.04	0.88	0.01
F16	66	6.8	19	0.02	19	0.23	0.06	0.42	0.01
F17	186	5.1	32	0.55	56	1.9	0.37	1.15	0.02
F18	29	5.0	17	0.01	18	0.04	0.03	0.66	0.01
F19	90	4.2	27	0.01	25	0.14	0.05	1.32	0.02

The pH values of the soil samples were in the range of 3.8 (F1, F3 and F5) to 7.6 (F10 and F11). Most of the samples had pH value less than 7. The lowest pH values were measured in the soil samples (F1, F3, and F5) that were collected from northern part of the study area, old mine/ tailing site (Figs 2.5 and 4.1). The highest pH values were observed in soil samples F10 and F11, from the sludge pool area (Table 5.1, Fig 2.5 and 4.1).

5.3 Total organic and inorganic carbon (TOC and TIC)

TOC and TIC results are given in percent of total soil (%TS). The TOC and TIC of the soil samples were quite low (less than 1% for most of the samples). TIC results were lower than TOC in all tailing samples, except in F11 (Table 5.1). The minimum and maximum TIC analyzed in the Folldal soil samples were about <0.01 %TS (F3- F5 and F13) and 1.5 %TS (F11) correspondingly. The lowest and highest TOC results were about and 0.2 and 6.9 %TC respectively. The minimum TOC values were obtained in the tailing samples, F11, F13, and F14 (collected from sludge pool area (see Table 5.1, Figs 2.5 and 4.1). The maximum TOC values were detected in the samples collected from main depot (S) area, in F7, F8 and F9 (Table 5.1, Figs 2.5 and 4.1).

5.4 Acid Potential (AP) and Neutralization Potential (NP)

The AP and NP of the mine tailings in the study area were estimated by applying the method described in section 4.5.1. The AP of the soil sample range from 0.2 t $CaCO_3$/1000 t (F14) to 62.5 t $CaCO_3$/1000 t (F11) (Table 5.2). The minimum and maximum NP of the samples were <0.17 t $CaCO_3$/1000 t (F3 - F5 and F13) and 25 t $CaCO_3$/1000 t (F11). Apart from soil samples F10 and F14, the net neutralization potential (NNP) of all the samples were negative (< 0), this means that the materials have a potential to produce AMD (Table 5.2). In addition neutralization potential ratio (NPR), the ratio of AP to NP in the majority of the samples were less than 1, which supported that the soil samples from Folldal mining area have a capacity to generate AMD (Table 5.2).

Table 5.2: The calculated results of Acid Potential (AP), Neutralization Potential (NP) and Net Neutralization Potential (NNP) and Neutralization Potential Ratio (NPR) in the soil samples by using static test method.

Sam-ple	TIC (%)	TIC (g/kg)	NP (t $CaCO_3$/1000 t)	S (g/kg)	AP (t $CaCO_3$/1000 t)	NNP (t $CaCO_3$/1000 t)	NPR (t $CaCO_3$/1000 t)
F1	0.01	0.12	0.2	0.93	2.91	-2.71	0.07
F2	0.04	0.41	0.68	1.4	4.38	-3.69	0.16
F3	<0.01	<0.1	<0.17	2.3	7.19	-7.02	<0.02
F4	<0.01	<0.1	<0.17	0.52	1.63	-1.46	<0.10
F5	<0.01	<0.1	<0.17	0.83	2.59	-2.42	<0.07
F6	0.04	0.41	0.68	1.3	4.06	-3.38	0.17
F7	0.32	3.24	5.4	0.66	2.06	3.34	2.62
F8	0.04	0.37	0.62	0.48	1.5	-0.88	0.41
F9	0.02	0.16	0.27	0.81	2.53	-2.26	0.11
F10	0.15	1.53	2.55	0.68	2.13	0.43	1.2
F11	1.48	14.8	24.67	20	62.5	-37.83	0.39
F12	0.01	0.12	0.2	0.14	0.44	-0.24	0.45
F13	<0.01	<0.1	<0.17	1.2	3.75	-3.58	<0.05
F14	0.11	1.11	1.85	0.05	0.16	1.69	11.56
F15	0.01	0.14	0.23	0.11	0.34	-0.11	0.68
F16	0.01	0.12	0.2	0.23	0.72	-0.52	0.28
F17	0.02	0.17	0.28	1.9	5.94	-5.65	0.05
F18	0.01	0.1	0.17	0.08	0.25	-0.14	0.68
F19	0.02	0.19	0.32	0.14	0.44	-0.12	0.73
K3*	0.02	0.23	1.92	51.4	160.63	-158.71	0.01

*Soil sample in the large column test

5.5 Leachate chemistry of humidity cell (small column tests)

Based on the activities onsite at the Folldal mining area, the study area is classified into 5 sub areas: 1, old tailing (N), 2) main depot (S), 3) sludge storage area (A), 4) industrial area (C) 5 background (B) modified from (NGI, 2014 , Fig 2.5). In total 16 small column tests were carried out (see section 4.3). Based on the NNP results (lowest NNP from each sub area) in the soil, 6 small column tests were selected. I.e., F1 and F3 (old tailing), F6 (main depot), F11 (sludge storage), F17 (industrial) and F18 (background) sub areas were selected. In the following, results from a selected number of columns from each area are presented (Figs 5.2- 5.7). All the results from the small column tests are given in Appendix B (Fig_As 1- 9). The graphs (Figs 5.2- 5.7) show the tot-S, Fe, Al, Cu and Zn concentrations, EC and pH of the leachate samples.

5.5.1 Sulphur -Sulphate mass release

The sulphur measured in the leachate samples was assumed that it was in the form of sulphate and released from sulphide minerals. In order to evidence this, both sulphate and sulphur concentrations in the samples were measured the first 4 weeks. The results showed that most of the tot-S measured in the leachate samples were in the form of SO_4^{2-} (Fig 5.1 and Table 5.3). The values of the calculated S were quite comparable with measured tot-S in the leachate samples.

The sulphur concentrations in the leachate samples decreased rapidly in the first 3-5 weeks in the all small columns, except F6 which first showed an increase after 1 week (Figs 5.2-5.7). The SO_4^{2-} in the leachate sample F1, F3, and F17 showed an increase after week 4 and then slightly decreased again (Figs 5.2, 5.3 and 5.6). The results of SO_4^{2-} in the leachate sample F6 elevated from week 1 (31000 µg/L) to week 3 (42000 µg/L) and then decreased quickly 1500 µg/L (week 10). In the last 10 weeks the concentrations of sulphur were almost constant (Fig 5.4). The SO_4^{2-} concentrations in leachate samples F11 were extremely high, varying from 62000 to 480000 µg/L (Fig 5.5). The highest SO_4^{2-} concentration was observed in the initial week, while the lowest concentration in the last leachate sample. Fig 5.5 shows rapid decrease SO_4^{2-} concentrations in the first 3 weeks and then slightly increase from week 3 to 5. In the remaining 15 weeks the concentrations of SO_4^{2-} decreased slightly. The SO_4^{2-} concentrations in F18 leachate samples showed rapid reduction the first 5 weeks and a slightly decrease in the remaining 15 weeks (Fig 5.7).

Table 5.3: Tot-S and SO_4^{2-} concentration in leachate water in the first four weeks and calculated tot-S from SO_4^{2-} analyses.

Sample code	Week	Tot-S (mg/L)	SO_4^{2-} (mg/L)	Calculated S (mg/L)
F1	1	17	53	17.8
F1	2	15	49	16
F1	3	9	31	10
F1	4	6	21	7
F3	1	45	151	50
F3	2	17	54	18
F3	3	9	33	11
F3	4	9	27	9.
F6	1	31	98	32.7
F6	2	42	136	45
F6	3	16	51	17
F6	4	7	24	8
F11	1	480	1680	560
F11	2	410	1460	486.7
F11	3	290	1410	470
F11	4	420	1340	446.7
F17	1	37	119	39.7
F17	2	30	103	347
F17	3	18	57	19
F17	4	15	47	15.7
F18	1	2	5.4	1.8
F18	2	1	2	0.7
F18	3	1	1.7	0.6
F18	4	1	2	0.7

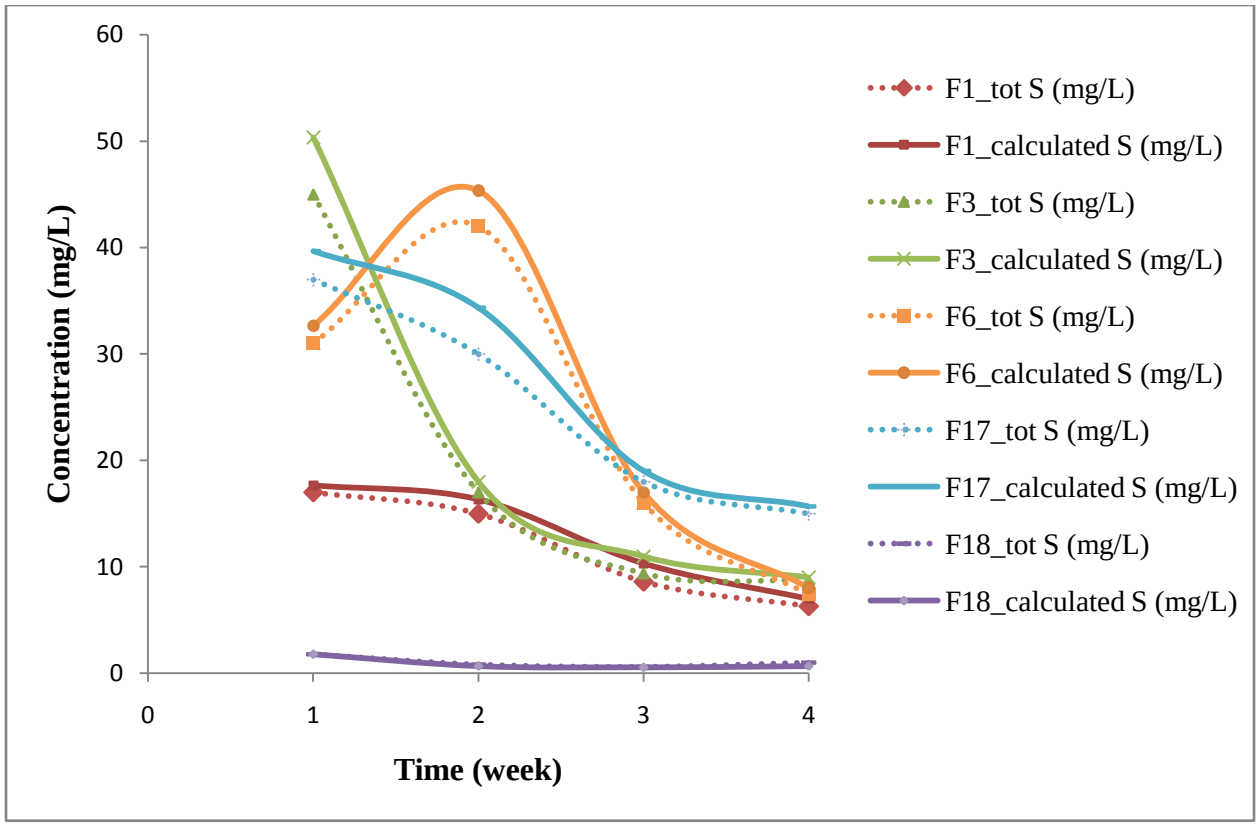

Fig 5.1 Scatter plot of measured total sulphur (S) and calculated sulphur from $SO4^{2-}$ concentrations of the leachate samples

5.5.2 EC and pH of leachate samples

Similar to the soil samples the EC and pH of the leachate samples varied considerable within the study area and also over time. Generally, for all columns, the EC of the leachate indicated a rapid decrease in the initial 5 weeks (Figs 5.2 - 5.7). However, from week 5 to 15, EC values of most of the leachates slightly decreased, and in the last 5 weeks were relatively constant (Figs 5.2 - 5.7). The EC trend followed the sulphate concentration trend within the time.

The pH in the leachate samples showed no general trend. The pH values of sample F1 (old mining area) slightly decreased from pH 4.2 (week 1) to 3.97 to (week 8) and then steadily increased to 4.10 (week 20) (Fig 5.2). Within the last 10 weeks the pH gradually increased.

The pH values of sample F3 (old mining area) from week 1 to 20 varied from 3.7 to 4.3, the maximum values were measured during weeks 4 and 5 (Fig 5.3). After week 5 pH values substantially decreased until week 20.

Column F6 (main depot area, see Figs 2.5 and 4.1) showed an increased pH values in the neutral area the first 3 weeks and generally decreased from week 3 (pH=7.4) to week 19 (pH=6.8) (Fig 5.4). At weeks 6 and 14 possible outliers are assumed. The pH versus time had similar trends as the sulphur concentrations versus time. Similar to pH, the sulphur concentrations of the leachate sample in F6 increased in the initial 3 weeks and then decreased gradually in the remaining experimental periods (see section 5.5.1).

The values of pH in leachate sample F11 (sludge pool area) were above pH 7 throughout the whole experiment (Fig 5.5). Although the highest sulphur concentration was detected in this sample, the neutral pH values obtained in the leachate samples of this column might be because the acid generating due to pyrite oxidation was buffered by carbonate minerals exposed at this site. This is supported by the elevated TIC and NP values observed in the soil sample F11 (Table 5.2). Even though there were some variations in the pH values in the leachate samples of F11, the values increased generally from week 1 to 16. After the week 16, the pH values started decreasing slowly (Fig 5.5).

The pH results from the leachate sample 17 (industrial area) increased rapidly from week 1 to week 3 and decreased gradually in the remaining weeks (Fig 5.6). The observation at week 16 and 19 assumed to be outliers. In general the pH results of this leachate samples were in the range of 6 and 7.

The pH results measured in the leachate sample of F18 (background) within 20 weeks varied from 5.4 to 6.7 thus slightly acidic to neutral (Fig 5.7). The pH values slowly decreased from week 1 to week 8 and then starting to increase slowly from week 9.

5.5.3 Iron and Aluminium concentration

Fe and Al concentrations in most of the leachate samples decreased rapidly in the first few weeks (Figs 5.2 -5.7). However, there is a large variation in concentration levels between the columns. In column F1, the concentrations of Fe and Al increased from week 4 to week 7. The

concentrations of these elements in the last 13 weeks slowly decrease (Fig 5.2). The minimum and maximum Fe concentration measured from this column was 1000 µg/l (at week 4) and 8300 µg/l (week 7) respectively.

Although soil samples F1 and F3 were collected near to each other, in the old mining area (N), the concentrations of Fe in column F3 (20 µg/L - 1600 µg/L) were significantly lower than column F1 (1000 µg/L -8300 µg/L) (see Figs 5.2 and 5.3). Al concentrations in F3 increased substantially from week 5 and maximum value was obtained in the leachate sample of week 20 (Fig 5.3). Increased Al concentration in this column is most likely due to pH decrease. Fe concentrations this column was rapidly decreasing after week 1 and approximately constant until week 15, when the values started increasing slowly.

The Fe concentrations in column F6 were below detect limit (0) in the initial 5 weeks and increased to 10 µg/l from week 6 to week 20 (Fig 5.4). This might be because of the secondary minerals that containing Fe was dissolved and increase Fe concentration in the solution. On the other hand maximum Al concentration (40 µg/l) was measured in the first week leachate sample. The value of Al concentration decreased considerable in week 2 sample and then roughly constant in the remaining weeks (Fig 5.4).

The concentration values of Fe in leachate samples from the F11 soil sample were low (less than limit of detection) in the almost entire weeks (Fig 5.5). However, there is an indication of increase of Fe concentration after 20 weeks of rinsing. It is difficult to interpreted because it might be outlier or from pyrite oxidation. The Al results showed gradually increase from week 1 to 20. The Fe and Al concentration obtained in F18 were greater than in the F17 (Figs 5.6 and 5.7). Relatively the leachate sample from soil sample F18 had high Fe and Al concentration than some soil samples collected from A and C areas.

5.5.4 Copper and Zinc concentration

Similar to the other parameters, Cu and Zn concentrations also showed a rapid reduction in the first few weeks and then a gradually decrease. The Cu and Zn concentrations versus time show a similar trend in column F1, F6, F11 and F17 (Figs 5.2, 5.4 -5.6). The Cu and Zn concentrations in F1 varied from 19 to 210 µg/L and 7.3 to 140 µg/L respectively (Fig 5.2). The Cu concentrations in F3 increased rapidly after 3 weeks of rinsing (from 40 µg/L to 240 µg/L) and

strongly correlated with Al concentration (Fig 5.3). The Zn concentration in this column gradually decreased from 40 (week 1) to 8 (week 19). The Cu and Zn concentrations in F6 considerable decreased in the first week and stayed mostly constant after week 3 (Fig 5.4). The concentrations of Cu and Zn in F11 decrease gradually from 40 µg/L to 1.3 µg/L and from 30 to 2.4 µg/L respectively (Fig 5.5). The Cu and Zn concentration in F17 were > through the experiments (Fig 5.6). Cu and Zn concentrations in F18 varied in between 20 µg/L and 3.3 µg/L and 40 µg/L and 4 µg/L correspondingly (Fig 5.7).

F1

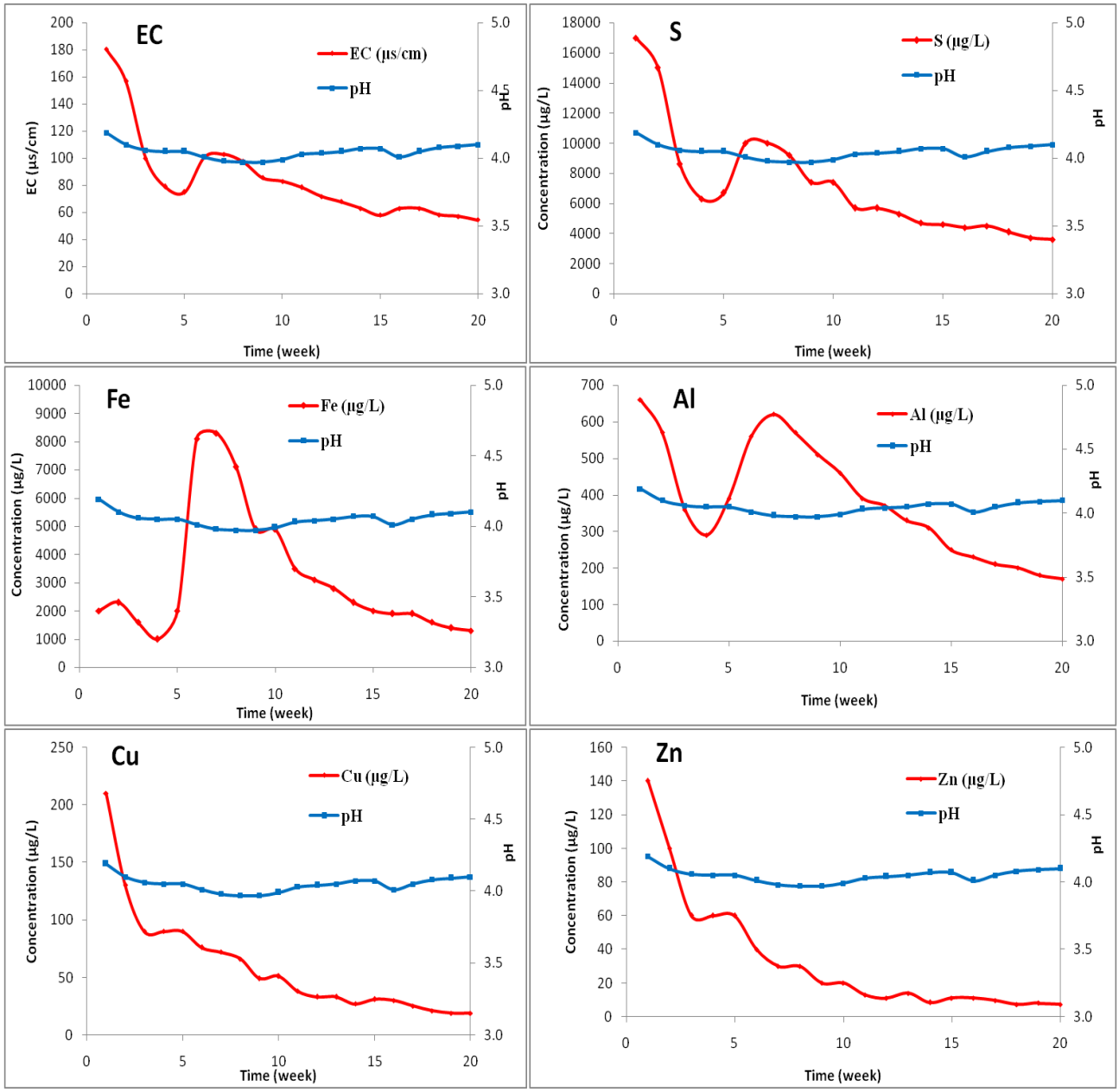

Fig 5.2 EC, pH, sulphate, iron, aluminium, copper and zinc vs. Time of leachate sample from F1 soil sample in N sub-area. The pH is shown in all diagrams to make a comparison better

F3

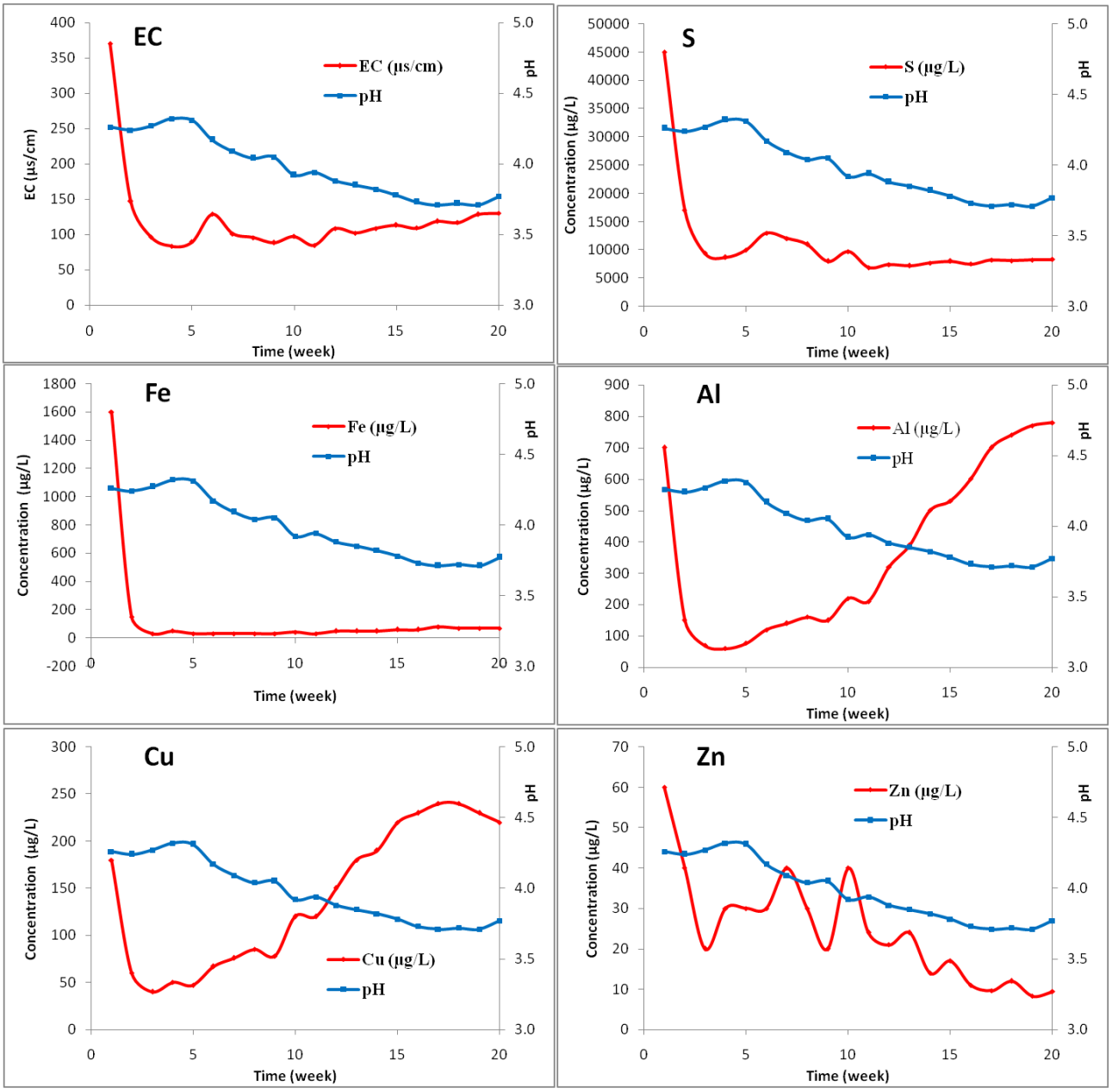

Fig 5.3 EC, pH, sulphate, iron, aluminium, copper and zinc vs. Time of leachate sample from F3 soil sample in N sub-area.

F6

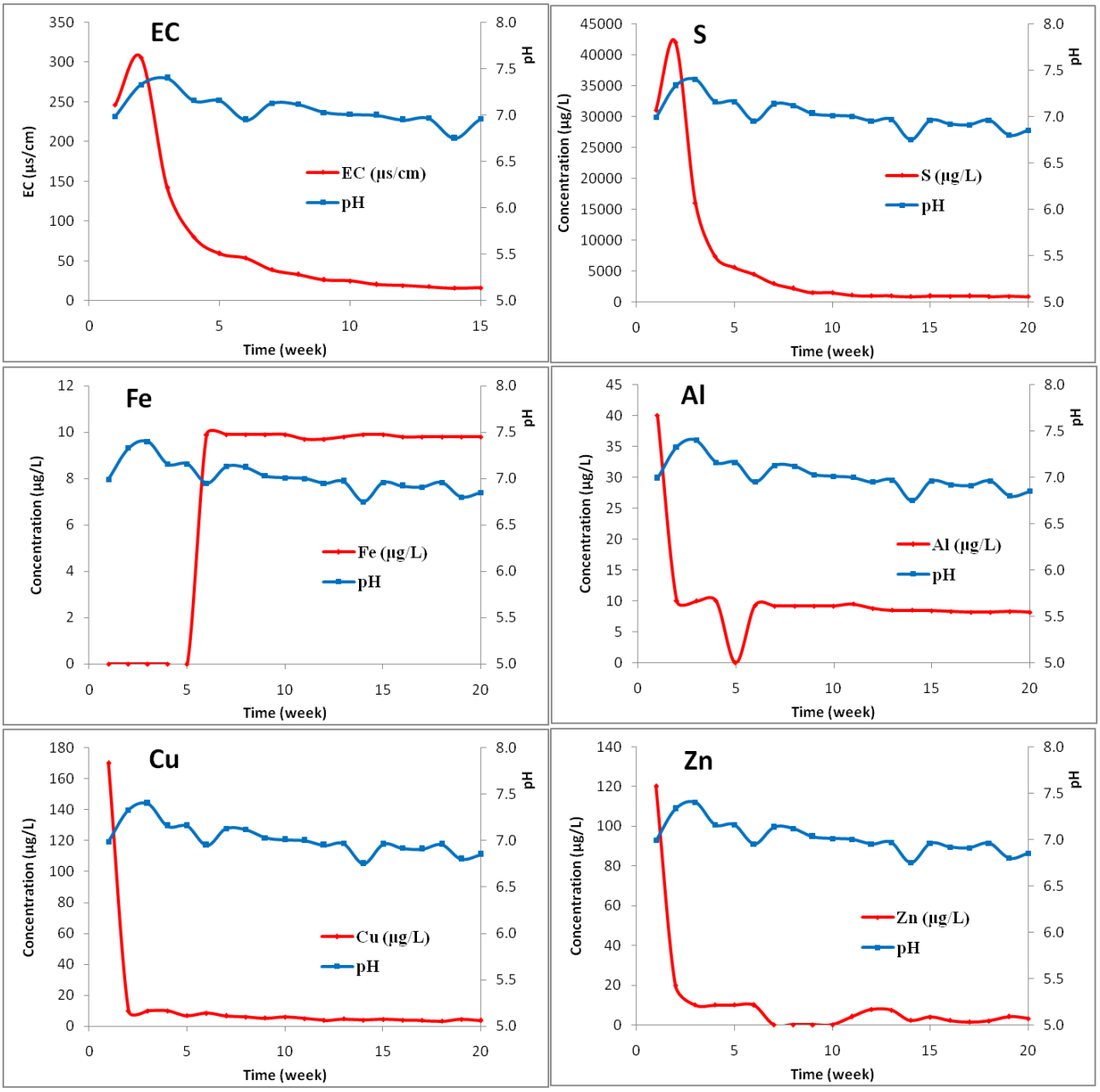

Fig 5.4 EC, pH, sulphate, iron, aluminium, copper and zinc vs. Time of leachate sample from F6 tailing sample in S sub-area.

F11

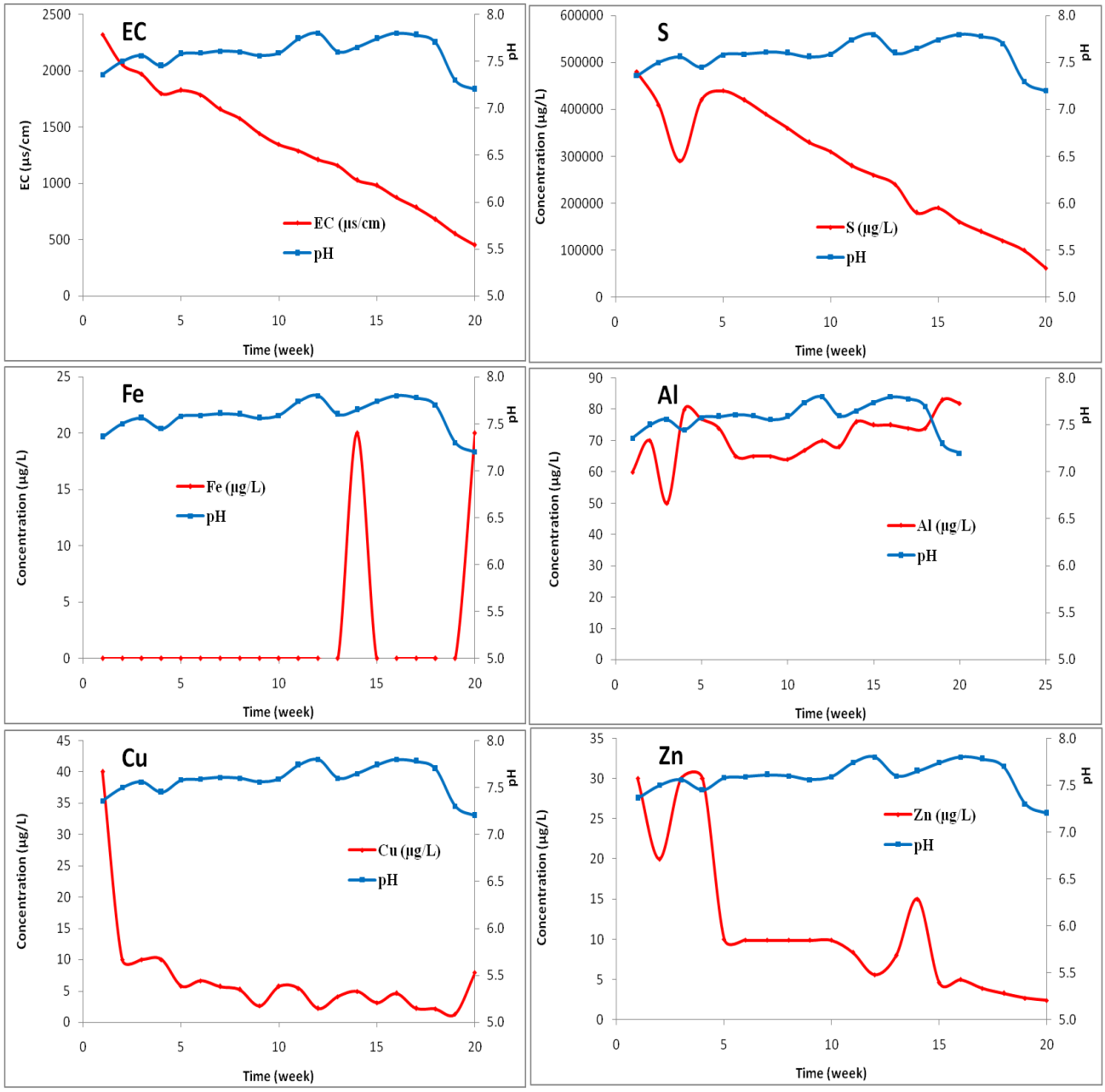

Fig 5.5 EC, pH, sulphate, iron, aluminium, copper and zinc vs. Time of leachate sample from F11 tailing sample in A sub-area.

F17

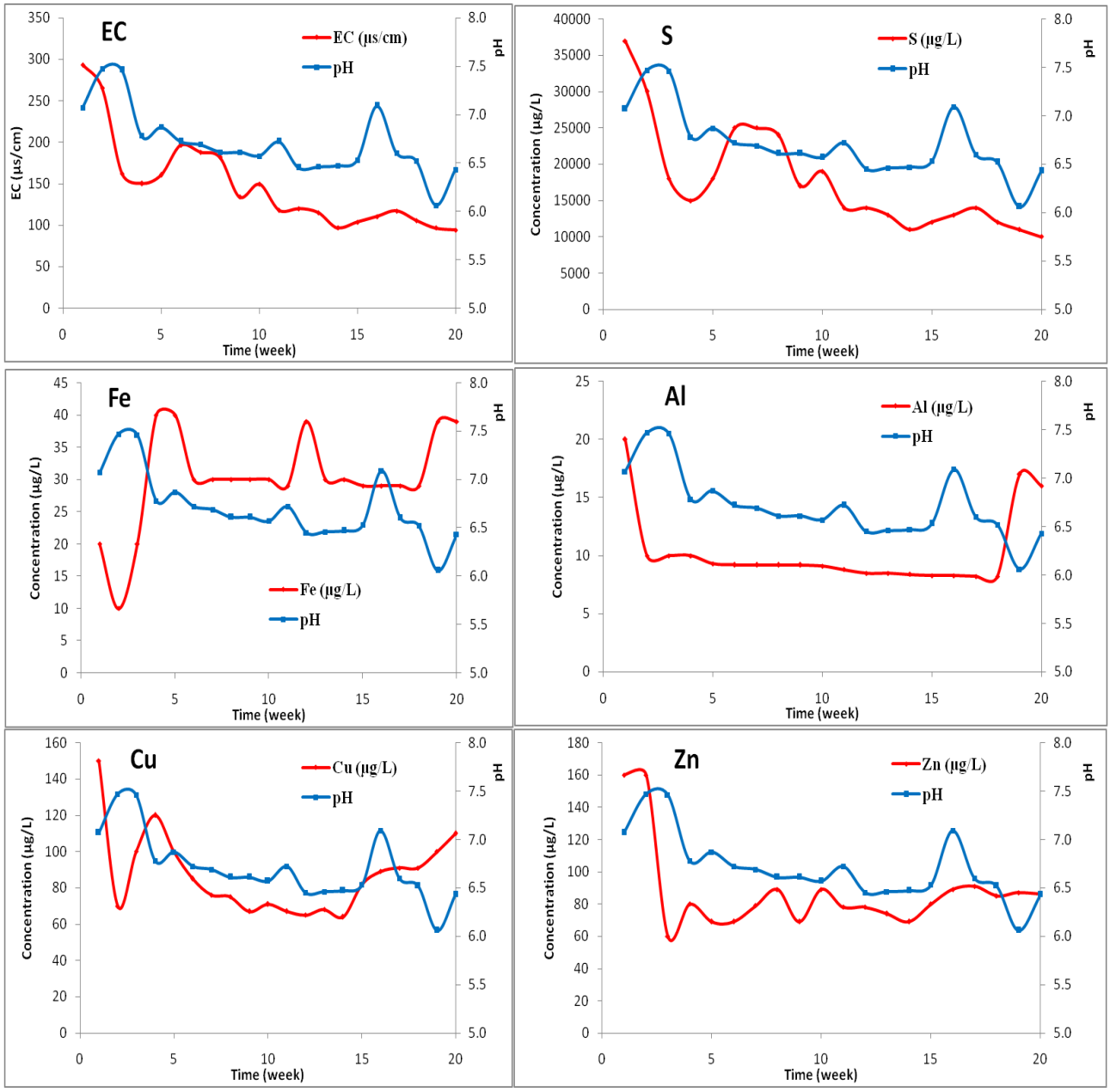

Fig 5.6 EC, pH, sulphate, iron, aluminium, copper and zinc vs. Time of leachate sample from F17 soil sample in C sub-area.

F18

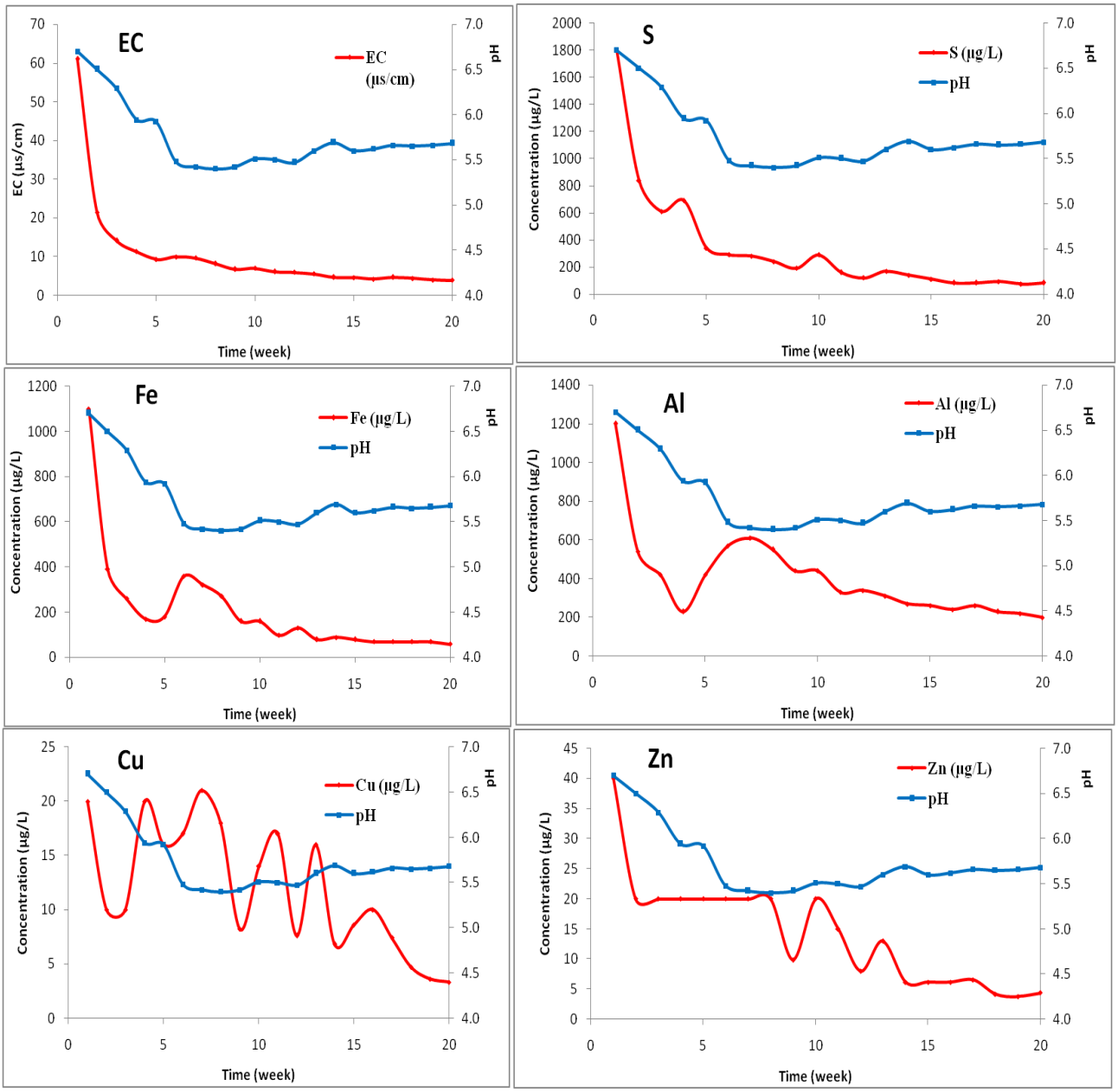

Fig 5.7 EC, pH, sulphate, iron, aluminium, copper and zinc vs. Time of leachate sample from F18 soil sample in B sub-area

5.6 Sulphate production rate

Since most of the tot-S measured in the leachate samples were in the form of SO_4^{2-} (see section 5.5.1), the sulphide oxidation rate of the samples were determined by calculating sulphate production rate by using Equation 4.7. The sulphate production rates calculated based on the leachate samples, show considerable variations between samples and over time (Table 5.4). The maximum sulphate production rates were observed in leachate sample F11 which also had the highest tot-S concentration. The minimum sulphate production rate values were observed in the background sample, F18 (Table 5.4).

In general, the sulphate production rates in all selected small columns decreased with time. For example, the SO_4^{2-} production rates decreased from 34 mg/kg/wk to 7.2 mg/kg/wk in F1; from 90 mg/kg/wk to 16 mg/kg/wk in F3, from 84 to 1.7 mg/kg/wk in F6 and from 652800 mg/kg/wk to 17856 mg/kg/wk in F11. After 20 weeks of leaching, there were noticeable high SO_4^{2-} production rates in most of the samples (>7 mg/kg/wk) (Table 5.4).

5.7 Cu and Zn leaching rate

Similar to sulphate production rates, maximum Cu and Zn leaching rates were observed in the initial weeks in all the samples except F3 (Table 5.5). Cu and Zn leaching rate in F1 had a similar trend and decreased gradually from week 1 to 20. The Cu leaching rates in F3 showed a sharp decrease in the first 3 weeks and increased steadily from week 3 to 18. The Cu leaching rates decreased in the remaining weeks (Table 5.5). In samples F6 and F11, the Cu and Zn leaching rate rapidly decreased in the first 3-5 weeks and stayed constant in the remaining experimental periods. The Cu and Zn leaching rates in F17 elevated after 15 days of rinsing. The Cu and Zn leaching rate in F18 had no general trend (Table 5.5).

Table 5.4: Sulphate production rate in Humidity Cell tests in seven selected soil samples from Folldal mining site

Time	F1	F3	F6	F11	F17	F18
Week	SO_4^{2-} (mg/kg/wk)	SO_4^{2-} (mg/kg/wk)	SO_4^{2-} (mg/kg/wk)	SO_4^{2-} (mg/kg/wk)	SO_4^{2-} (mg/kg/wk)	SO_4^{2-} (mg/kg/wk)
1	34.0	90.0	62.0	652800	74	3.60
2	30.0	34.0	84.0	492000	60	1.68
3	17.2	18.8	32.0	199520	36	1.22
4	12.6	17.4	14.8	211680	30	1.38
5	13.4	20.0	11.2	235840	36	0.68
6	20.0	26.0	9.0	336000	50	0.58
7	20.0	24.0	6.0	312000	50	0.56
8	18.4	22.0	4.4	264960	48	0.48
9	14.8	16.0	3.0	195360	34	0.38
10	14.8	19.4	3.0	183520	38	0.58
11	11.4	13.8	2.2	127680	28	0.32
12	11.4	14.8	2.0	118560	28	0.24
13	10.6	14.4	2.0	101760	26	0.34
14	9.4	15.4	1.7	67680	22	0.28
15	9.2	16.0	1.9	69920	24	0.22
16	8.8	15.0	1.8	56320	26	0.17
17	9.0	16.4	1.9	50400	28	0.17
18	8.2	16.2	1.8	39360	24	0.18
19	7.4	16.4	1.8	29600	22	0.15
20	7.2	16.6	1.7	17856	20	0.17

Table 5.5: Cu and Zn leaching rate (µg/kg/wk) in Humidity Cell tests in seven selected soil samples from Folldal mining site

Time	F1		F3		F6		F11		F17		F18	
Week	Cu	Zn	Cu	Zn	Cu	Zn	Cu	Zn	Cu	Zn	Cu	Zn
1	420	280	360	120	340.0	240	672	336	300	320	40	80
2	260	200	120	80	20.0	40	104	160	140	320	20	40
3	180	120	80	40	20.0	20	72	144	200	120	20	40
4	180	120	100	60	20.0	20	72	144	240	160	40	40
5	180	120	94	60	13.4	20	42	48	200	138	32	40
6	152	80	134	60	16.6	20	40	32	170	138	34	40
7	144	60	152	80	13.2	0	33	24	152	158	42	40
8	132	60	170	60	12.0	0	28	24	150	178	36	40
9	98	40	156	40	10.4	0	10	16	134	138	16	20
10	102	40	240	80	11.6	0	23	16	142	178	28	40
11	76	26	240	48	10.0	8	16	9	134	156	34	30
12	66	22	300	42	7.6	16	6	5	130	156	15	16
13	66	28	360	48	9.4	15	11	9	136	148	32	26
14	54	17	380	28	7.8	5	11	10.	128	138	14	12
15	62	22	440	34	8.8	8	8	4	164	160	17	12
16	60	22	460	22	7.6	5	11	4	178	178	20	12
17	50	19	480	19	7.4	3	4	3	182	182	15	13
18	42	15	480	24	6.4	4	4	2	182	170	9	8
19	38	16	460	17	8.6	8	2	2	200	174	7	8
20	38	15	440	19	7.2	6	12	1	220	172	7	9

5.8 Leachate chemistry of the large column test

EC and pH of the leachate samples over 18 months are given in Fig 5.8. The results show low pH values, mainly < pH 2.2 together with high EC values (>8 ms/cm). Both EC and pH values were noticeably different from the EC and pH of leachate samples from the small column/humidity cell test, which had lower EC and higher pH in all small columns except F11 where a similar EC was observed but a much higher pH (> 7) (see section 5.5.2). This is most likely because the soil sample tested in the large column was taken from a deeper level (>1m) where the soil was not oxidised.

Sulphur and iron concentrations decreased rapidly in the first 4 months and then increased slowly from 6 to 14 months (Fig 5.8 B), most likely due to pyrite oxidation.

Aluminium, magnesium and copper concentrations in the leachate samples decreased rapidly in the initial 4 months and then increased in the remaining months (Fig 5.8 C). Zinc, manganese and potassium results were also decreased in the first few months and then approximately constant throughout the remaining months (Fig 5.8 D).

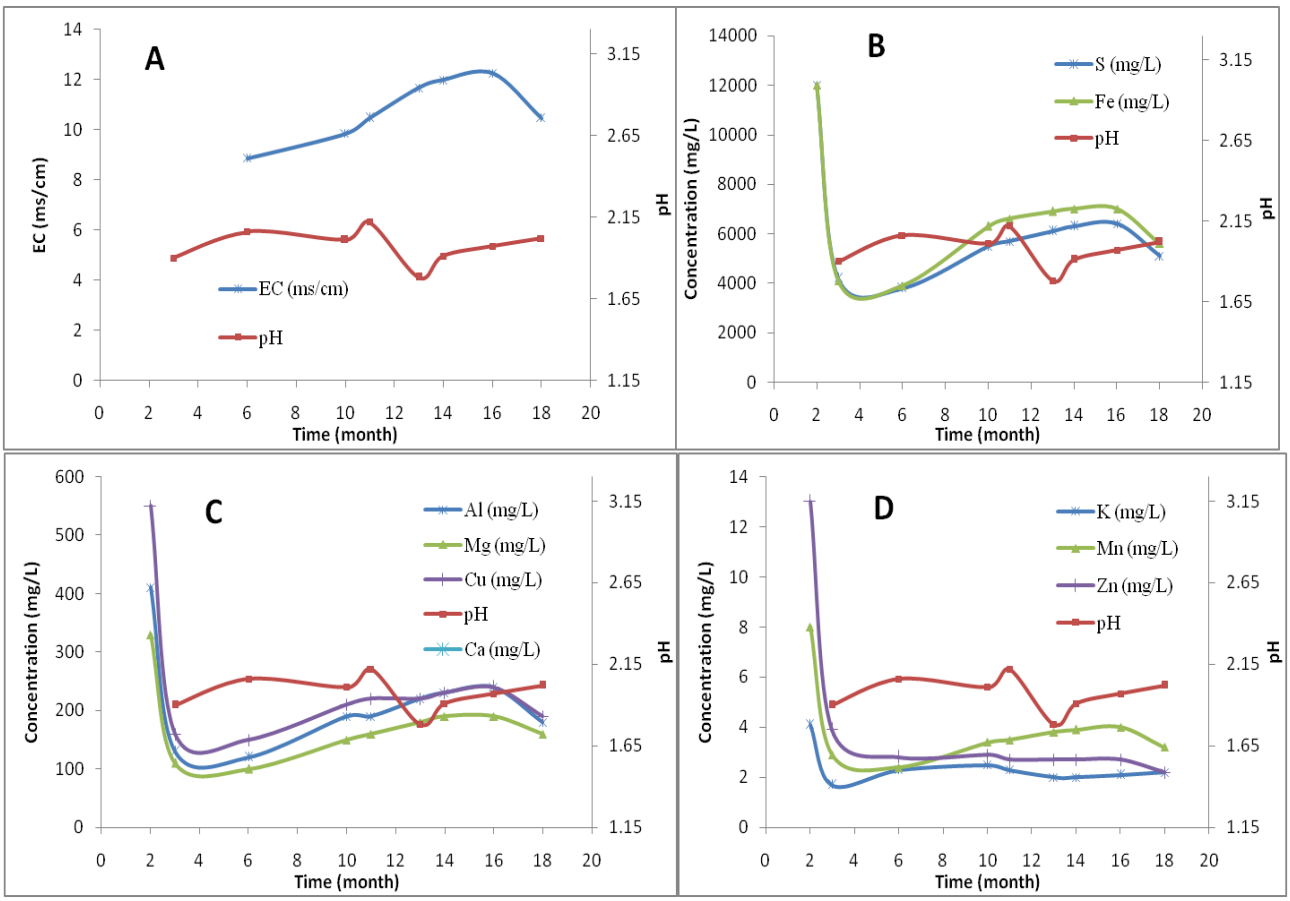

Fig 5.8 Analytical results from leachate samples from the large column test with reactive tailings material from Folldal mining area. EC and pH of the samples (A), sulphur and iron concentrations (B), aluminium, magnesium, copper and sodium concentrations (C) and potassium, manganese and zinc concentrations (D) versus time.

5.9 Geochemical simulation results

5.9.1 Reactant phases

The inverse modelling calculations showed that 10 different possible models Table 5.6 may describe the specific dissolution and precipitation reactions that are most likely to be responsible for the observed changes in water composition resulting from interaction with Folldal mine tailings.

In general, the results for the dissolution/precipitation fraction of the phases are similar. All the models have similar amounts of halite, chalcopyrite, and sphalerite dissolving and jarosite and

albite precipitation. The differences between the models were in the amount of pyrite dissolving (from $2.2.10^{-3}$ to $1.2.10^{-1}$ mol/L), schwertmannite dissolving ($3.8.10^{-2}$ to $2.7.10^{-1}$ mol/L), K-mica dissolving (2.10^{-3} to $5.2.10^{+3}$ mol/L) and chlorite dissolving ($7.2.10^{-4}$ to $9.1.10^{-4}$ mol/L); the presence of dissolution of pyrrhotite and gypsum and, dissolution/precipitation of K-feldspar. The models also varied by presence and precipitation of amorphous iron hydroxide ($Fe(OH)_3(a)$) and gibbsite (Table 5.6). In most of the models the Fe dissolving comes from pyrite.

From the ten inverse models, model 6 (Table 5.7) was selected as the best model based on: (1) geology/mineralogy (2) field observation (3) literature review of the Folldal mining area. There were reddish-brownish soil exposed in the study area (Fig 2.7), which supported the precipitation of jarosite and $Fe(OH)_3$.

Table 5.6: Ten possible models and phases identified on the inverse modelling simulation in PHREEQC from the leachate sample from the large column test and rainwater from Appelo and Postma (2005). Positive mole transfers indicate dissolution, negative mole transfers indicate precipitation. In italics the valid model chosen.

Phases	Model 1	Model 2	Model 3	Model 4	Model 5	***Model 6***	Model 7	Model 8	Model 9	Model 10
Pyrite	1.2E-01	1.2E-01	1.2E-01	2.2E-01		***2.4E-02***	2.2E-03			
$O_2(g)$	4.3E-01	3.5E-01	4.3E-01		5.2E-01	***3.1E-01***		5.2E-01		
Pyrrhotite					3.0E-02			3.0E-02	4.7E-04	4.7E-04
Schwertmannite	3.8E-02	3.9E-02	3.8E-02	2.7E-01	2.6E-02	***2.3E-01***	2.7E-01	2.6E-02	2.7E-01	2.7E-01
Chalcopyrite	2.5E-03	2.5E-03	2.5E-03	2.5E-03	2.5E-03	***2.5E-03***	2.5E-03	2.5E-03	2.5E-03	2.5E-03
Jarosite	-1.2E-01	-1.2E-01	-1.2E-01	-1.2E-01	-1.2E-01	***-1.2E-01***	-1.2E-01	-1.2E-01	-1.2E-01	-1.2E-01
K-feldspar	1.2E-01	-5.2E+03		1.2E-01	1.2E-01	***-5.2E+03***			1.2E-01	
Sphalerite	6.0E-05	6.0E-05	6.0E-05	6.0E-05	6.0E-05	***6.0E-05***	6.0E-05	6.0E-05	6.0E-05	6.0E-05
Chlorite	9.1E-04	7.2E-04	9.1E-04	9.1E-04	9.1E-04	***7.2E-04***	9.1E-04	9.1E-04	9.1E-04	9.1E-04
K-mica	2.0E-03	5.2E+03	1.2E-01	2.0E-03	2.0E-03	***5.2E+03***	1.2E-01	1.2E-01	2.0E-03	1.2E-01
Halite	1.2E-01	1.2E-01	1.2E-01	1.2E-01	1.2E-01	***1.2E-01***	1.2E-01	1.2E-01	1.2E-01	1.2E-01
Gypsum	3.0E-03		3.0E-03	3.0E-03	3.0E-03		3.0E-03	3.0E-03	3.0E-03	3.0E-03
$Fe(OH)_3(a)$				-1.7E+00		***-1.4E+00***	-1.7E+00		-1.7E+00	-1.7E+00
Gibbsite		-1.0E+04	-2.3E-01				-2.3E-01	-2.3E-01		-2.3E-01
Albite	-1.2E-01	-1.2E-01	-1.2E-01	-1.2E-01	-1.2E-01	***-1.2E-01***	-1.2E-01	-1.2E-01	-1.2E-01	-1.2E-01

Table 5.7 Selected model (model 6) and molar transfers calculated by PHREEQC

Mineral phase	Formula	Mole transfer (mol/L)
Pyrite	FeS_2	2.4E-02
$O_2(g)$	O_2	3.1E-02
Pyrrhotite	FeS	—
Schwertmannite	$Fe_8O_8(OH)_6SO_4$	2.3E-03
Chalcopyrite	$FeCuS_2$	2.5E-03
Jarosite	$KFe_3(SO_4)_2(OH)_6$	-1.2E-01
K-feldspar	$KAlSi_3O_8$	-5.2E+03
Sphalerite	ZnS	6.0E-05
Chlorite	$Mg_5Al_2Si_3O_{10}(OH)_8$	7.2E-04
K-mica	$KAl_3Si_3O_{10}(OH)_2$	5.2E+03
Halite	NaCl	1.2E-01
Gypsum	$CaSO_4 \cdot 2H_2O$	—
$Fe(OH)_3(a)$	$Fe(OH)_3$	-1.4E+00
Gibbsite	$Al(OH)_3$	—
Albite	$NaAlSi_3O_8$	-1.2E-01

Values in moles per litter (positive values indicate dissolution and negative values indicate precipitation). Dashes indicate phase not used in model.

5.9.2 Acid mine drainage formation

The simulation of the kinetic of pyrite oxidation in the Folldal mine tailings shows a fast reduction in pH in the initial 4 months (from pH 5.6 to 3.6) (Fig 5.9), which might be due to oxidation of pyrite. The pH values were approximately constant starting from month 4 (Fig 5.9). On the other hand the concentration of Fe^{2+} increased rapidly the first 4 months (from about 0 µmol/L to 102 µmol/L). After that the concentrations stayed above 100 µmol/L for the remaining 14 months. This is because pyrite oxidation increases Fe^{2+} and H^{+} concentration (Equation 3.5).

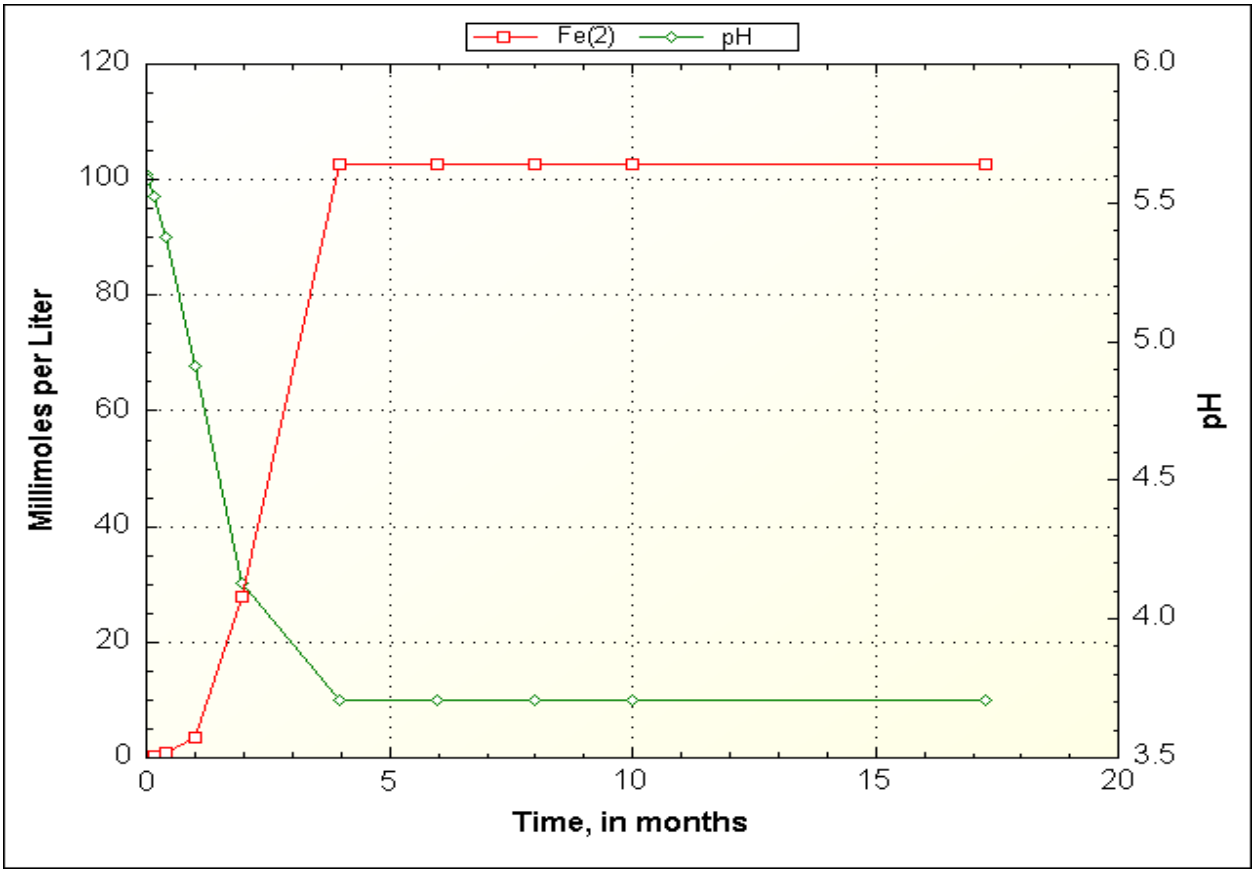

Fig 5.9 Fe^{+2} concentration and pH variation over 18 months in the study area due to pyrite oxidation

6 Discussions

The results obtained from humidity cell (small column) tests, large column test, geochemical models and literature review are integrated in this section to describe hydrogeochemical characteristics of Folldal mining site.

6.1 Hydrogeochemical characteristics of Folldal mining area

The results from soil and leachate analyses show that Folldal mining site has high concentration of sulphur/sulphate, iron, aluminium and heavy metals (Cu and Zn) with high potential risk of contaminating ground- and surface water. The water resources (groundwater and Folla river) in the study area also show substantially elevated concentration of these pollutants as shown by (NGI,2014). Furthermore, Rodés (2014) investigated the groundwater in the old mining area (upper part of the mining area) and in the mine tailings, showing that was highly polluted.

The values of pH, EC, Fe, SO_4^{2-}, Al, Cu and Zn in soil samples (Table 5.1) and leachate samples (Fig 6.1) show considerable variations within the study area. These wide variations in soil and water chemistry could be explained by the heterogeneity of the materials deposited/exposed in the Folldal mining area. The analyses of soil samples from Folldal mine tailings showed that the tailings are very heterogeneous, consisting of a mixture of different types of material, in terms of mineralogy, weathering and texture (NGI, 2014). Furthermore, Geologically the study area consists of poorly sorted glacial deposit (Aanes, 1980; Bjerkgård and Bjørlykke, 1994b) which supported the variation of analytical results observed in the Folldal mining area. In addition various activities carried out at different sites in the Folldal mining area (see Fig 2.5) can be the reason for the observed variations.

The pH in the soil and water investigated at the Folldal mining area, varied from extremely acidic to alkaline. This is in according to literature, where pH of mine waters may vary from alkaline/ neutral to highly acidic (Singh, 1987). The pH values in the leachate samples from the humidity cell tests were in between 3 and 8 (Fig 6.1). Although, the pH is not a quantitative measure of acidity, it reflects the degree of acidity or alkalinity in the leachate water. The lower pH values were measured in the upper part of the study area, in old mine area (see Figs 2.5 and 4.1). The pH results of leachate samples from large column from this part of study area were also

very low (Fig 5.8). It could be due to severe oxidation of pyrite. The oxidation of pyrite increases the amount H^+, Fe^{2+}/Fe^{3+} and SO_4^{2-} ions in the soil and water (see chapter 3). The extremely high values of total Fe and SO_4^{2-} (> 4000 mg/L) in the leachate sample of large column test supported the intensive pyrite oxidation carried out in this part of Folldal mining area (Fig 5.8). Previous researchers mapped this area as one of the main acid producing area (NGI, 2014).

The highest pH values measured in leachate samples of the small column F11, is most likely because calcium carbonate minerals present in the soil sample buffer the acidity. The high TIC measured (Table 5.1) and acid neutralization potential calculated (Table 5.2) in this sample illustrated that there was elevated carbonate minerals which can buffer the pH. Aanes (1980) observed thin layer of limestone in the study area, indicating that soil and tailings may contain carbonates.

From the leachate sample analyses results (small column test), no correlation between pH and EC has been detected (Figs 5.2-5.8 and 6.1). Various authors have reported the absence of a correlation between pH and electrical conductivity (EC) in AMD environments (Grande et al., 2005a, 2005b; Lyew and Sheppard, 2001). However, the EC of the leachate samples were closely linked to the sulphate concentration (Fig 6.1). This phenomenon was interpreted by Lyew and Sheppard (2001), where they suggested that EC appears strongly correlated to SO_4^{2-} content and the presence of dissolved solids and, to a lesser extent, to metal load.

Similar to EC, highest SO_4^{2-} was analysed in leachate sample F11 (Fig 6.1), which indicate that high content of sulphide minerals at this site. However, the pH values observed in this sample were high. According to Singh (1987) such low acidity (high pH) together with elevated SO_4^{2-} concentrations indicate that alkalinity produced from calcareous materials consequently neutralise H^+ produced by sulphide oxidation. The lowest SO_4^{2-} was observed in the background soil (Fig 6.1), where there is limit impact of mine wastes. Rodes (2014) observed good quality groundwater in the forest area; where there is insignificant mine wastes impact. The level of SO_4^{2-} in the water is most likely to be affected by amount of reactive pyrite minerals Singh (1987).

There was no general order of the dissolved metals in the leachate samples of humidity cell (small column tests) of Folldal mining area (Fig 6.1). In some leachate samples, Cu was the

dominant, while in other samples Fe or Al were the dominant elements (Fig 6.1). On the other hand, the order of these dissolved metals in large column was: Fe > Cu > Al > Zn (Fig 5.8). However, Gurung (2001) found that the overall mean concentration of dissolved metals concentrations in abandoned mine impacted surface waters in Tasmanian, Australia were in the order Fe > Al > Zn > Cu. The variations observed in the order of dissolved metals could be explained by mineralogical variation between the two areas. The extent and degree of dissolved metals concentrations in the tailings vary depending upon geochemical characteristics and degree of mineralization of the tailings (Johnson et al., 2000). The results indicate that there is a higher content of Cu-minerals in the Folldal mining area compared to Tasmanian abandoned mine tailings.

The Cu concentrations of some leachate samples (particularly in F3) were considerably correlated with Al concentrations (Fig 6.1). Thus, Cu will dissolve together with aluminosilicate at lower pH. This is in accordance with Gurung (2001) who observed a significant correlation between Cu and Al in the leachate at an abandon mines in Tasmanian, Australia. In most leachate samples from Folldal mining area Cu and Zn were noticeably correlated to each other. Explanation of this phenomenon could lie in the fact that the origin of heavy metals might be the same rocks that are in the vicinity of the mine.

The elevated acidity, SO_4^{2-}, Fe, Al, and heavy metals concentrations observed in the leachate samples from large column test is most likely generating from elevated pyrite oxidation. In general, such high acid/high sulphate water is originated from mine sites that contain exposed sulphide minerals (mainly pyrite) undergoing active oxidation (Gurung, 2001).

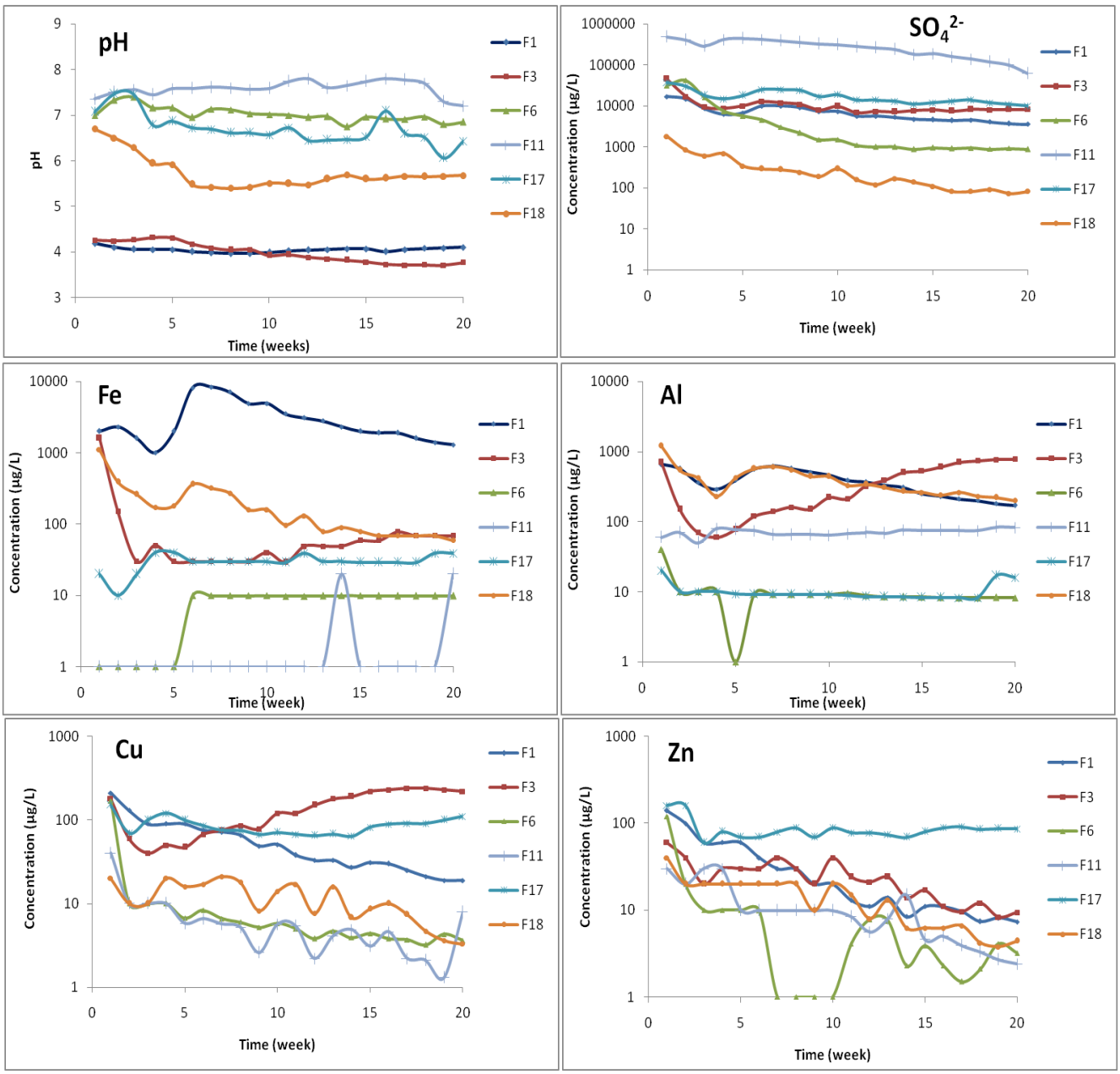

Fig 6.1 Water quality corresponding to the humidity cell tests carried out seven Folldal mine tailings samples.

6.2 Acid Mine Drainage (AMD) prediction

6.2.1 AMD prediction by static test

Acidity increases as the iron is oxidised (Equation 3.5 and Fig 3.1). Nevertheless, this oxidised iron usually precipitates out at the base of drainage due to low solubility, unless the pH is very low. However, sulphate content remains constant and can be used to approximate the degree of acidity present before neutralisation took place (CEN/TR, 2012a; Nordstrom and Alpers, 1999; Price, 2009; Williamson and Rimstidt, 1994).

The net neutralization potential (NNP) values in most of the topsoil samples from the Folldal mining area are negative. From these results, most of the samples can be classified as having a potentially acid-forming capacity, according to Dold (2017, 2014); Morin and Hutt (2001) and Sherlock (1995).

However, Robertson and Kirsten (1989) suggested classification criteria for the acid-generation potential of the tailings as following:

- If the tailings NNP is higher than +20 t $CaCO_3$/1000 t, the sample is considered non acid generating,
- If the tailings NNP is lower than -20 t $CaCO_3$/1000 t, the sample is considered acid generating,
- If the tailings NNP is between -20 and +20 t $CaCO_3$/1000 t, the sample is in an uncertain zone.

Fig 6.2 shows the classification of acid generating potential in the soil samples from Folldal based on NNP calculation. All the topsoil samples collected from Folldal mine tailings except soil sample F11 are classified in the uncertain zone, thus possible acid generating. The NNP of soil sample F11 was about -38 t $CaCO_3$/1000 t and this sample is classified as high acid generating potential. The AP and NNP of the topsoil samples of the Folldal mining area were not as high as expected in the most acidified environment. The majority of the soil samples were most likely oxidised and most of the elements were leached to the subsoil, explaining the relatively low AP and NNP.

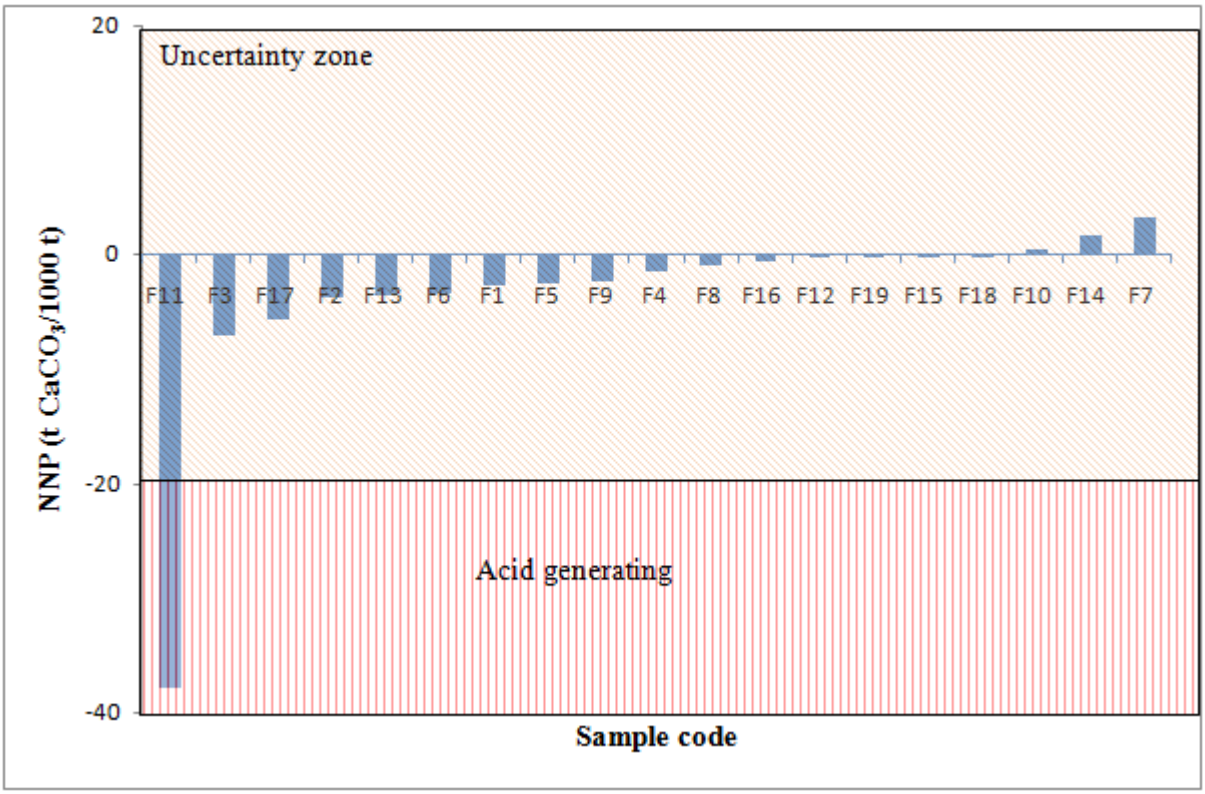

Fig 6.2 Acid generating potential in soil samples from Folldal mining area according to Robertson and Kirsten (1989) classification.

Adam et al. (1997) used neutralization potential ratio (NPR) i.e. NP to AP ratio and recommended the following classification benchmarks:

- If the NPR is higher than 2.5, the material is considered non-acid generating,
- If the NPR is in between 2.5 and 1, the sample is in an uncertain zone,
- If NPR is lower than 1, the material is considered as acid generating.

The NPR of most the topsoil samples were < 1 (Table 5.2) and classified as having a potentially acid-forming capacity (Fig 6.3). Since the NPR of samples F7 and F14 were > 2.5, the two samples can be considered as non-acid generating. The NPR value estimated from the soil sample F10 was 1.2 and the sample is in the uncertainty zone (Adam et al., 1997; Benzaazoua et al., 2004).

The deviation between the two classification system is due to Robertson and Kirsten (1989) used wider uncertainity zone (-20 to +20 t $CaCO_3$/1000 t) than Adam et al. (1997) 1- 2.5). The Soil sample F11 classified as acid producing in both classification criteria.

The considerable low NNP (-159 t $CaCO_3$/1000 t) and NPR (0.01) observed in the subsoil sample used in the large column test has a substantial potential to produce acidity (Table 5.2). Such extremely low NNP and NPR can be explained by high SO_4^{2-} concentration generated from weathering (sulphide oxidation) in the fresh (unoxidised) mine tailings than in the weathered ones (Plante et al., 2011). Based on the field observations and NPR results of most of the soil samples as well as the NNP results of F11, it can be concluded that soil and mine tailings in the Folldal area have a potential to generate acidity. That the topsoil has a potential to generate acidity, also after many years of weathering.

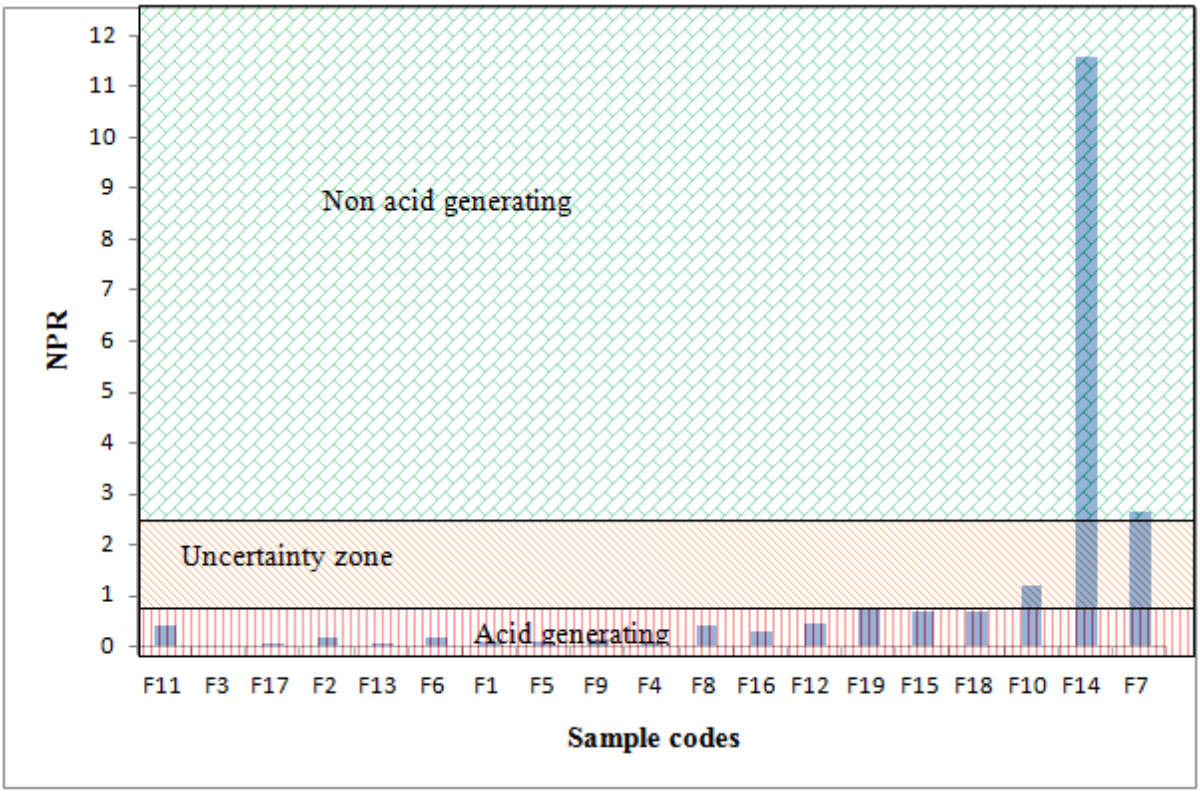

Fig 6.3 Acid generating potential in soil samples from Folldal mining area according to Adam et al. (1997) classification.

6.2.2 AMD prediction by kinetic tests

The high concentration of SO_4^{2-}, Al, Cu and Zn observed in most of the samples from the small columns in the initial week (Figs 5.2- 5.8) might be due to dissolution of ultra-fine particles (Furrer and Stumm, 1986) and dissolution at highly reactive surface sites on the fresh mineral surfaces (Werhli, 1989). In accordance with Hakkou et al. (2005) the rapid initial dissolution of sulphate is due to already oxidized sulphides in the soil samples. Adsorbed weathering products may then be rapidly released when the particles are rinsed with water.

6.2.2.1 Sulphate production rate

Sulphate production rates (SPR) in the leachate samples from Folldal mining area tended to increase with increasing tot-S concentration in the solid (Fig 6.4), which support that the detected sulphur in the soil samples is mainly from pyrite oxidation. Therefore if the sample initially has high pyrite content, high SPR will be expected. This can be exampled by sample F11 in which the highest tot-S and SPR observed (Fig 6.4 and Table 5.1). Lapakko and Antonson (2006) found similar phenomenon in the humidity cell leachate samples from Archean greenstone rock, Minnesota.

The leachate samples from humidity cell (small column) tests show a clear decrease in sulphate production rate over times (Fig 6.6). This is most likely because of the depletion of the reactants (pyrite), depletion of ultra-fine particles, precipitation of secondary minerals (Furrer and Stumm, 1986; Werhli, 1989), and coating of the reacting minerals surfaces by secondary phase (Cruz et al., 2001). Hakkou et al. (2005) also obtained similar observation i.e., decrease SPR over times in the leachate samples collected from Kettara mine site, Moroco.

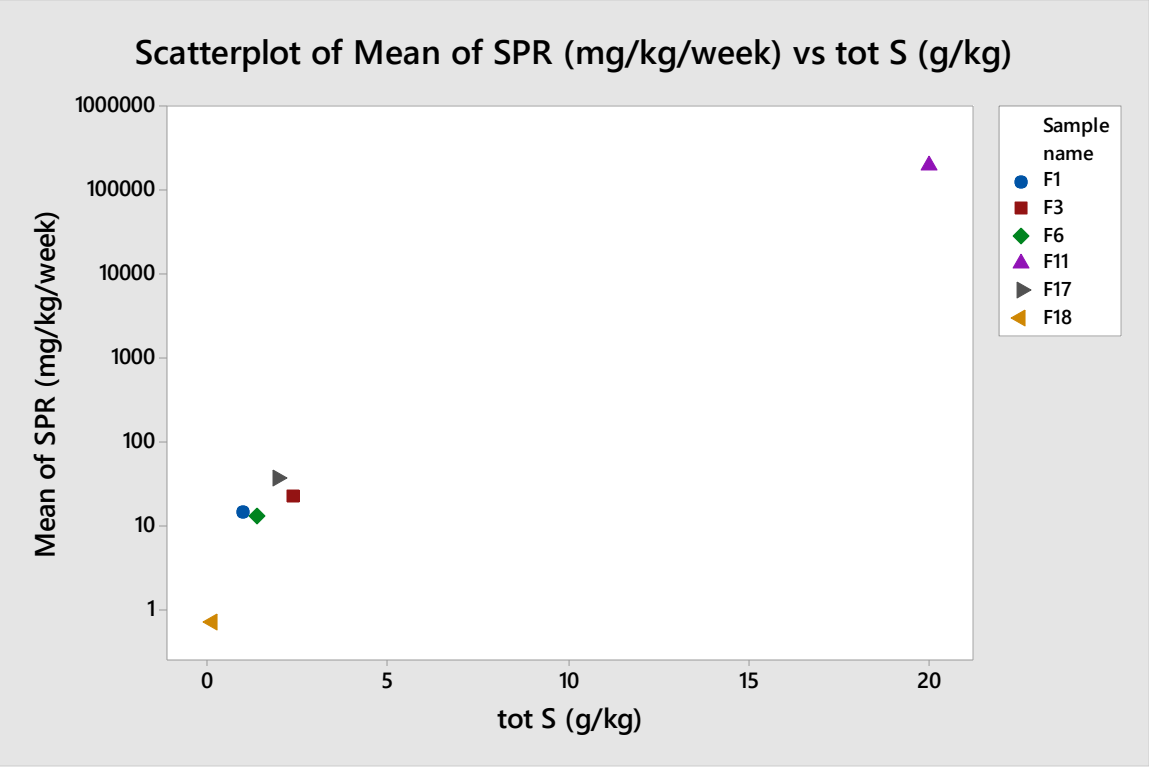

Fig 6.4 The relation between tot-S in the solid and the mean of sulphate production rate (SPR) in the leachate samples

The leachate samples from the Folldal mining area can be classified into 3 sections (low acid/low sulphate, low acid/high sulphate and high acid/high sulphate) based on the pH and SPR of the leachate samples (Table 6.1). Most of the samples are classified as low acid/low sulphate, which is most likely to be depleted with sulphate by forming sulphate minerals (e.g. jarosite). Low acid/high sulphate was obtained in the leachate sample F11 (Figs 6.5 and 6.6), and high acid (low pH)/high sulphate were observed in the subsoil samples used in large column test (Fig 5.8).

Table 6.1: The relation between the acidity (pH) and sulphate production rate

Low acid/low sulphate	Low acid/high sulphate	High acid/high sulphate
F6	F11	Large column test
F13		
F17		
F18		

Gurung (2001) interpreted the relationship of acidity and sulphate production rate in the mine tailings as follows:

- High acid/high sulphate water represents mine sites that contain exposed or disturbed sulphide materials undergoing active oxidation.
- Low acid/high sulphate water represents residual sulphate accumulated from periodic acid generation at the site and due to presence of neutralization minerals (e.g., calcium carbonate)
- Low acid/low sulphate waters are most likely to be depleted with sulphate, which is likely to be incorporated in the formation of sulphate minerals such as jarosite, alunite and gypsum.

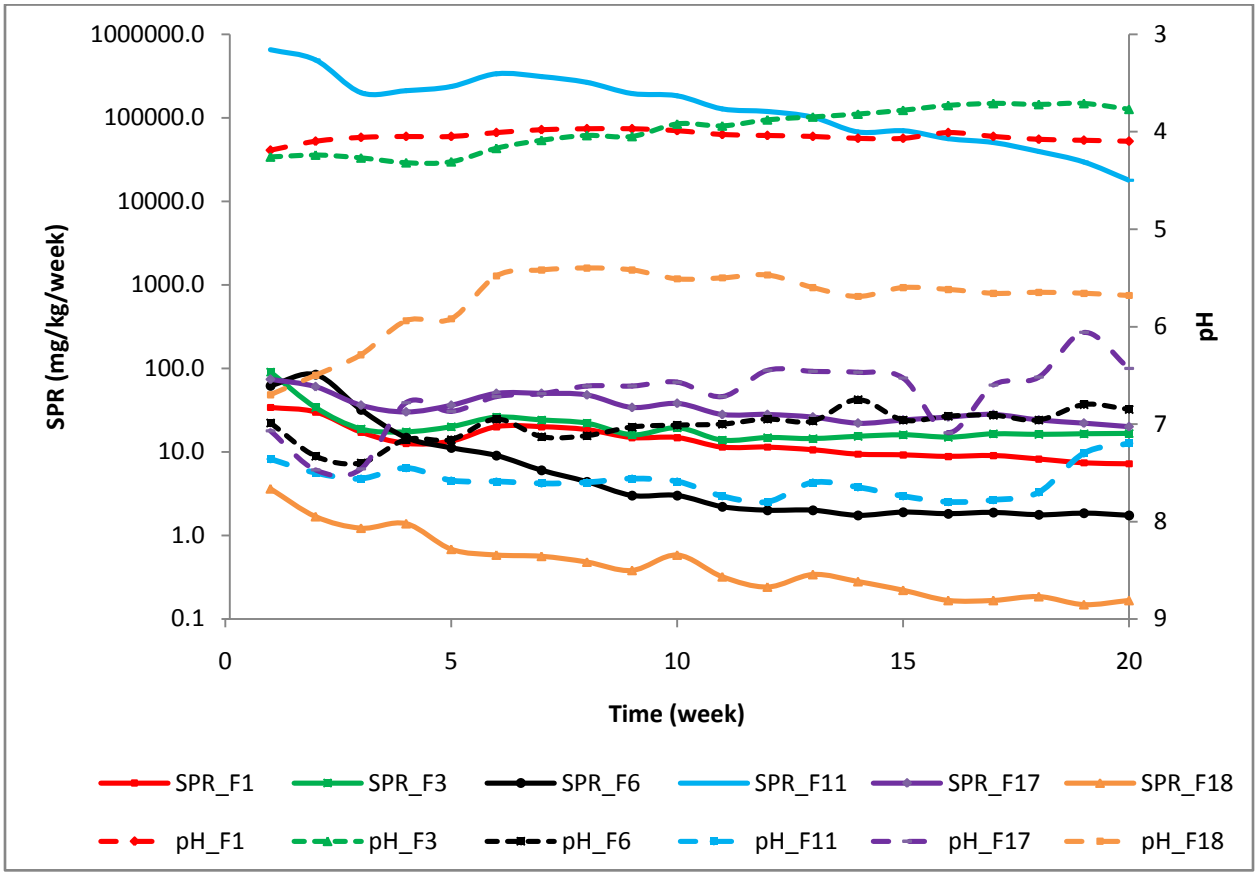

Fig 6.5 Sulphate production rate (SPR) and pH of the 6 samples (F1, F3, F6 , F11, F17 and F8) from small column test.

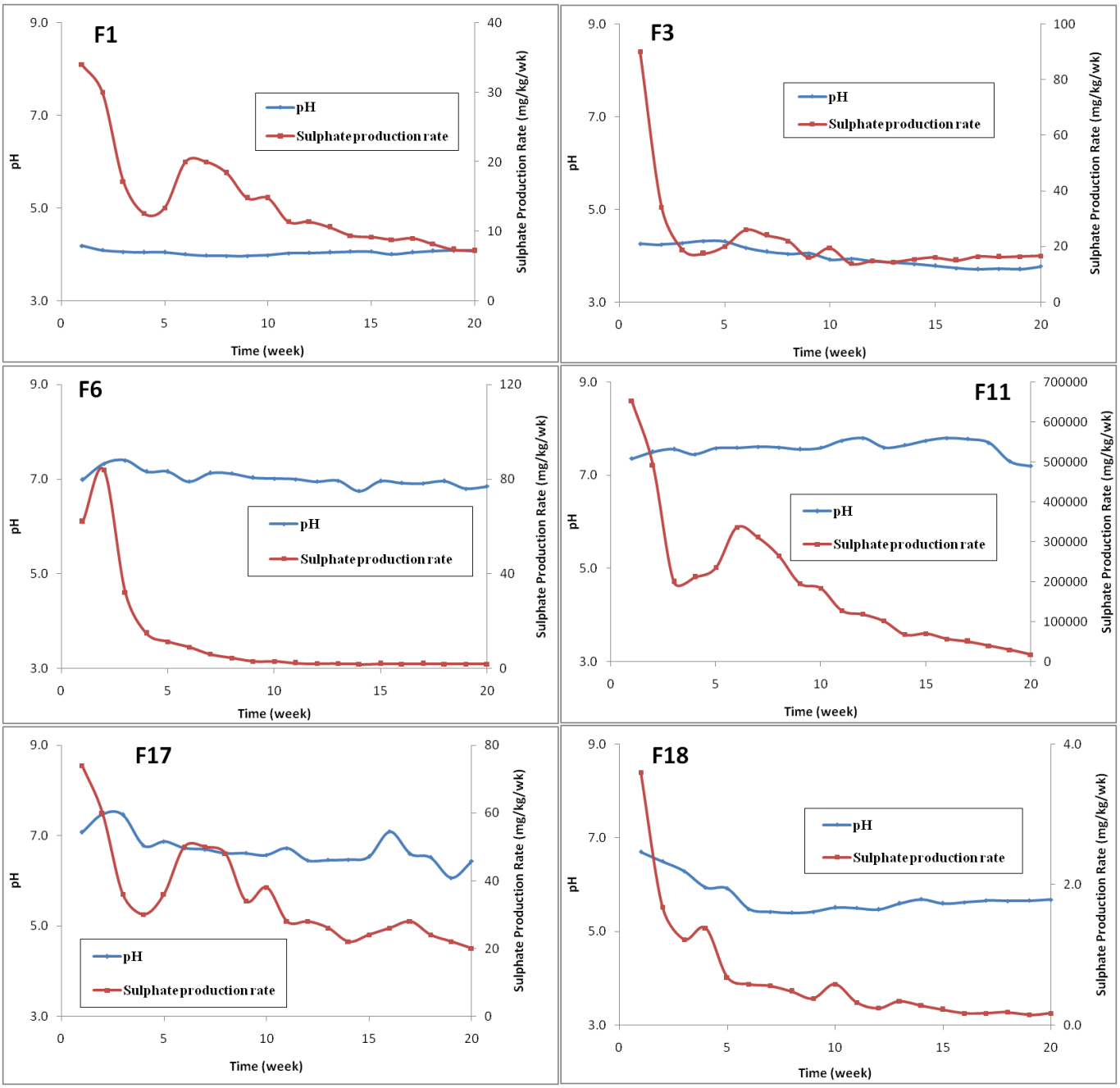

Fig 6.6 pH and rates of sulphate production in humidity cell tests in selected soil samples from Folldal mining site.

The sulphate production rate in all the leachate samples except F6 and F18, was > 10 mg/kg/week, even after 20 weeks of rinsing/leaching, which indicate that the tailing continuously release acid after 20 weeks of leaching (Fig 6.6). In addition, the cumulative sulphate release in

all the leachate samples except F6 and F18 increased throughout the experimental time (Fig 6.7) that evidenced the oxidation sulphide minerals and producing AMD. Hakkou et al., (2005) observed mean sulphate release rate of 5379 mg/kg/week in Kettara mine tailings which is lower than the one obtained in F11 (18140 mg/kg/week) and higher than in the remaining samples. They also observed a continuous increase of cumulative released sulphates.

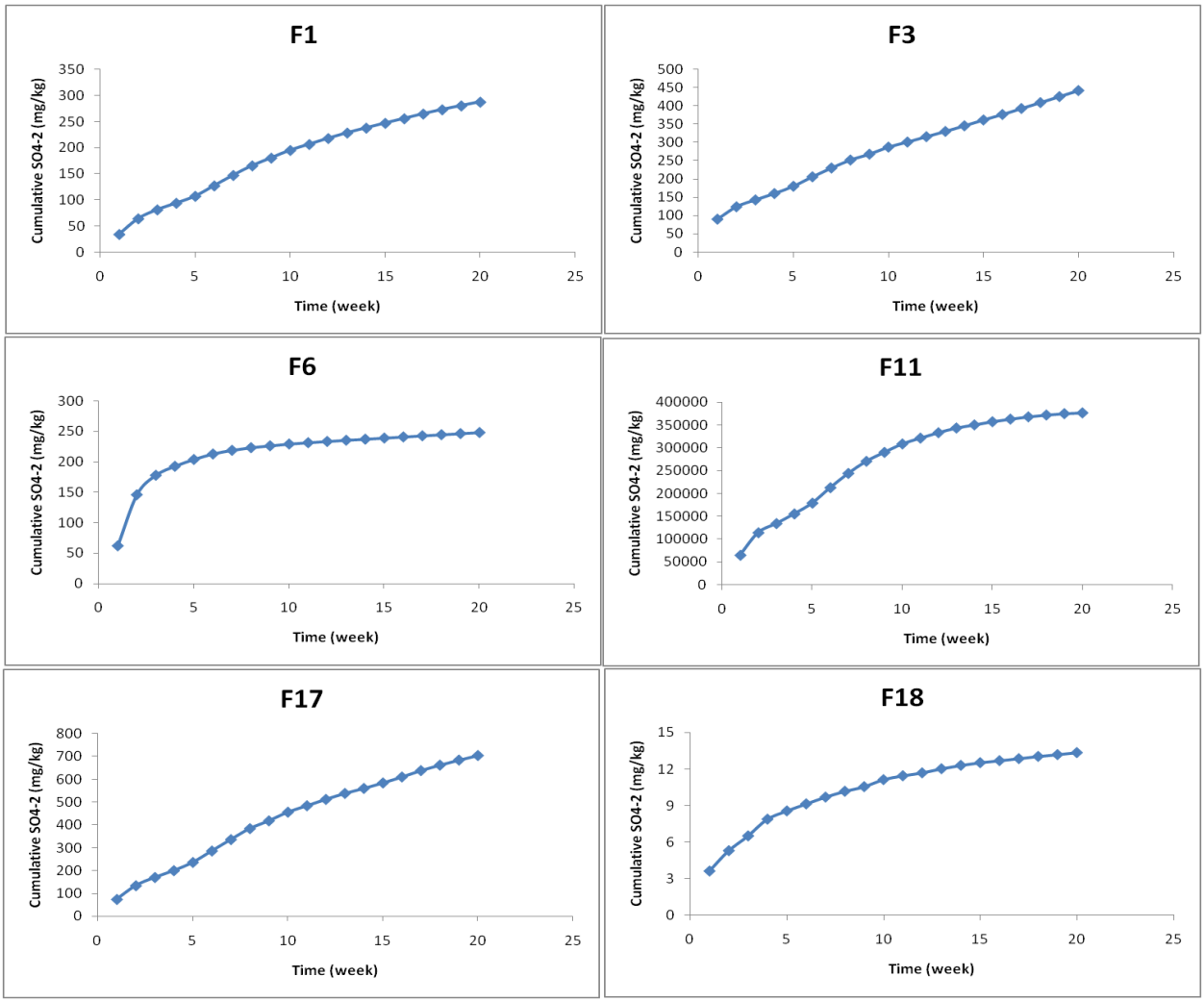

Fig 6.7 Evolution of cumulative sulphate loads obtained from water quality corresponding to humidity cell tests carried out samples F1, F3, F6, F11, F17 and F18.

6.2.2.2 Oxidation-neutralization curve

Fig 6.8 shows the accumulative mass of sulphates (SO_4^{2-}) obtained in the leachate samples from the large column test plotted versus the accumulative amount of calcium and magnesium (Ca + Mg). The sulphate in this plot represents the main oxidation products while the term Ca + Mg represents the main carbonate or silicate dissolution product (Hakkou et al., 2005; Méndez-Ortiz et al., 2007). The obtained curve, called oxidation-neutralization curve reflects the geochemical evolution of the acidic and neutralization potentials during the kinetic tests (Benzaazoua et al., 2001). The Folldal subsoil show a linear-shaped oxidation-neutralization curve in the large column test (Fig 6.8). The linear relation (with $R^2 = 1$) between the neutralizing and acidification materials in the system suggests that sulphate production exceeds the neutralizing capacity in sample. The ratio of the accumulative SO_4^{2-} (acidification) to the Ca + Mg (neutralizing) is about 20:1. However the ratio of the accumulative SO_4^{2-} to the Ca + Mg in neutral (non acid producing soil should be less than or equal to 0.32 =32/100). Thus, the sulphide oxidation capacity (acidification) is substantially greater than the neutralizing capacity and indicate this type of the Folldal mine tailings is producing significant acid mine drainage. The neutralization rate, which can also be defined as the slope of the obtained curve is 0.042. This value is lower than those obtained by (Hakkou et al., 2005), which varies between 0.19 and 0.10; (Benzaazoua et al., 2004), which vary between 0.36 and 0.42 and (Méndez-Ortiz et al., 2007) which is 0.5. The smaller the slope of the oxidation-neutralization curve, the higher the acid generating potential of the mine wastes (Méndez-Ortiz et al., 2007).

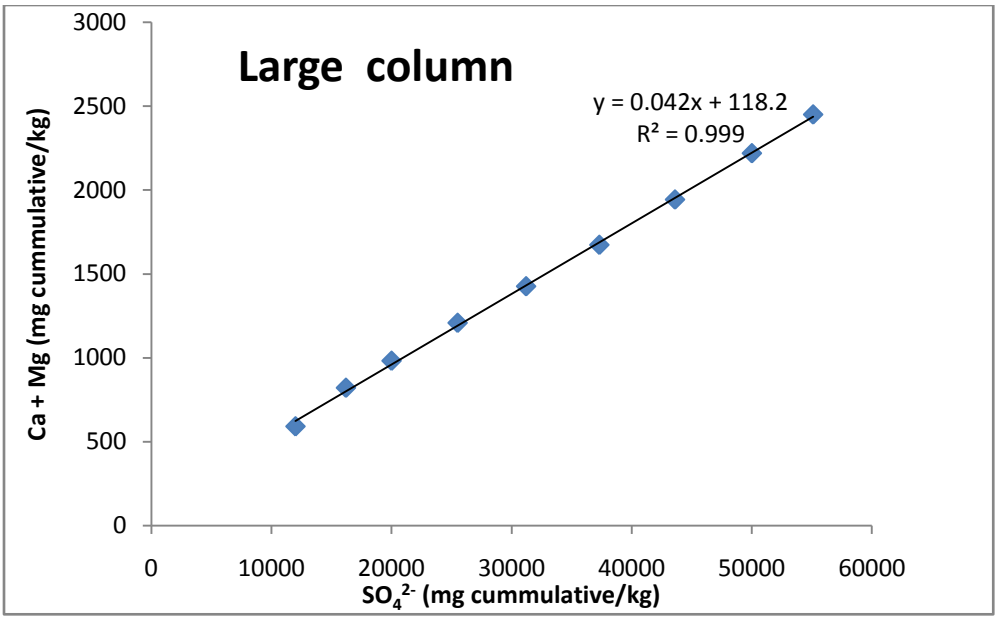

Fig 6.8 Oxidation-neutralization curves for leachates obtained from the large column test of Folldal mine tailings.

6.2.2.3 Cu and Zn leaching rate

Cu and Zn leaching rate in the Folldal mine tailings were determined by using humidity cell tests. Similar to sulphate production rates, the leaching rates of Cu and Zn showed substantial decrease in the initial few weeks of leaching (Fig 6.9 and Table 5.5). The leaching rates of heavy metals such as Cu, Zn and Pb have been determined by various kinetic tests. For instance, Namaghi and Li (2016) used column tests to study heavy metal attenuation and mobility in the mine waste, while Morin and Hutt (2001) used humidity cell tests to investigate the Cu and Zn leaching rate in various mine tailings.

In samples F1 and F3 the leaching rate of Cu was higher than Zn throughout the experiments (Fig 6.9), which might be due to higher concentration of Cu than Zn in the host rock at this site (Tables 4.5 and 5.7). This is in accordance with literature, where the concentration of heavy metals in acid drainage commonly reflects their relative abundance in the host rocks (Gurung, 2001). There were no clear trend between the leaching rate of Cu and Zn in the leachate samples F6, F11, F17, and F18 (Fig 6.9). In addition to host rocks, deposit type, physiography, density of drainage pattern and environmental conditions have a predominant influence on the variation in

the heavy metal concentrations and in acid drainage quality sourced from impacted sites (Gurung, 2001).

Gurung (2001) concluded that at low pH, dissolved Cu was the most common metal while Zn remained mobile throughout the pH range of 2–8. This is presumably because of Cu has a higher tendency to adsorb to soil particles, it is the dominant species found acidic waters while Zn, which has a limited adsorption capacity, is predominantly mobile at a wider pH range. This phenomenon might be the other possible reason why significantly high leaching rates of Cu were observed in the humidity cell (small column) tests of soil samples F1 and F3 (Fig 6.9) and large column test in subsoil sample (Fig 5.8) than Zn.

The concentrations of Cu and Zn in the leachate sample from the large column test reached values as high as 550 and 13 mg/L (see Fig 5.8). This is in the same range as measured in the AMD from the Folldal mine (approximately 60 and 40 mg/L for Cu and Zn respectively) (Klimpel, 2017).The oxidation of chalcopyrite and sphalerite is most likely the primary source of dissolved Cu and Zn in the leachate samples, as shown by Hakkou et al., 2005.

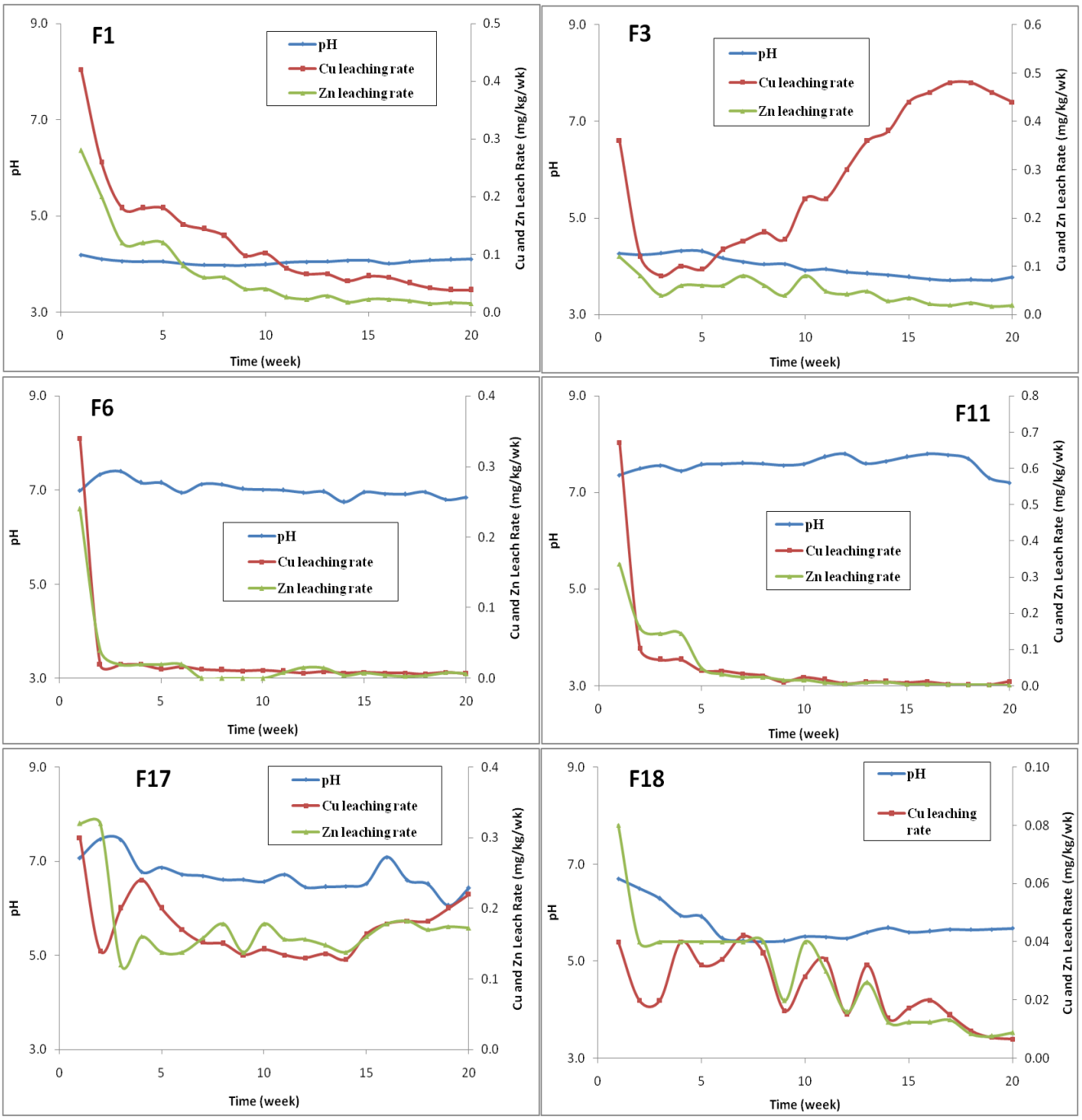

Fig 6.9 pH and leaching rates of Copper and Zinc in Humidity Cell/small column tests on seven soil samples collected from Folldal mining area

6.2.3 Geochemical models for AMD at Folldam mining site

6.2.3.1 Inverse modelling

The inverse geochemical model simulation was carried out to identify specific dissolution and precipitation reactions that are most likely to be responsible for the observed changes in water composition resulting from interaction of Folldal mine tailings. Inverse modelling, using observed mineral assemblages and minerals inferred from PHREEQC, can reveal the roles of mineral dissolution and precipitation in establishing the drainage chemistry (Seal et al., 2008).

The results of the inverse models indicated that from the sulphide minerals, pyrite dissolution by oxidation was the most important contributor to the drainage chemistry in the study area, which required proportional amounts of dissolved O_2 for oxidation (Tables 5.7 and 5.8). The high sulphate and iron values observed in the leachate samples of the large column test (Fig 5.8) were most probably caused by dissolution of pyrite, chalcopyrite, schwertmannite and sphalerite. The elevated concentrations of copper and zinc in the study area are from dissolution of chalcopyrite, and sphalerite. The inverse geochemical simulations supported that the aluminosilicate minerals present in the tailings are also dissolving and neutralizing the acid formed from sulphides oxidation (Table 5.7). K-mica was the highest dissolving aluminosilicate mineral followed by chlorite.

Inverse modelling suggested that K-feldspar, jarosite, amorphous $Fe(OH)_3$, and albite were the dominant precipitates (Table 5.7). The precipitation of K-feldspar and albite could explain the low content of potassium and sodium obtained in the leachate samples. The considerable low values of iron concentration obtained in most of the leachate samples from humidity cell (small column) test (see section 5.5.3) supported the precipitation of iron (as jarosite and $Fe(OH)_3$)(a).

6.2.3.2 Kinetic modelling

The PHREEQC results, based on inverse modelling of the Folldal tailing material, showed that high Fe^{2+} concentration will be released due to pyrite oxidation (Fig 5.9). This is in accordance with literature where pyrite oxidation releases sulphate and iron as direct oxidation products (Molson et al., 2005).

Fig 6.10 shows rapid increase of the modelled Fe^{2+} concentration in the first 4 months, followed by a constant concentration of 102 mmol/L (5712 mg/L) for the remaining time. The Fe

concentration released from the large column test varied from 70 mmol/L to 214 mmol/L, thus in the same range as modelled by PHREEQC (see Fig 6.10). Fe concentration observed in the large column test and modelled results showed inverse relationship in the first 3 months. This phenomena can be explained by the geochemical model does not take dissolution of ultra-fine particles (rich in pyrite mineral) in to account (Furrer and Stumm, 1986). Furthermore, the impact of microbial activities on pyrite oxidation (see chapter 3) is not included in the model. In addition the model does not account for coating of the reacting minerals surfaces by secondary phase (Cruz et al., 2001), which may decrease the rate of oxidation and subsequently Fe concentration. After approximately week 4 the Fe concentration observed in the large column are comparable with the modelled results (Fig 6.10), thus the model describes the Fe release quite well.

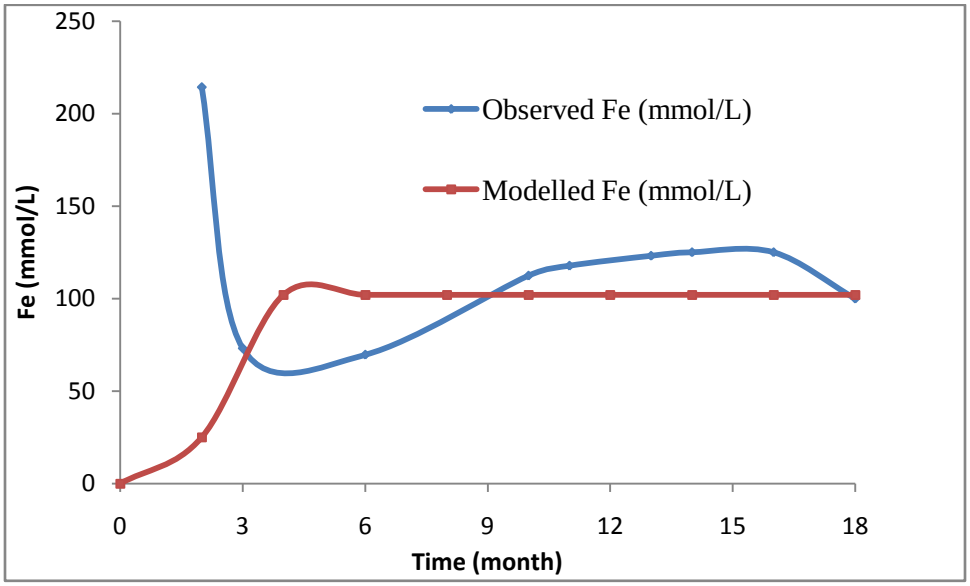

Fig 6.10 Comparison of Fe observed in the leachate samples from the large column and obtained from geochemical simulation by PHREEQC.

The pH values obtained from the model considerable low (3.6) after month 4. Based on the pH values obtained from model, it would expect lower Fe concentration in the Folldal mining area. This is in accordance with literature where the lower pH increase the solubility of Fe (Appelo and Postma, 2005).

However, the pH values observed in the leachate samples from the large column test (approximately 2) were substantial lower than the pH results quantified by the models (range from 3.6 to 5.6). The absent of considering the impact of the microbial activities that catalysts pyrite oxidation in the geochemical simulation can be the reason why higher pH values were obtained from the model.

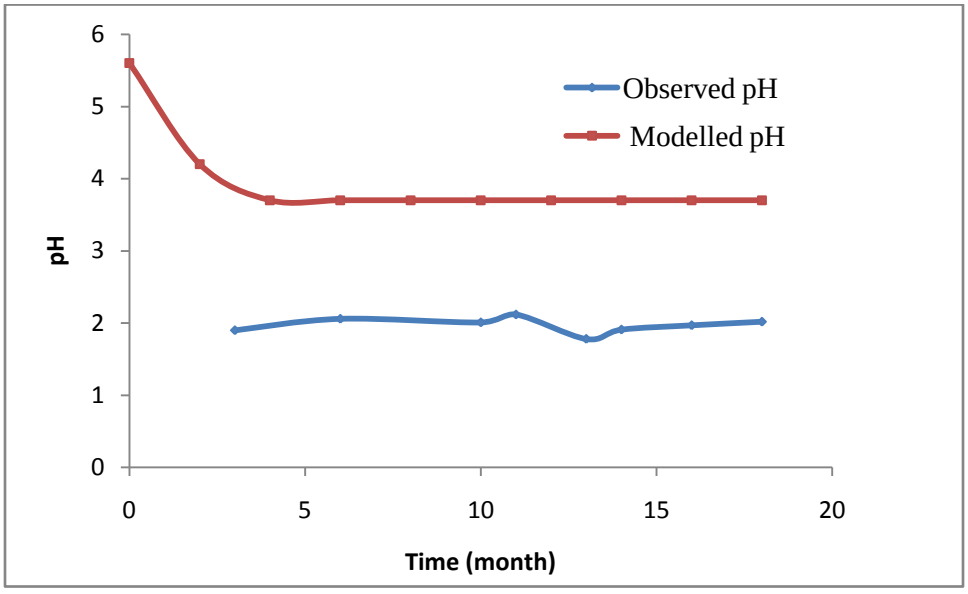

Fig 6.11 Comparison of pH observed in the leachate samples from the large column and obtained from geochemical PHREEQC model.

7 Conclusions and recommendations

7.1 Conclusions

For the topsoil in the Folldal, only using static tests makes it difficult to predict the acid producing potential of the topsoil (uncertain zone). Including kinetic tests as the leaching tests provide a much better information. The main aims of this thesis work were to predict acid producing capacity of Folldal mine tailings by integrating static and kinetic tests and to develop models to quantify leachates composition. Effective remediation measures including legislative regulations to reduce the impact of acid mine drainage on the environment can only be designed based on proper assessment of the key geochemical processes and precise prediction of acid producing potential of the mining tailing.

The net neutralization potential (NNP) and neutralization potential ratio (NPR) of the soil samples determined by acid base accounting (ABA) method of static test samples were negative (< 0 t $CaCO_3$/1000 t) and < 1 respectively which indicating that the Folldal mine tailings materials, also on the surface (topsoil) have a potential to produce acid mine drainage (AMD). However based on the classification system of Robertson and Kirsten (1989), all the topsoil samples collected from Folldal mine tailings except soil sample F11 are in the uncertain zone. The NNP of soil sample F11 was about -38 t $CaCO_3$/1000 t, and this sample could be classified as high acid generating potential. Therefore, based on the field observations and NPR results of most of the soil samples as well as the NNP results of F11, it can be concluded the topsoil from the Folldal mine tailings have a potential to generate acidity, also after many years of weathering.

The results from soil and leachate analyses show that Folldal mining site has high concentration of sulphur/sulphate, iron, aluminium and heavy metals (copper and zinc) with high potential risk of contaminating ground- and surface water. However, the values of these parameters as well as pH and EC show considerable variations within the mining area, which might be due to the heterogeneity of the materials deposited/exposed in the area. For example, the pH values varied from pH 3 to 8. The highest pH value observed in the topsoil is most likely due to calcium carbonate present in the soil sample which buffer the acidity.

The electrical conductivity (EC) and SO_4^{2-} values in most of the leachate samples were strongly correlated and suggested that sulphide minerals oxidation might be the reason for high concentrations of the dissolved metals and account for high EC in the Folldal mining area.

Cu and Zn concentrations in leachate of the topsoil samples were also correlated to each other that might be because the origins of these elements are the same rocks. The concentrations of Cu and Zn in the leachate sample of large column test reached values as high as 550 and 13 mg/L, which is in the same range as measured in the AMD from the Folldal mine (approximately 60 and 40 mg/L for Cu and Zn respectively).

The sulphate production rate (SPR) in nearly all the leachate samples of the topsoil was >10mg/kg/week, even after 20 weeks of rinsing/leaching, which indicate that even the tailing material on the surface continuously release acid after 20 weeks of leaching. Furthermore, the ratio of the accumulative SO_4^{2-} (acidification) to the Ca + Mg (neutralizing) for the subsoil tailing sample is about 20:1, which is substantial high compare to 8:25 ratio in neutral (non acid producing) soil. Thus, the sulphide oxidation capacity (acidification) is substantially greater than the neutralizing capacity and indicating the Folldal mine tailings is producing significant acid mine drainage.

The results of inverse geochemical modelling showed the possible dissolution of pyrite, chalcopyrite, schwertmannite, sphalerite, K-mica and chlorite; precipitation of K-feldspar, jarosite, amorphous $Fe(OH)_3$, and albite. The dissolutions of these minerals accounted for the high sulphate, Fe, Al, Cu and Zn observed in the study area. However the geochemical model for kinetic oxidation rate of pyrite, did not describe the observed large column test data sufficiently, probably because the PHREEQC model does not take account for: 1) the dissolution of ultra-fine particles, 2) impact of microbial activities and 3) coating of the reacting minerals surfaces by secondary phase.

7.2 Recommendations

Since the results from static and kinetic tests indicating the Folldal mine tailings is producing significant acid mine drainage, remediation measures have to be taken to reduce long-term impacts on ecosystems and human health.

In this thesis Ca and Mg concentration in the small samples were not determine, however concentration of these elements are quite important in oxidation-neutralization curve, which use to determine acid producing potential by kinetic test.

Since sulphide is the dominant form of sulphur in the Folldal mining area, the future analytical efforts and costs can be reduced by analyzing for total sulphur only, instead of measuring both tot-S and sulphate concentrations.

In order calibrate the inverse modelling, the mineralogical analyses are strongly recommended. In addition the concentration measured in the leachate samples do not always reflect the geochemical processes occurring within the soils submitted to kinetic testing. In fact, precipitation often occurs to a greater or lesser extent during testing. Therefore, during the dismantling of the large column test, taking samples at different depths and analyses for soil total concentrations will be recommended.

8 References

Aanes, K.J., 1980. A Preliminary Report from A Study on The Environmental Impact of Pyrite Mining and Dressing in A Mountain Stream in Norway, in: Flannagan, J.F., Marshall, K.E. (Eds.), Advances in Ephemeroptera Biology. Springer, Boston, MA, p. 24.

Adam, K., Kourtis, A., Gazea, B., Kontopoulos, A., 1997. Evaluation of static tests used to predict the potential for acid drainage generation at sulphide mine sites. Inst. Min. Metall. Trans. Sect. A Min. Ind. 106, 1–8.

Agrawal, A., Sahu, K.K., 2009. An overview of the recovery of acid from spent acidic solutions from steel and electroplating industries. J. Hazard. Mater. 171, 61–75.

Akcil, A., Koldas, S., 2006. Acid Mine Drainage (AMD): causes, treatment and case studies. J. Clean. Prod. 14, 1139–1145.

Appelo, C.A.J., Postma, D., 2005. Geochemistry, Groundwater and Pollution, 2nd ed. A.A. Balkema.

Armienta, M.A., Villaseñor, G., Rodriguez, R., Ongley, L.K., Mango, H., 2001. The role of arsenic-bearing rocks in groundwater pollution at Zimapán Valley, México. Environ. Geol. 40, 571–581.

Banks, D., Younger, P.L., Arnesen, R.T., Iversen, E.R., Banks, S.B., 1997. Mine-water chemistry: The good, the bad and the ugly. Environ. Geol. 32, 157–174.

Belkhiri, L., Mouni, L., Boudoukha, A., 2012. Geochemical evolution of groundwater in an alluvial aquifer: Case of El Eulma aquifer, East Algeria. J. African Earth Sci. 66–67, 46–55.

Benzaazoua, M., Bussiere, B., Dagenais, a M., 2001. Comparison of kinetic tests for sulfide mine tailings, in: International Conference on Tailings and Mine Waste. pp. 263–272.

Benzaazoua, M., Bussière, B., Dagenais, A.M., Archambault, M., 2004. Kinetic tests comparison and interpretation for prediction of the Joutel tailings acid generation potential. Environ. Geol. 46, 1086–1101.

Bjerkgård, T., Bjørlykke, A., 1996. Sulfide deposits in folldal, southern trondheim region caledonides, Norway: Source of metals and wall-rock alterations related to host rocks. Econ. Geol. 91, 676–696.

Bjerkgård, T., Bjørlykke, A., 1994a. The stratabound sulphide deposits in the Folldal area, southern Trondheim region, Norway. Nor. Geol. Tidsskr. 74, 213–237.

Bjerkgård, T., Bjørlykke, A., 1994b. Geology of the Folldal area, southern Trondheim Region Caledonides, Norway. Norges Geol. Undersøkelse Bull. 426, 53–75.

Blodau, C., 2006. A review of acidity generation and consumption in acidic coal mine lakes and their watersheds. Sci. Total Environ. 369, 307–332.

Bouzahzah, H., Benzaazoua, M., Bussière, B., 2012. Modification and Automation of the Humidity Cell Test Protocol to Favor Tailings Reactivity, in: 9th International Conference on Acid Rock Drainage (ICARD). Ottawa, Ontario, pp. 1–12.

Bouzahzah, H., Benzaazoua, M., Bussiere, B., Plante, B., 2014. Prediction of Acid Mine Drainage: Importance of Mineralogy and the Test Protocols for Static and Kinetic Tests. Mine Water Environ. 33, 54–65.

Bussière, B., 2007. Colloquium 2004: Hydrogeotechnical properties of hard rock tailings from metal mines and emerging geoenvironmental disposal approaches. Can. Geotech. J. 44, 1019–1052.

CEN/TR, 2012a. Characterization of waste Kinetic testing for assessing acid generation potential of sulfidic waste from extractive industries: PD CEN/TR 16363, BSI Standards Publication.

CEN/TR, 2012b. Characterization of waste — Overall guidance document for characterization of waste from the extractive industries: PD CEN/TR 16376:2012, BSI Standards Publication.

Chen, Y.T., Li, J.T., Chen, L.X., Hua, Z.S., Huang, L.N., Liu, J., Xu, B.B., Liao, B., Shu, W.S., 2014. Biogeochemical processes governing natural pyrite oxidation and release of acid metalliferous drainage. Environ. Sci. Technol. 48, 5537–5545.

Coastech Research Inc., 1989. Investigation of Prediction Techniques for Acid Mine Drainage.

MEND project 1.16.1, Canada Centre for mineral and energy technology, Energy, Mines and Resources Canada.

Cruz, R., Méndez, B.A., Monroy, M., González, I., 2001. Cyclic voltammetry applied to evaluate reactivity in sulfide mining residues. Appl. Geochemistry 16, 1631–1640.

CSIR, 2009. Acid Mine Drainage in South Africa, Natural Resources and the Environment.

Dai, Z., Samper, J., Ritzi, R., 2006. Identifying geochemical processes by inverse modeling of multicomponent reactive transport in the Aquia aquifer. Geosphere 2, 210–219.

Desbarats, A.J., Parsons, M.B., Percival, J.B., Beauchemin, S., John Kwong, Y.T., 2011. Geochemistry of mine waters draining a low-sulfide, gold-quartz vein deposit, Bralorne, British Columbia. Appl. Geochemistry 26, 1990–2003.

Dold, B., 2017. Acid rock drainage prediction: A critical review. J. Geochemical Explor. 172, 120–132.

Dold, B., 2014. Evolution of Acid Mine Drainage Formation in Sulphidic Mine Tailings. Minerals 4, 621–641.

Eary, L.E., Williamson, M.A., 2006. Simulations of the Neutralizing Capacity of Silicate Rocks in Acid Mine Drainage Environments. J. Am. Soc. Min. Reclam. 564–577.

Folldal Gruver, 2018. Stiftelsen Folldal Gruver. URL http://folldalgruver.no/english/ (accessed 1.12.18).

Frostad, S., Klein, B., Lawrence, R.W., 2002. Evaluation of Laboratory Kinetic Test Methods for Measuring Rates of Weathering. Mine Water Environ. 21, 183–192.

Furrer, G., Stumm, W., 1986. The coordination chemistry of weathering: I. Dissolution kinetics of [delta]-Al2O3 and BeO. Geochim. Cosmochim. Acta 50, 1847–1860.

Geological Survey of Norway, 2014. Map services: Bedrock, Soil, Mineral resources. Available at: http://www.ngu.no/no/hm/Kart-og-data/.

Georgopoulou, Z.J., Fytas, K., Soto, H., Evangelou, B., 1996. Feasibility and cost of creating an

iron-phosphate coating on pyrrhotite to prevent oxidation. Environ. Geol. 28, 61–69.

Grande, J.A., Andujar, J.M., Aroba, J., Torrea, M.L. de la, Beltran, R., 2005a. Precipitation, pH and metal load in AMD river basins: an application of fuzzy clustering algorithms to the process characterization. J. Environ. Monit. 7, 325–334.

Grande, J.A., Beltrán, R., Sáinz, A., Santos, J.C., De La Torre, M.L., Borrego, J., 2005b. Acid mine drainage and acid rock drainage processes in the environment of Herrerías Mine (Iberian Pyrite Belt, Huelva-Spain) and impact on the Andevalo Dam. Environ. Geol. 47, 185–196.

Gurung, S., 2001. Acid drainage from abandoned mines in Tasmania: Report 1 Acid drainage from abandoned mines in Tasmania 1–28.

Hakkou, R., Benzaazoua, M., Bussière, B., 2005. Environmental characterization of the abandoned Kettara mines wastes (Morocco). Post - Min. 1–14.

Hansen, R.N., 2015. Contaminant leaching from gold mining tailings dams in the Witwatersrand Basin, South Africa: A new geochemical modelling approach. Appl. Geochemistry 61, 217–223.

Holmstrom, H., 2000. Geochemical processes in sulphidic mine tailings Field and laboratory studies performed in northern Sweden at the Laver, Stekenjokk and Kristineberg mine-sites. Luleå University of Technology.

Hudson-Edwards, K.A., Jamieson, H.E., Lottermoser, B.G., 2011. Mine Wastes: Past, Present, Future. Elements 7, 375–380.

Hudson-Edwards, K.A., Macklin, M.G., Miller, J.R., Lechler, P.J., 2001. Sources, distribution and storage of heavy metals in the Río Pilcomayo, Bolivia. J. Geochemical Explor. 72, 229–250.

Johnson, R.H., Blowes, D.W., Robertson, W.D., Jambor, J.L., 2000. The hydrogeochemistry of the Nickel Rim mine tailings impoundment, Sudbury, Ontario. J. Contam. Hydrol. 41, 49–80.

Kartverket, 2005. Norge i Bilder WMS.

Kefeni, K.K., Msagati, T.A.M., Mamba, B.B., 2017. Acid mine drainage: Prevention, treatment options, and resource recovery: A review. J. Clean. Prod. 151, 475–493.

Kim, J.Y., Chon, H.T., 2001. Pollution of a water course impacted by acid mine drainage in the Imgok creek of the Gangreung coal field, Korea. Appl. Geochemistry 16, 1387–1396.

Klimpel, F., 2017. Natural neutralization of acid mine drainage : A possible remedial measure for the Folldal and Sulitjelma mines? Master thesis, Oslo University. p 113.

Kossoff, D., Dubbin, W.E., Alfredsson, M., Edwards, S.J., Macklin, M.G., Hudson-Edwards, K.A., 2014. Mine tailings dams: Characteristics, failure, environmental impacts, and remediation. Appl. Geochemistry 51, 229–245.

Lapakko, K.A., Antonson, D.A., 2006. Pyrite Oxidation Rates From Humidity Cell Testing of Greenstone Rock. J. Am. Soc. Min. Reclam. 1007–1025.

Lapakko, K.A., White III, W.W., 2000. Modification of the ASTM 5744-96 kinetic test, in: Proceedings of the Fifth International Conference on Acid Rock Drainage. pp. 631–639.

Lindsay, M.B.J., Moncur, M.C., Bain, J.G., Jambor, J.L., Ptacek, C.J., Blowes, D.W., 2015. Geochemical and mineralogical aspects of sulfide mine tailings. Appl. Geochemistry 57, 157–177.

Lyew, D., Sheppard, J., 2001. Use of conductivity to monitor the treatment of acid mine drainage by sulphate-reducing bacteria. Water Res. 35, 2081–2086.

MacIngova, E., Luptakova, A., 2012. Recovery of metals from acid mine drainage. Chem. Eng. Trans. 28, 109–114.

Méndez-Ortiz, B.A., Carrillo-Chávez, A., Monroy-Fernández, M.G., 2007. Acid rock-drainage and metal leaching from mine waste material (tailings) of a-Pb-Zn-Ag skarn deposit: Environmental assessment through static and kinetic laboratory tests. Rev. Mex. Ciencias Geol. 24, 161–169.

Molson, J.W., Aubertin, M., Bussière, B., Joanes, A.-M., 2004. Simulating acid mine drainage

through mine wastes constructed with capillary barrier covers, in: 57th Canadian Geotechnical Conference and the 5th Joint CGS-IAH Conference. pp. 29–36.

Molson, J.W., Fala, O., Aubertin, M., Bussieere, B., 2005. Numerical simulations of pyrite oxidation and acid mine drainage in unsaturated waste rock piles. J. Contam. Hydrol. 78, 343–371.

Morin, K. a, Hutt, N.M., 2001. Environmental geochemistry of minesite drainage: practical theory and case studies. MDAG Publishing.

Namaghi, H.H., Li, S., 2016. Acid-Generating and Leaching Potential of Soils in a Coal Waste Rock Pile in Northeastern China. Soil Sediment Contam. 25, 776–791.

NGI, 2014. Folldal gruver. Vurdering av mulige tiltak mot avrenning fra tidligere gruvevirksomhet.

Nicholson, R. V, Scharer, J.M., 1994. Laboratory Studies of Pyrhotite Oxidation Kinetics. Environ. Geochemistry Sulfide Oxid. 14–30.

Nordstrom, D.K., Alpers, C.N., 1999. Geochemistry of acid mine waters, in: Plumlee, G.S., Logsdon, M.J. (Eds.), The Environmental Geochemistry of Mineral Deposits. pp. 133–160.

Norsk Standard, 2011. Characterization of waste Static test for determination of acid potential and neutralisation potential of sulfidic waste: NS-EN15875, Standard Norge.

Papassiopi, N., Zaharia, C., Xenidis, A., Adam, K., Liakopoulos, A., Romaidis, I., 2014. Assessment of contaminants transport in a watershed affected by acid mine drainage, by coupling hydrological and geochemical modeling tools. Miner. Eng. 64, 78–91.

Parbhakar-Fox, A., Lottermoser, B.G., 2015. A critical review of acid rock drainage prediction methods and practices. Miner. Eng. 82, 107–124.

Parkhurst, B.D.L., Appelo, C. a J., 1999. User's Guide To PHREEQC (version 2) — a Computer Program for Speciation, and Inverse Geochemical Calculations:, U.S Geological Survey.

Parkhurst, D.L., Appelo, C.A.J., 2013. Description of Input and Examples for PHREEQC Version 3 — A Computer Program for Speciation , Batch-Reaction , One-Dimensional

Transport , and Inverse Geochemical Calculations., in: Groundwater Modeling Techniques 6. U.S. Geological Survey, p. 6–43A.

Plante, B., Benzaazoua, M., Bussière, B., 2011. Predicting Geochemical Behaviour of Waste Rock with Low Acid Generating Potential Using Laboratory Kinetic Tests. Mine Water Environ. 30, 2–21.

Plante, B., Bussière, B., Benzaazoua, M., 2012. Static tests response on 5 Canadian hard rock mine tailings with low net acid-generating potentials. J. Geochemical Explor. 114, 57–69.

Price, W., 2009. Prediction manual for drainage chemistry from sulphidic geologic materials: MEND Report1.20.1, CANMET Mining and Mineral Sciences Laboratories.

Robertson, S., Kirsten, 1989. Draft Acid Rock Drainage Technical Guide Volume 1. BC AMD Task Force.

Rodés, S.P., 2014. Hydrogeological characteristics and numerical modeling of groundwater flow and contaminant transport in the Folldal mining site. Master thesis, Oslo University. p 112.

Ruihua, L., Lin, Z., Tao, T., Bo, L., 2011. Phosphorus removal performance of acid mine drainage from wastewater. J. Hazard. Mater. 190, 669–676.

Salmon, S.U., 2003. Geochemical modelling of acid mine drainage in mill tailings: Quantification of kinetic processes from laboratory to field scale.

Sapsford, D.J., Bowell, R.J., Dey, M., Williams, K.P., 2009. Humidity cell tests for the prediction of acid rock drainage. Miner. Eng. 22, 25–36.

Seal, R.R., Hammarstrom, J.M., Johnson, A.N., Piatak, N.M., Wandless, G.A., 2008. Environmental geochemistry of a Kuroko-type massive sulfide deposit at the abandoned Valzinco mine, Virginia, USA. Appl. Geochemistry 23, 320–342.

Sharif, M.U., Davis, R.K., Steele, K.F., Kim, B., Kresse, T.M., Fazio, J.A., 2008. Inverse geochemical modeling of groundwater evolution with emphasis on arsenic in the Mississippi River Valley alluvial aquifer, Arkansas (USA). J. Hydrol. 350, 41–55.

Sherlock, E., 1995. Evaluation of static and kinetic prediction test data and comparison with field

monitoring data. Mend Rep.

Simate, G.S., Ndlovu, S., 2014. Acid mine drainage: Challenges and opportunities. J. Environ. Chem. Eng. 2, 1785–1803.

Singh, G., 1987. Mine water quality deterioration due to acid mine drainage. Int. J. Mine Water 6, 49–61.

Skousen, J., Rose, A., Geidel, G., Foreman, J., Evans, R., Hellier, W., 1998. Handbook of technologies for avoidance and remediation of acid mine drainage, The National Mine Land Reclqmqtion Center. West Virginia.

Sobek, A.A., Schuller, W.A., Freeman, J.R., Smith, R.M., 1978. Field and Laboratory Methods Applicable to Overburdens and Minesoils. Industrial Environmental Research Laboratory.

Sracek, O., Choquette, M., Gélinas, P., Lefebvre, R., Nicholson, R. V., 2004. Geochemical characterization of acid mine drainage from a waste rock pile, Mine Doyon, Québec, Canada. J. Contam. Hydrol. 69, 45–71.

Stumm, W., Morgan, J.J., 1996. Aquatic Chemistry, 3rd ed. Wiley and Sons, New York.

Sutthirat, C., 2011. Geochemical Application for Environmental Monitoring and Metal Mining Management, in: EO, E. (Ed.), Environmental Monitoring.

Tvedten, M.K., 2016. The performance of multilayered covers for limiting acid mine drainage from tailings in Folldal , Norway: A laboratory column experiment. Master thesis, Oslo Univesity. p 86.

Werhli, B., 1989. Monte Carlo simulations of surface morphologies during mineral dissolution. J. Colloid Interface Sci. 132, 230–242.

Williamson, M.A., Rimstidt, J.D., 1994. The kinetics and electrochemical rate-determining step of aqueous pyrite oxidation. Geochim. Cosmochim. Acta 58, 5443–5454.

Appendixes

Appendix A: Certified materials

Table_A 1: Environmental matrix reference material certificate analysis IO-96.4

Environmental Matrix Reference Material

Certificate of Analysis

ION-96.4

Natural river water from the Grand River, Ontario

ION-96.4 was collected from the mouth of the Grand River in Southern Ontario during 2009

Measurand	Value in mg/L
Alkalinity, Total (as $CaCO_3$)	245 ± 12
Boron	0.043 ± 0.0059
Calcium	95.5 ± 7.5
Chloride	74.0 ± 3.8
Colour (units)	14.0 ± 3.7
Conductivity (µS/cm, 25^{o}C)	830 ± 27
Dissolved Inorganic Carbon (DIC)	57.3 ± 6.4
Dissolved Organic Carbon (DOC)	4.67 ± 0.73
Fluoride	0.122 ± 0.035
Hardness, Total (as $CaCO_3$)	344 ± 26
Magnesium	25.5 ± 2.1
Nitrate +Nitrite (as N)	2.86 ± 0.3
pH (units, 25^{o}C)	8.39 ± 0.18
Potassium	3.5 ± 0.3
Silica (as Si)	0.275 ± 0.035
Sodium	43.3 ± 4.3
Sulphate	76.3 ± 4.2
Total Nitrogen	3.2 ± 0.29

Table_A 2: Certified Values (a) (Dry-Mass Basis) for Selected Elements in SRM 2709a

Element	Mass Fraction (%)	Element	Mass Fraction (mg/kg)
Aluminium	7.37 ± 0.16	Antimony	1.55 ± 0.06
Calcium	1.91 ± 0.09	Barium	979 ± 28
Iron	3.36 ± 0.07	Cadmium	0.371 ± 0.002

Magnesium	1.46 ± 0.02	Chromium	130 ± 9
Phosphorus	0.0688 ± 0.0013	Cobalt	12.8 ± 0.2
Potassium	2.11 ± 0.06	Lead	17.3 ± 0.1
Silicon	30.3 ± 0.4	Manganese	529 ± 18
Sodium	1.22 ± 0.03	Strontium	239 ± 6
Titanium	0.336 ± 0.007	Vanadium	110 ± 11
Zirconium	195 ± 46		

(a) Certified values for all elements except cadmium and lead are the equally weighted means of results from two or three analytical methods.

Table_A 3: Reference Values (a) (Dry-Mass Basis) for Selected Elements in SRM 2709a

Element	Mass Fraction (mg/kg)
Arsenic	10.5 ± 0.3
Cerium	42 ± 1
Cesium	5.0 ± 0.1
Copper	33.9 ± 0.5
Europium	0.83 ± 0.02
Gadolinium	3.0 ± 0.1
Lanthanum	21.7 ± 0.4
Mercury(b)	0.9 ± 0.2
Nickel	85 ± 2
Rubidium	99 ± 3
Scandium	11.1 ± 0.1
Thallium	0.58 ± 0.01
Thorium	10.9 ± 0.2
Uranium	3.15 ± 0.05
Zinc	103 ± 4

(a) Reference values for all elements are based on results from one analytical method at NIST.

Table_A 4: 1643H Standard values

Element	Mass Concentration (µg/L)		
Aluminum	141.8	±	8.6
Antimony	58.30	±	0.61
Arsenic	60.45	±	0.72
Barium	544.2	±	5.8
Beryllium	13.98	±	0.17
Boron	157.9	±	3.9
Cadmium	6.568	±	0.073
Calcium	32 300	±	1 100
Chromium	20.40	±	0.24
Cobalt	27.06	±	0.32
Copper	22.76	±	0.31
Iron	98.1	±	1.4
Lead	19.63	±	0.21
Lithium	17.4	±	1.7
Magnesium	8 037	±	98
Manganese	38.97	±	0.45
Molybdenu	121.4	±	1.3
Nickel	62.41	±	0.69
Potassium	2 034	±	29
Rubidium	14.14	±	0.18
Selenium	11.97	±	0.14
Silver	1.062	±	0.075
Sodium	20 740	±	260
Strontium	323.1	±	3.6
Tellurium	1.09	±	0.11
Thallium	7.445	±	0.096
Vanadium	37.86	±	0.59
Zinc	78.5	±	2.2

Elements added, µg/L

U	Th	S	Si	P	Cs	La	Ce	Pr	Nd	Sm	Eu	Gd	Dy	Ho	Er	Tm	Yb	Lu	Zr	Nb	Ga
1	1	2500	2500	2500	1	1	1	1	1	1	1	1	1	1	1	1	1	1	5	1	1

Appendix B: Leachate samples analyses in humidity cell tests/small column tests

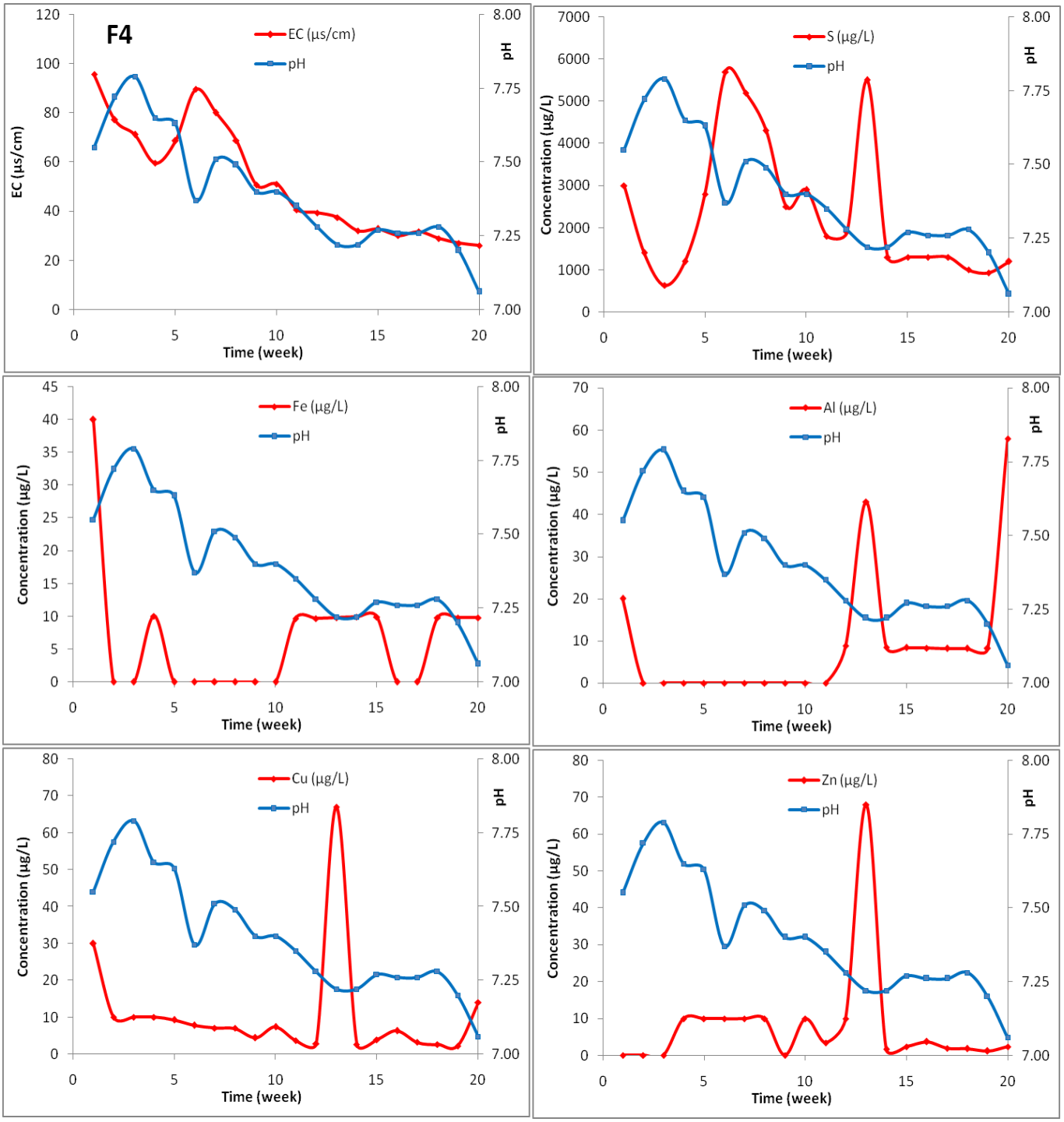

Fig_A 1 EC, pH, sulphate, iron, aluminium, copper and zinc vs. Time of leachate sample in F4 soil sample

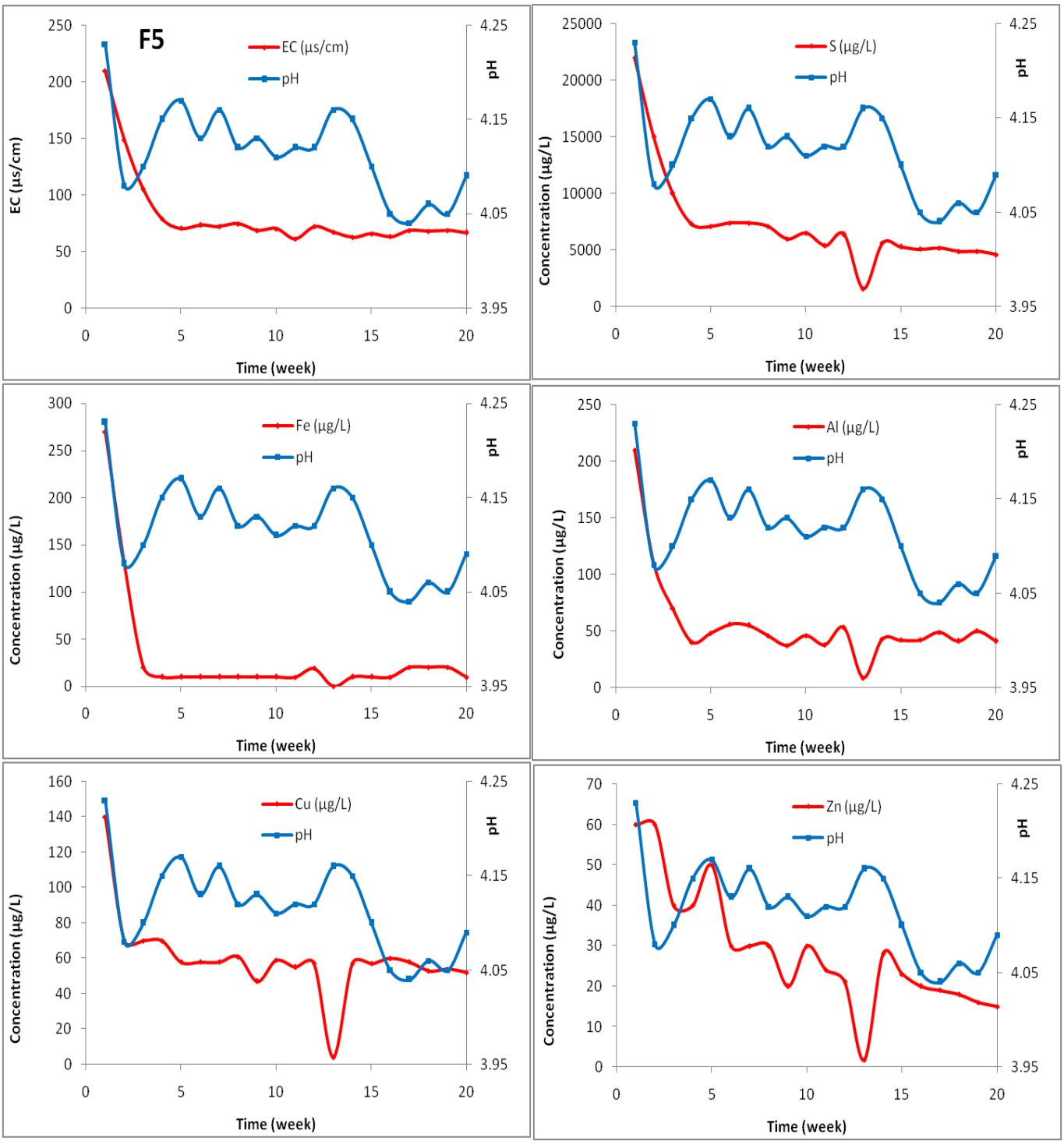

Fig_A 2 EC, pH, sulphate, iron, aluminium, copper and zinc vs. Time of leachate sample in F5 soil sample

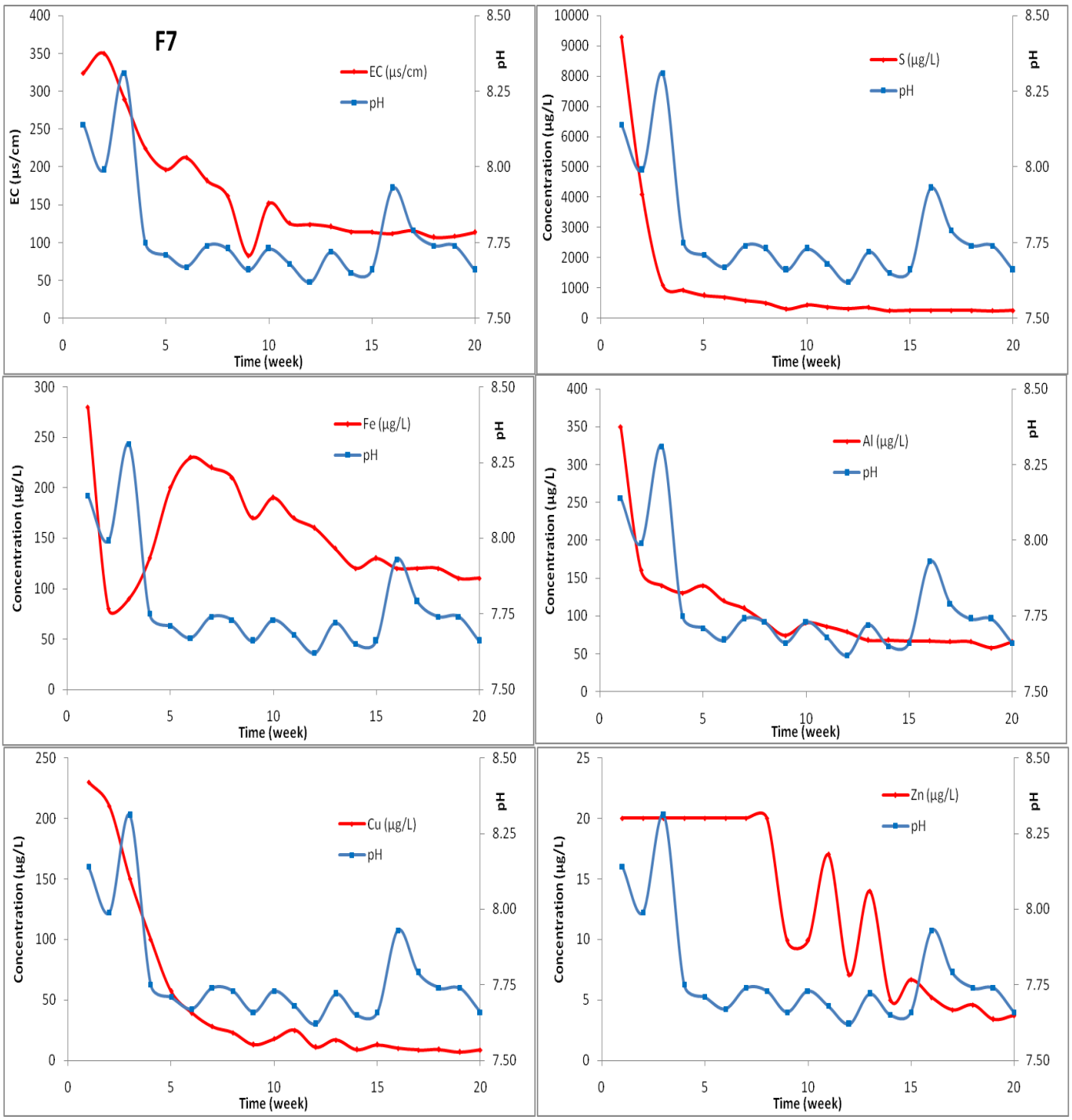

Fig_A 3 EC, pH, sulphate, iron, aluminium, copper and zinc vs. Time of leachate sample in F7 soil sample

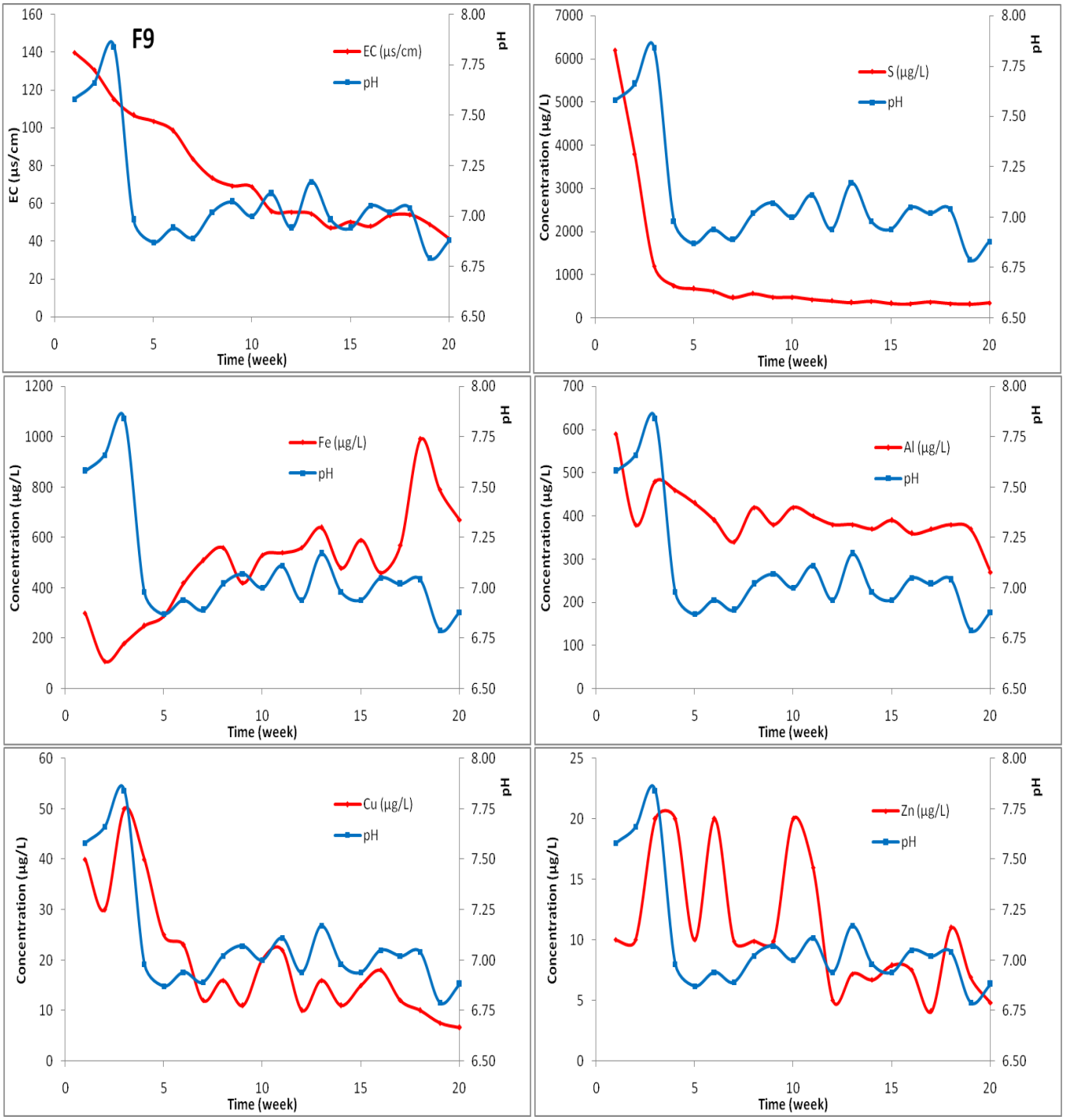

Fig_A 4 EC, pH, sulphate, iron, aluminium, copper and zinc vs. Time of leachate sample in F9 soil sample

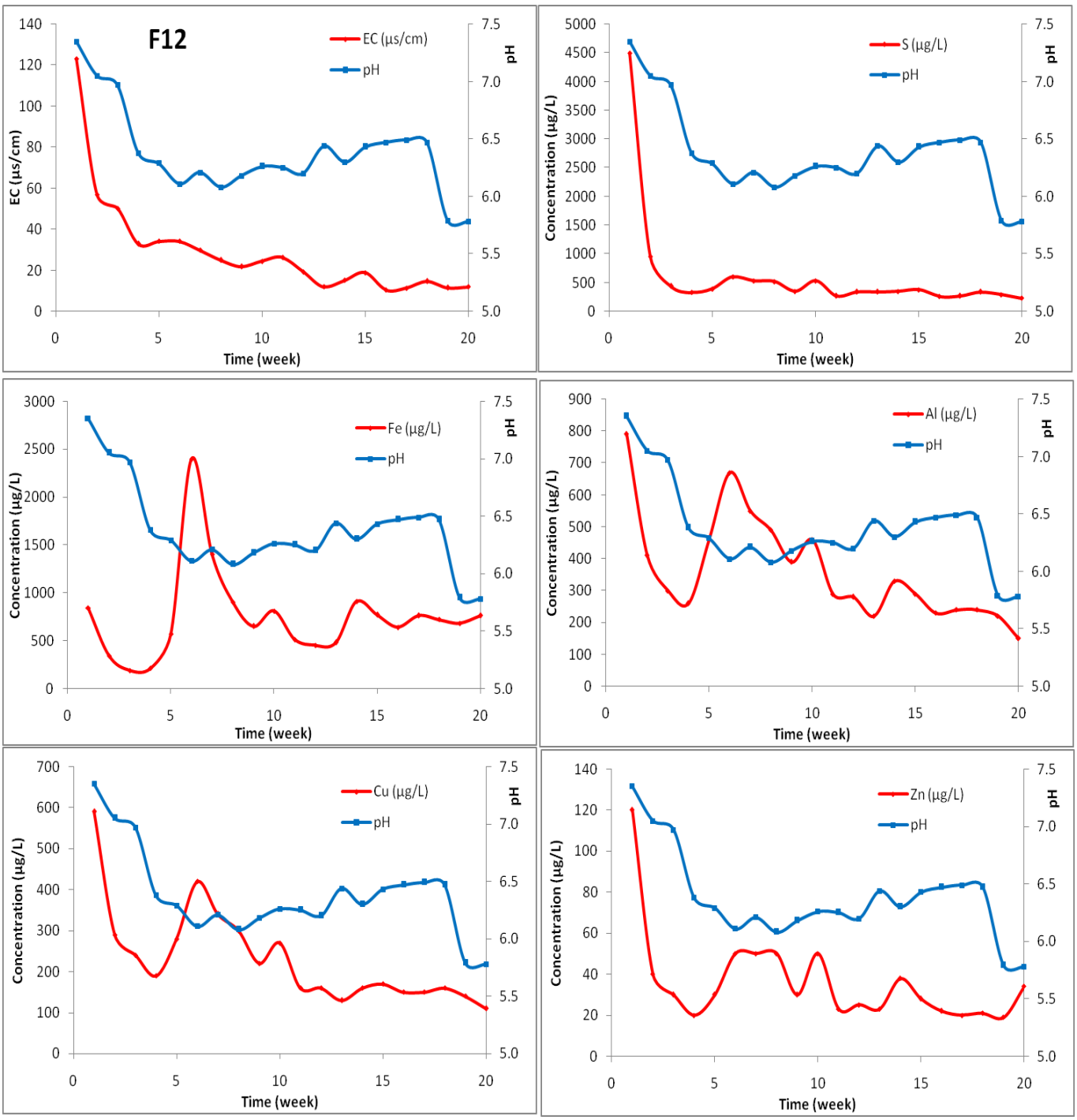

Fig_A 5 EC, pH, sulphate, iron, aluminium, copper and zinc vs. Time of leachate sample in F12 soil sample

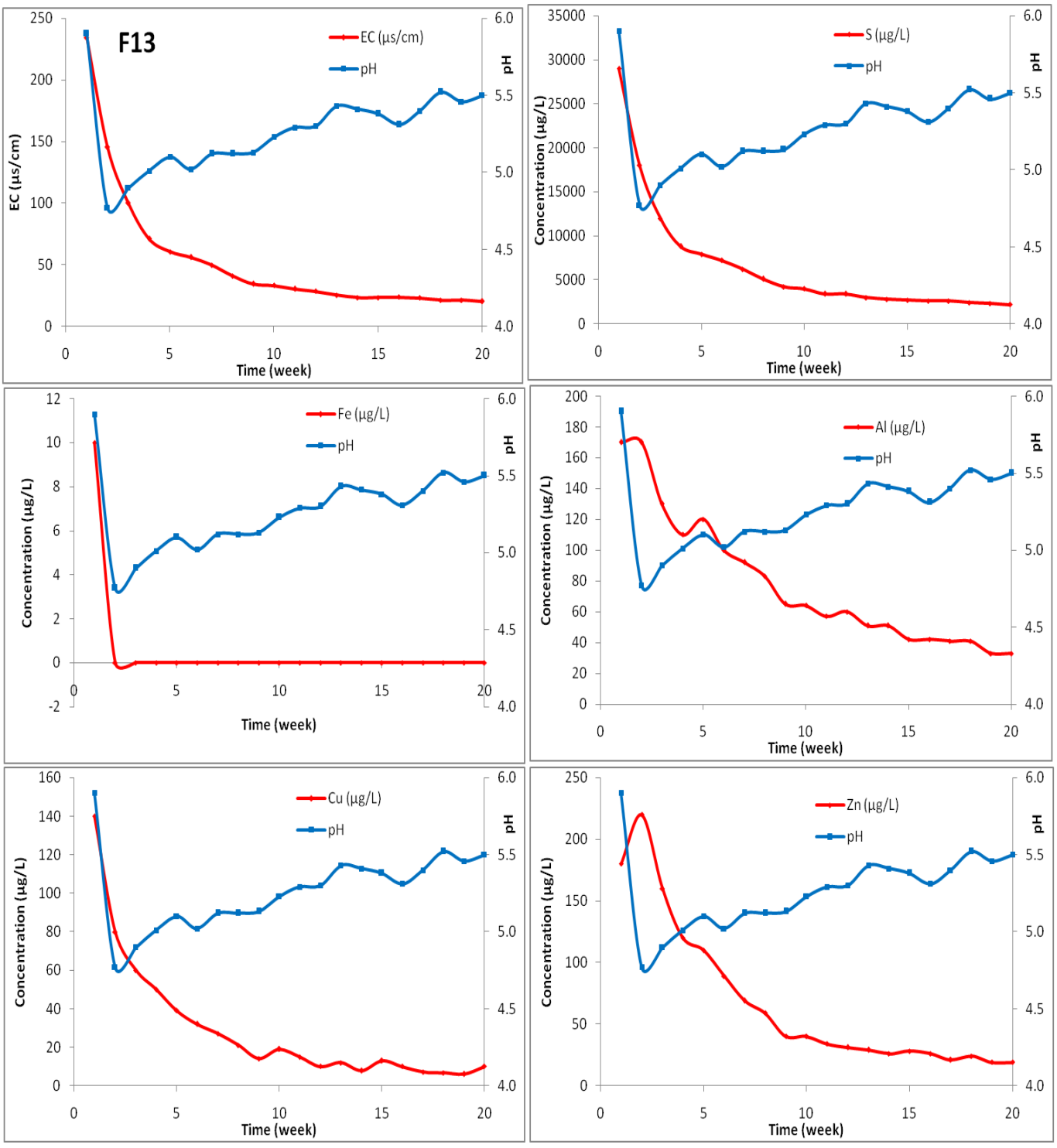

Fig_A 6 EC, pH, sulphate, iron, aluminium, copper and zinc vs. Time of leachate sample in F13 soil sample

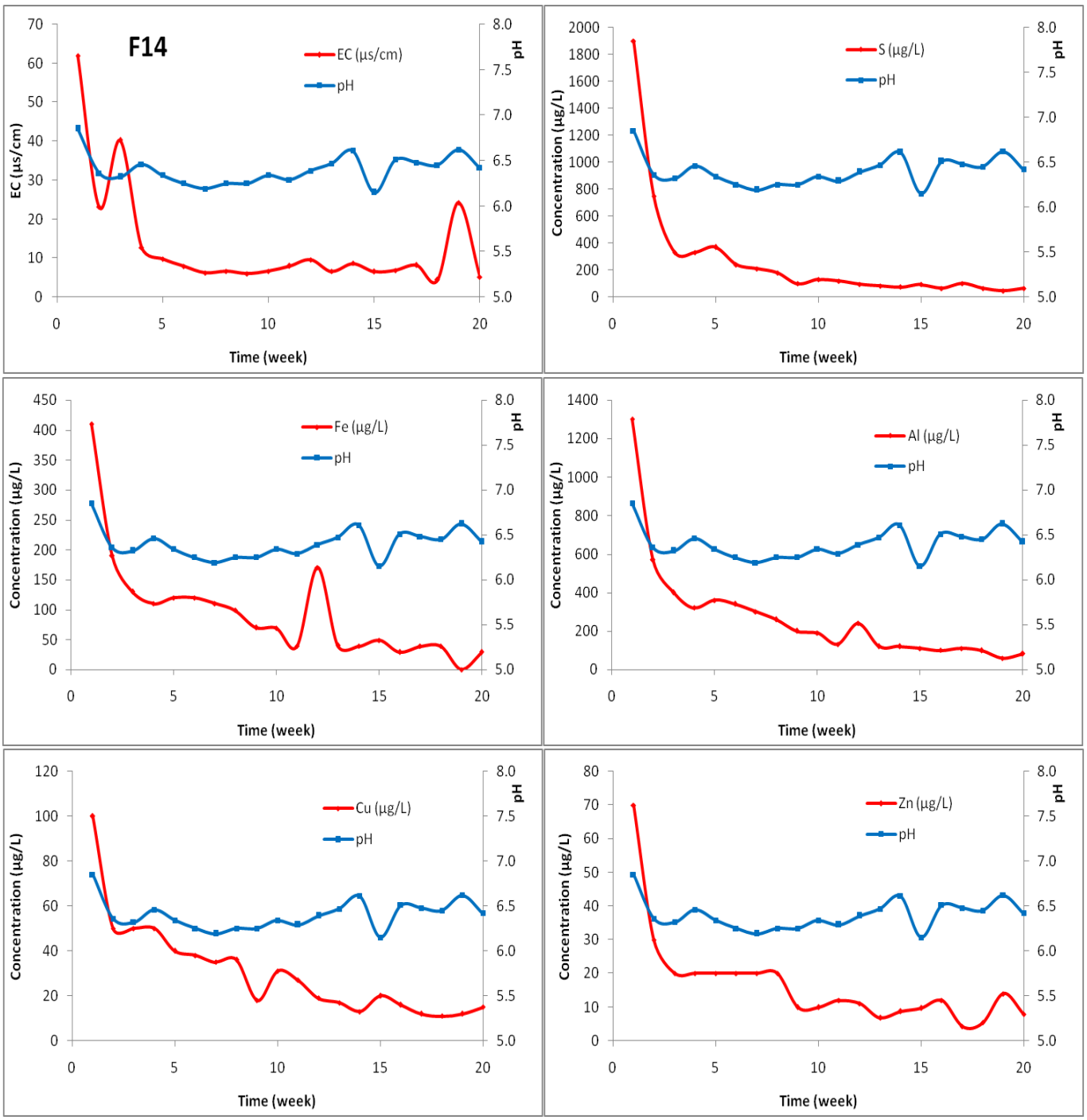

Fig_A 7 EC, pH, sulphate, iron, aluminium, copper and zinc vs. Time of leachate sample in F14 soil sample

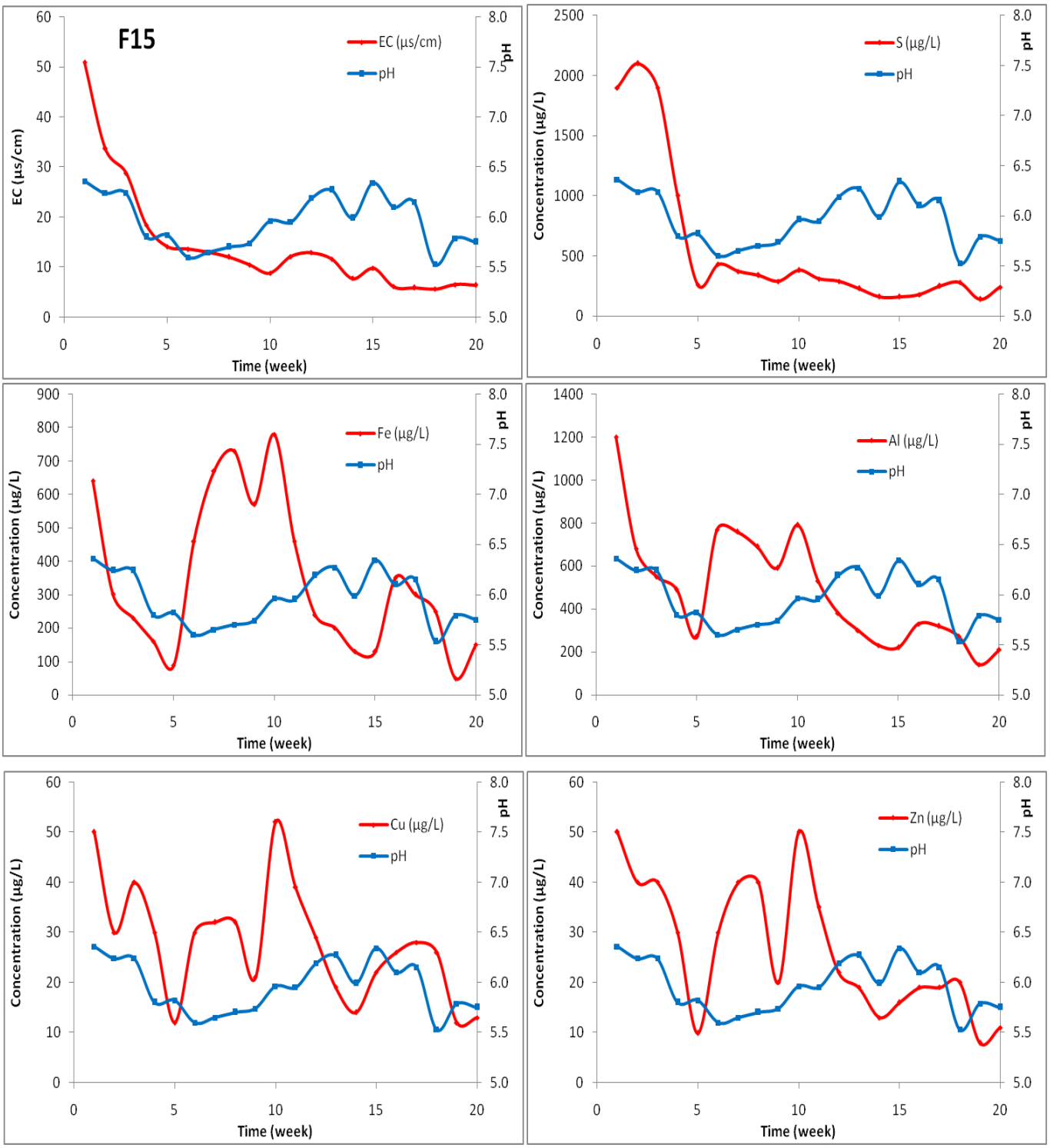

Fig_A 8 EC, pH, sulphate, iron, aluminium, copper and zinc vs. Time of leachate sample in F15 soil sample

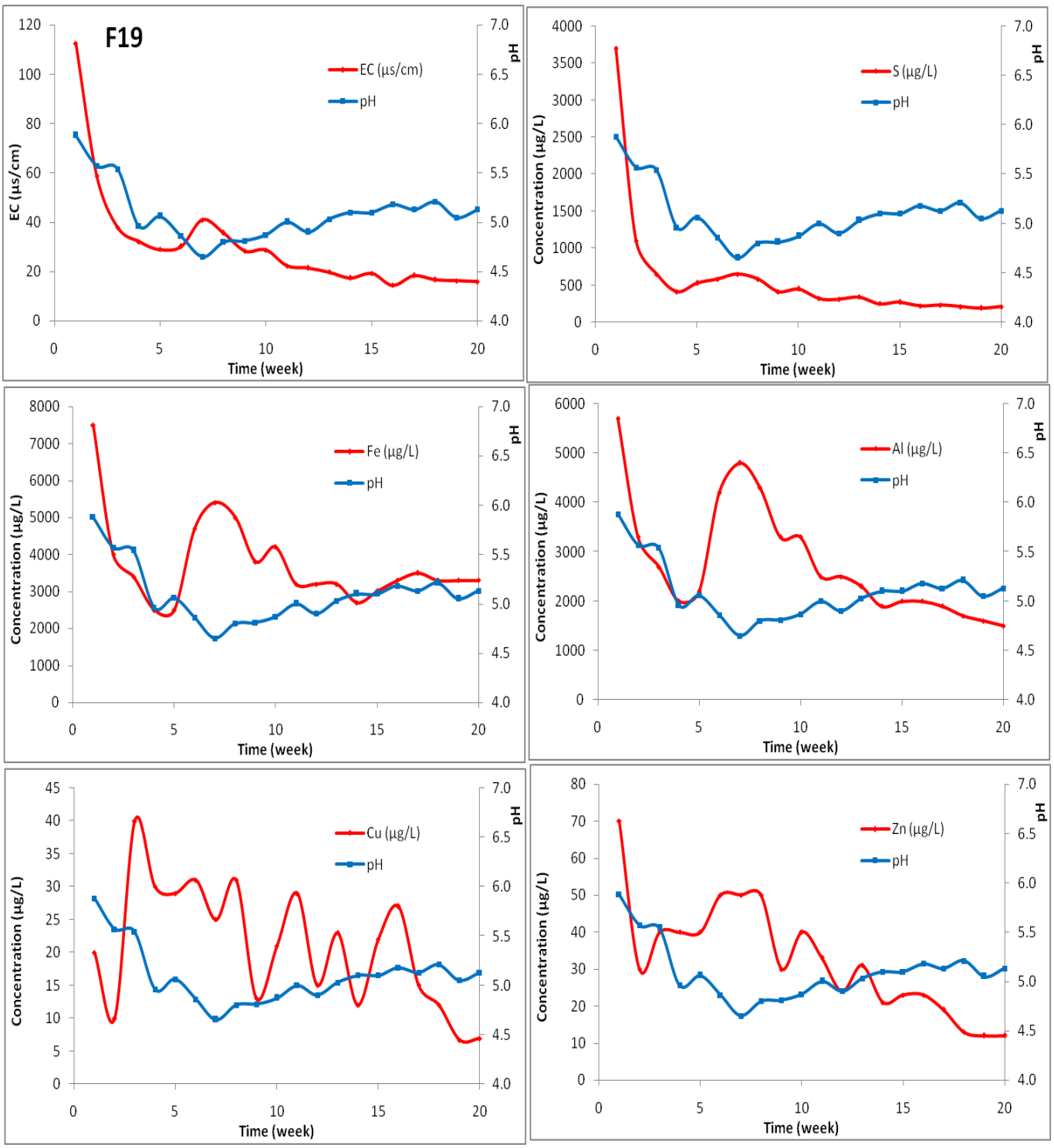

Fig_A 9 EC, pH, sulphate, iron, aluminium, copper and zinc vs. Time of leachate sample in F19 soil sample

Appendix C: Total soil concentrations

Table_A 5: Total elements concentration, pH and EC in the soil samples from Folldal mining area.

Sample	EC (µs/cm)	pH	**Al (g/kg)**	**Ca (g/kg)**	**Cu (g/kg)**	**Fe (g/kg)**	**K (g/kg)**	**Mg (g/kg)**	**Mn (g/Kg)**	**Na (g/kg)**	**P (g/kg)**	**S (g/kg)**	**Zn (g/kg)**
F1	181.1	3.8	28.00	20.00	0.10	53.00	2.80	11.00	0.50	1.20	0.40	0.93	0.07
F2	182.6	7.5	26.00	18.00	0.18	40.00	5.80	11.00	0.43	0.91	0.43	1.40	0.12
F3	236.2	3.8	19.00	9.10	0.09	43.00	4.10	7.40	0.29	0.78	0.36	2.30	0.04
F4	88.9	7.2	36.00	35.00	0.12	46.00	2.30	16.00	0.60	1.60	0.40	0.52	0.15
F5	154.4	3.8	28.00	13.00	0.12	52.00	4.80	14.00	0.43	1.20	0.39	0.83	0.08
F6	317.6	5.9	17.00	7.10	0.28	27.00	2.40	11.00	0.41	0.50	0.28	1.30	0.11
F7	224.2	7.2	19.00	24.00	0.08	19.00	3.50	7.60	0.35	0.62	0.42	0.66	0.22
F8	128.5	7.2	20.00	12.00	0.10	23.00	3.90	8.40	0.41	0.69	0.37	0.48	0.32
F9	100.1	6.4	24.00	15.00	0.03	21.00	4.00	10.00	0.31	0.76	0.49	0.81	0.07
F10	195.9	7.6	19.00	19.00	0.08	27.00	2.90	9.20	0.38	0.75	0.43	0.68	0.12
F11	2109.0	7.6	9.60	33.00	1.10	55.00	0.52	11.00	0.54	0.28	0.20	20.00	2.00
F12	55.6	5.1	23.00	13.00	0.20	26.00	3.00	9.10	0.57	0.85	0.43	0.14	0.10
F13	179.3	4.3	22.00	14.00	0.12	41.00	3.70	11.00	0.42	1.00	0.62	1.20	0.09
F14	32.0	4.9	24.00	8.90	0.04	24.00	5.50	9.20	0.39	0.60	0.39	0.05	0.05
F15	50.0	4.8	20.00	8.60	0.02	21.00	3.10	4.80	0.37	0.53	0.27	0.11	0.04
F16	65.6	6.8	19.00	11.00	0.02	19.00	3.10	6.60	0.35	0.62	0.38	0.23	0.06
F17	186.5	5.1	32.00	16.00	0.55	56.00	4.80	18.00	0.48	1.10	0.68	1.90	0.37
F18	28.8	5.0	17.00	11.00	0.01	18.00	1.90	6.00	0.27	0.68	0.38	0.08	0.03
F19	90.1	4.2	27.00	8.20	0.01	25.00	6.50	9.80	0.29	0.69	0.23	0.14	0.05

Appendix D: Large column data

Table_A 6: pH, EC and concentrations of elements in large column test

Column	Date	pH	EC	Na (mg/L)	Mg (mg/L)	Al (mg/L)	S (mg/L)	K (mg/L)	Ca (mg/L)	Mn (mg/L)	Fe (mg/L)	Cu (mg/L)	Zn (mg/L)
K3	06/17/16			9.7	330	410	12000	4.1	260	8	12000	550	13
K3	07/20/16	1.90			110	130	4200	1.7	120	2.9	4100	160	3.9
K3	10/21/16	2.06	8.87		100	120	3800	2.3	61	2.4	3900	150	2.8
K3	02/03/17	2.01	9.85		150	190	5500	2.5	76	3.4	6300	210	2.9
K3	03/28/17	2.12	10.47		160	190	5700	2.3	58	3.5	6600	220	2.7
K3	05/24/17	1.78	11.66		180	220	6100	2	67	3.8	6900	220	2.7
K3	06/22/17	1.91	11.98		190	230	6300	2	80	3.9	7000	230	2.7
K3	08/25/17	1.97	12.25		190	240	6400	2.1	86	4	7000	240	2.7
K3	10/05/17	2.02	10.48		160	180	5100	2.2	71	3.2	5600	190	2.2

Appendix E: Geochemical modelling inputs

E1: Inverse modelling

```
#Inverse modeling
SOLUTION 1 # Rain water from Appelo 2005
    temp      1
    pH        5.6
    pe        4
    redox     pe
    units     umol/l
    density   1
    Ca        16
    Cl        11 charge
    K         5
    Mg        5
    Na        13
    O(0)      865
    S(6)      31.1

    -water    1 # kg
SOLUTION 2 #leachate samples from large column test
    temp      4.5
    pH        1.9
    pe        6.8
    redox     pe
    units     mg/l
    density   1
    Al        130
    Ca        120
    Cl        145.2 uMol/l     charge
    Cu        160
    Fe        4100
    K         1.7
    Mg        110
    Na        9.7
    S(6)      4200
    Zn        3.9
    -water    1 # kg
EQUILIBRIUM_PHASES 1
    O2(g)     -0.69 10
INVERSE_MODELING 1
    -solutions      1        2
    -uncertainty    0.05     0.05
    -phases
        Pyrite              dis
        O2(g)               dis
        Pyrrhotite          dis
        Schwertmannite
        Chalcopyrite
        Jarosite-K
        K-feldspar
```

```
        Sphalerite
        Chlorite(14A)        dis
        K-mica               dis
        Halite
        Gypsum
        Fe(OH3(a)          pre
        Gibbsite             pre
        Albite
    -tolerance         1e-10
    -mineral_water     true
    -multiple_precision     true
    -mp_tolerance 1e-12
    -censor_mp 1e-20
PHASES
Halite
    NaCl = Cl- + Na+
    log_k     0
Chalcopyrite
    FeCuS2 + 4O2 = Cu+2 + Fe+2 + 2SO4-2
    log_k     0
Sphalerite
    ZnS + 2O2 = Zn+2 + SO4-2
    log_k     0
Pyrrhotite
    FeS + H2O + 1.5O2 = Fe+2 + 2H+ + SO4-2
    log_k    10
Schwertmannite
    Fe8O8(OH)6SO4 + 22H+ = 8Fe+3 + 14H2O + SO4-2
    log_k     0

END
```

E2: kinetic modelling

```
SOLUTION 1 #rainwater (from Appelo and POstma)
temp 10; pH 5.6
units umol/l
density 1
Ca 16
Cl 11
K 5
Mg 5
Na 27
S(6) 21
O(0) 1 O2(g) -0.68
-water 1 # kg
RATES
    Pyrite
-start
  1 A = 120 * m0
 10 if SI("Pyrite")>0 then goto 100
 20 fH = mol("H+")
 30 fFe2 = (1 + tot("Fe(2)") / 1e-6)
```

```
 40 if mol("O2") < 1e-6 then goto 80
 50 rO2 = 10^-8.19 * mol("O2")^0.5 * fH^-0.11
 60 rO2_Fe3 = 6.3e-4 * tot("Fe(3)")^0.92 * fFe2^-0.43
 70 goto 90
 80 rem
 81 rFe3 = 1.9e-6 * tot("Fe(3)")^0.28 * fFe2^-0.52 * fH^-0.3
 90 rate = A * (m/m0)^0.67 * (rO2 + rO2_Fe3 + rFe3) * (1 - SR("Pyrite"))
100 save rate * time
-end
KINETICS 1
Pyrite
    -formula  Pyrite  1
    -m0       1.32 # mols of Pyrite/L
    -tol      1e-08
-steps  100  400  3100  10800  21600  5.04e4  8.64e4  1.728e5  1.8e6  1.8e7  4.67e7
4.67e7 # seconds
-step_divide 1e-4
-cvode true
INCREMENTAL_REACTIONS True

USER_PUNCH 1
    -headings Days Fe(2) pH
    -start
10  PUNCH  SIM_TIME  /  3600  /  24/30,  TOTAL("Fe(2)")*1e3,  TOTAL("Fe(3)")*1e3,  -
LA("H")
    -end
USER_GRAPH 10
    -headings Fe(2) pH
    -axis_titles  "Time, in months" "Millimoles per Litre" "pH"
    -initial_solutions      false
    -connect_simulations    true
    -plot_concentration_vs  t
  -start
20 GRAPH_X TOTAL_TIME/3600/24/30
30 GRAPH_Y tot("Fe")*1e3
40 GRAPH_SY -LA("H+")
    -active                 true
-end
 END
```

Norges miljø- og biovitenskapelige universitet
Noregs miljø- og biovitskapelege universitet
Norwegian University of Life Sciences

Postboks 5003
NO-1432 Ås
Norway